CTU
CZECH TECHNICAL UNIVERSITY IN PRAGUE

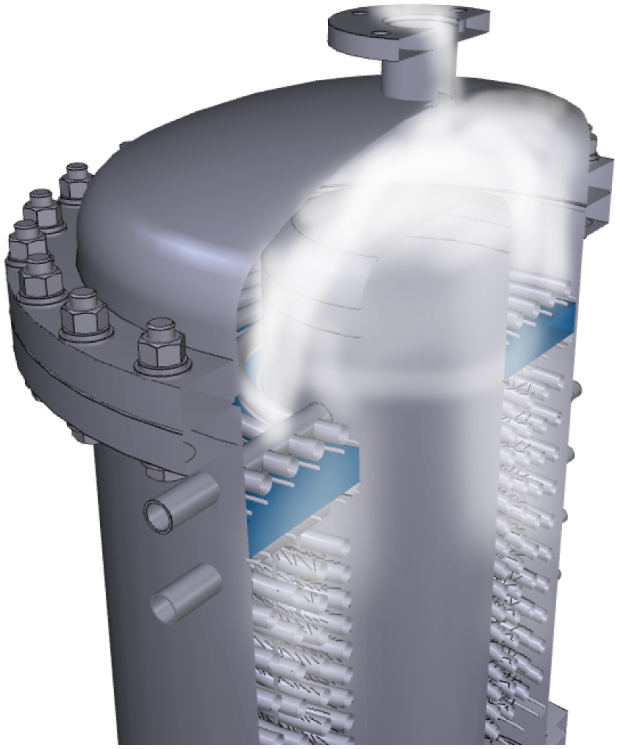

Design of Experimental Unit Based on Absorption Power Cycle with LiBr Solution Working Fluid

Master's thesis in Master Programme *Strojní inženýřství - Energetika*

DÁVID JURAJ SZÜCS

Department of Energy Engineering, Faculty of Mechanical Engineering
CZECH TECHNICAL UNIVERSITY
Prague, Czech Republic 2019

Prohlášení

Prohlašuji, že jsem svou bakalářskou prací s názvem Návrh experimentální jednotky založeném na absorpčním oběhu pro konání práce a využívající roztok LiBr (Design of Experimental Unit Based on Absorption Power Cycle with LiBr Solution Working Fluid) vypracoval samostatně a použil jsem pouze podklady (literaturu, projekty, SW atd.) uvedené v seznamu.

Nemám závažný důvod proti užití tohoto školního díla ve smyslu § 60 zákona č. 121/2000 Sb., o právu autorském, o právech souvisejících s právem autorským a o změně některých zákonů (autorský zákon).

V Praze dne: .....

Podpis: .....

Design of Experimental Unit Based on Absorption Power Cycle with LiBr Solution Working Fluid
Master's Thesis

DÁVID JURAJ SZÜCS

Supervisor: Ing. Václav Novotný, Faculty of Mechanical Engineering, CTU and in cooperation with University Centre of Energy Efficient Buildings CTU in Prague

Master's Thesis 2019
Department of Energy Engineering
Faculty of Mechanical Engineering
Czech Technical University in Prague
Prague, Czech Republic
energetika.cvut.cz

Cover: 3D visualization of vapour absorption in the absorber of the APC (modified model from CERBET)

Typeset in LaTeX
Printed by CTU
Prague, Czech Republic 2019

Design of Experimental Unit Based on Absorption Power Cycle with LiBr Solution Working Fluid

DÁVID JURAJ SZÜCS
Department of Energy Engineering
Faculty of Mechanical Engineering
Czech Technical University

Abstract

Continuous efforts for better fuel utilization and efficiency amelioration in both commercial and scientific circles have led the research towards an exploration of very-low-temperature heat sources for power generation. Such very-low temperature sources have an upper temperature limit of approximately 150 °C, thus approaching the beginning of the feasible range of already well-established organic Rankine cycles (ORCs). Absorption cycles, of which, e.g. Kalina cycle has already proven both thermodynamic advantages and practical implementations, seem to become perspective systems for the low-temperature heat source, such as last-stage bottoming cycle or small scale waste heat recovery. The working fluid of Kalina cycles has, however, caused multiple operational problems and for this reason, a solution of Lithium-Bromide salt in water as the working fluid of an absorption power cycle (APC) has been proposed by some of the researchers. The absorption technology with a solution of H_2O-LiBr has only been practically known from cooling industry, but theoretical publications have demonstrated a possible adjustment for power generation. A design methodology of an absorption power cycle (APC) with a solution of H_2O-LiBr is discussed and presented in this work. Following the methodology prepared, a proof-of-concept experimental unit is being constructed upon the design proposed. The experimental unit is to be set as a bottoming cycle of an organic Rankine circle (ORC) with generator inlet temperature of 90 °C and heat input to the APC of 20 kW. The APC unit is expected to have a gross power output of 0.5 kW. Nevertheless, a temperature glide during the heat addition and rejection result in higher exergy efficiency, and significant volumetric flow rate of vapour allows to build an efficient turbine for small power output. The technology of additive manufacturing from plastic is used for the expander. Under experimental conditions, on the other hand, the design results willingly in the components' over-sizing, which is expected to cover the uncertainties of the model and the character of the fluid. This thesis presents a thermodynamic model of the cycle, methodology for sizing of the components and a final design proposal of the APC unit. Once the construction of the APC is finalized, future work is expected to bring results of the operation, approval of the concept, size optimization and possible economic feasibility study that would determine future commercialization of the system.

Keywords: APC, absorption power cycle, absorption cycle design, low-temperature sources, microgeneration, decentralized sources, waste heat recovery

Návrh experimentální jednotky založeném na absorpčním oběhu pro konání práce a využívající roztok LiBr

DÁVID JURAJ SZÜCS
Ústav energetiky
Fakulta strojní
České vysoké učení technické v Praze

Abstrakt

Neustálé úsilí o lepší využitelnost primárních zdrojů a vyšší účinnost energetických systémů vedla v posledních letech komerční i vědecké společnosti k výzkumu i velmi nízkoteplotních zdrojů elektrické energie. Tyto velmi nízkoteplotní zdroje dosahují předpokládané teplotní hranice kolem 150 °C, což představuje začátek běžného rozsahu teplot organických Rankinových cyklů (ORC). Mezi absorpční cykly patří například cyklus Kalinův, který je již řadu let známý jako teoreticky výhodný v nízkoteplotních aplikacích výroby elektrické energie, ovšem se značnými nedostatky projevujícími se v praktickém užití. Tyto nedostatky se zdají být částečně odstraněny například použitím jiného pracovního média v absorpčním cyklu. Tato diplomová práce se věnuje právě využití vodního roztoku bromidu lithného (H_2O-LiBr) v absorpčním produkčním cyklu (APC), který v teoretické rovině slibuje dobré termodynamické vlastnosti. Technologie absorpce je již dlouho známa z chladicího průmyslu a publikace různých autorů potvrzují možnost implementace těchto postupů k výrobě elektrické energie. Tato práce navazuje na předešlé zdroje výzkumu APC a předkládá metodiku návrhu komponent jednotlivých částí pro aplikaci ve výrobě elektrické energie. Metodika návrhu je pak následována samotnou stavbou zařízení, která je v čase psaní této práce v průběhu. Experimentální zařízení APC předpokládá zdroje tepla z nadřazeného organického Rankinova cyklu (ORC) o teplotě 90 °C a přenášeného tepelného výkonu 20 kW. Expandér, který je vyráběn aditivním 3D tiskem z plastu předpokládá výkon necelých 0.5 kW. Navzdory malému výkonu je díky exergetické účinnosti a dostatečně velkému objemovému toku dosahováno vyšší účinnosti expandéru. V experimentálních podmínkách je zařízení značně naddimenzováno z důvodu prakticky neověřených procesů a nejistot v chování média. Práce předkládá termodynamický model cyklu, metodiku návrhu a praktické provedení konstrukce. Toto je nutným a prvním krokem k dalšímu výzkumu na zařízení, které po absolvování prvotní fáze ověření konceptu může v budoucích pracích pokračovat optimalizací velikosti zařízení či studií komerční proveditelnosti.

Klíčová slova: APC, absorpční produkční cyklus, návrh absorpčního zařízení, nízkoteplotní zdroj tepla, mikrogenerace, decentralizovaná energetika, odpadní teplo

Acknowledgements

The author is grateful for the team at the University Centre for Energy Efficient Buildings, that was crucial for the initiation and completion of the project. This namely concerns the supervisor Ing. V. Novotný and colleagues Bc. J. Špale, Ing. J. Pavličko, and others. Similarly, thanks are reserved for Czech Technical University for the deep and thorough knowledge received. Last, but not the least, the ultimate gratitude is saved to the author's family that has always provided love, trust and support for things achieved and to-be achieved.

Dávid Juraj Szücs, Prague, May 2019

Contents

List of Figures

List of Tables

Nomenclature

Abbreviations

ACC	Absorption cooling cycle
APC	Absorption power cycle
CCP	Combined cooling and power
CHP	Combined heat and power
CTU	Czech Technical University
DC	Dry cooler
GDP	Gross domestic product
HX	Heat exchanger
MC	Moisture content
NPSH	Net positive suction head
NPT	National pipe thread
ORC	Organic Rankine cycle
PCM	Phase change material
SLS	Selective laser sintering
T-CO_2	Transcritical CO_2 cycle
TEG	Thermoelectric generator
TFC	Trilateral flash cycle
TTD	Terminal temperature difference
UCEEB	University Centre for Energy Efficient Buildings

Symbols

α	Conductive heat transfer coefficient	$kW/(m^2\,K)$
Δp	Pressure difference	bar
δ	Film thickness	m
$\dot{m}$	Mass flow	kg/s
$\dot{Q}$	Heat flow	kW
$\dot{q}$	Heat flux	kW/m^2
$\dot{V}$	Volumetric flow	m^3/s
η	Efficiency	

Γ	Mass flow per lenght	$kg/s \cdot m$
λ	Darcy friction factor	
$\mathfrak{D}$	Diffusivity	m^2/s
μ	Dynamic viscosity	$Pa\,s$
ρ	Density	kg/m^3
σ	Surface tension	N/m
ξ	mass fraction of water in solution (if not specified otherwise)	
ζ	Local pressure loss coefficient	
c	concentration)	
d_h	Characteristic diameter	m
e	Exergy	kJ/kg
h	Specific enthalpy	kJ/kg
h_{fg}	Difference in enthalpy between sat. liquid and sat. vapour	kJ/kg
j	Mass flux	$kg/s \cdot m$
k	Thermal conductivity	$kW/(m\,K)$
k_l	Mass transfer coefficient	m/s
l	Length	m
n	number)	
Nu	Nusselt number)	
P	Power	kW
p	Pressure	bar
Pr	Prandtl number)	
R	Surface area	m^2
R	Thermal resistance	K/kW
Re	Reynolds number)	
s	Entropy	kJ/kgK
T	Temperature	°C
W	Power output/input	kW
w	Velocity	m/s
x	Vapour quality	
LHV	Lower heating value	MJ/kg

Subscripts

0	Ambient conditions
$1^{st}law$	Related to 1^{st} law efficiency
$boil$	boiling
bu	bundle
cf	Cooling fluid

cw	Cooling water
des	recuperator
exp	Expander
ext	External
f	friction
h	height
hp	High pressure
hs	Heat source
i	Element i; inner
ie	Isentropic
in	Input/inlet
l	liquid
lp	Low pressure
net	Net
o	outer
out	Output/outlet
p	Pump
rec	recuperator
rej	Rejected
sec	section
sh	shell
$surf$	surface
the	theoretical
tot	total
v	vapour
wf	working fluid

1

Introduction

Energy security is one of the most important goals of many countries. It is not only an existential requirement for society as a whole, but it is also a basis for the development of industries, private & public sector, infrastructure and services. Because of this, it is necessary to provide a secure, reliable and financially affordable source of energy. Demand and use of primary energy resources follow a global trend in positive economic growth, especially in developing countries. However, this might not be the case of the developed countries that invest in the rationalization of their energy sectors. This leads, in most cases, to a decrease in the usage of the primary energy resources. Such a measure is not solely a result of a sound budgeting, but it also reflects the accords on environmental protection, long-term & short-term health issues and the current geopolitical situation.

Developed countries of the European Union have worked extensively on fulfilling citizens' and companies' energy needs over the past decades. Since 2006, the European Union has succeeded to lower the total consumption of primary energy resources despite the constant increase in the gross domestic product (GDP). These trends, in total numbers on the European level, are depicted in Figure 1.1. One of the largest European programs that has a mission to support this trend is *Europe 2020*. This initiative is Europe's adoption of international accords, e.g. Kyoto agreement for economical and sustainable usage of primary resources. *Europe 2020* has a target of 20 % energy savings by 2020 in comparison to 1990s [12]. In 2018, even more courageous target of 30 % of energy savings by 2030 was set. The ultimate goals of this initiative are higher energy efficiency, lower energy expenditure, lower reliance on energy import and better protection of the environment. Despite the overall decrease in total energy consumption from the year 2006, the 2018 progress report has recorded a slight raise over the past three consecutive years (2014-2017), which makes it more difficult to reach the 2020 goal [11]. Based on this, the European Commission has proposed policies to boost improvements in energy efficiency. These consist of: support of energy efficient renovations, eco design for a variety of products, preparation of National Energy Efficiency Action Plans by EU coun-

tries, introducing smart meters for electricity & gas, or imposing regulation on large companies [13].

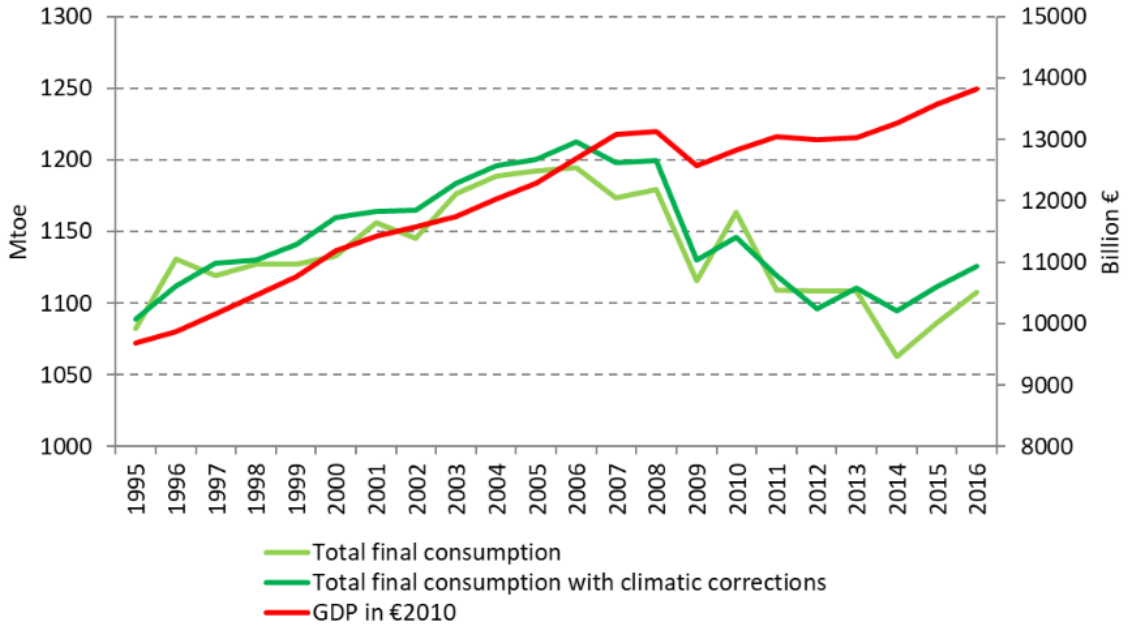

Figure 1.1: Development of total annual energy consumption and GDP in EU28 between years 1995 and 2016 [11]

Direct implications of such measures in the energy industry are an extensive research & development of new and already existing energy systems, combined heat & power production, trigeneration, or decentralization. While the EU has experienced a significant implementation of renewable energy resources, the 2018 EU progress report indicates that the development in thermal power generation has slowed down. Average annual change in *power output to fuel input* ratio of thermal power plants in the EU28 between years 2005 and 2016 accounts for 0,2 % [11]. Improvements in the conventional thermal cycle, i.e. the Rankine cycle, have already been studied extensively for the past decades. These cycles fall into a category of cycles with high-temperature sources. Although, there is not any universal consensus on a precise division of the cycles depending on the temperature of their heat sources, however, Table 1.1 summarizes the most common heat source categorization in the literature.

While recent studies have been concentrating on cycles for low-to-mid-temperature heat sources, represented by organic Rankine cycles (ORC) in most cases, significantly less research is focused on the utilization of low-temperature heat sources. Nevertheless, these low-enthalpy energy systems can apply to an enormous range of applications where such a low-temperature heat source is available. Low-temperature heat sources include naturally occurring heat sources (low-temperature solar collec-

Table 1.1: Categorization of cycles depending on the temperature of their heat sources

Heat source	Temperature range
High-temperature	> 500 °C
Medium-temperature	150 °C $\div$ 500 °C
Low-temperature	(50 °C)$\div$ 150 °C

tors, geothermal fluid or bedrock), waste heat from industries, or heat rejection from various topping power generation cycles. These low-temperature systems become especially interesting in the context of energy efficiency improvements, broadening the diversity of the resources and thus in bringing higher overall energy security. Low-temperature heat sources have already been widely used in space heating applications. If this heating is combined with topping power generation, it is known as combined heating and power (CHP) generation. Besides this most dominant use of low-temperature heat sources, it can also be utilized in a heat-induced cooling application or low-enthalpy power generation. Thus, in the context of better fuel utilization in power systems, this work is concentrating on the possibility of power generation from such a low-temperature heat source.

1.1 Electricity generation from low-temperature heat sources

Traditionally, electricity is generated from high-temperature steam Rankine cycles, which use fossil or nuclear fuel as a heat source, or from Brayton cycle gas turbines. Steam Rankine cycle as well as Brayton cycle, however, are not advantageous in lower temperature applications. This is mainly because, steam, in low-temperature applications and thus is low-pressure state, result in very low density. A low density of vapour is a cause of large volumetric flow and thus of an increase in components size. These properties would mostly result in complex multistage turbines and financially intensive solutions relative to the power produced. It is also expected of the Rankine cycle to have superheated steam in order to avoid droplet condensation at the end of the expansion process. For this reason, most of the power generation systems of a heat source with a temperature lower than 450 °C function on the principle of organic Rankine cycle (ORC) [24]. This cycle is very similar to the traditional Rankine cycle in the layout of the system, although it uses organic fluid instead of steam as a working fluid. The use of the organic fluid eliminates most of

the drawbacks of steam in low-pressure conditions mentioned. Thermo-economical analyses of the ORCs have shown significant advantages over the steam-operated Rankine cycles in the range of medium-temperature heat sources. Over the past decades of research and experiments, ORCs have proven the theoretical models. Thanks to this, many companies and institutions have turned the ORCs to reliable and now commercially available technology in their niche application, i.e. modular decentralized units and heat sources of temperature higher than 150 °C [33]. Forni et al. presented a division of ORC technologies by the type of the organic fluid used into three categories reflecting the suitable temperature ranges (this division can also be found in comparison with other low-temperature power systems in Figure 1.2) [14]:

- ORCs with *silicone* based working fluid (for biomass combustion, concentrated solar energy and other higher temperature heat sources such as moderate gas turbine exhaust or high-grade process waste heat)
- ORCs with *hydrocarbons* based working fluid (for high-temperature geothermal sources or medium-grade waste heat recovery)
- ORC with *fluorinated* organic fluid (for lower temperature geothermal sources and low-grade waste heat recovery, such as engine jacket water or process waste hot water)

The ORC was already also implemented for application of temperatures lower than 150 °C; it has not, however, proved to be economically interesting. Many systems have been proposed to cover this low-temperature range of heat sources, as they have shown potential thermodynamic advantages over the ORCs [26].

Cycles using a zeotropic mixture of fluids are becoming increasingly discussed alternatives. Zeotropic mixtures, thanks to different boiling points of the compounds, do not evaporate/condensate at constant temperature and provide better temperature match with the external fluids in heat exchangers. Such a cycle could be an ORC with a zeotropic organic mixture or better known Kalina cycle that uses a mixture of NH_3-H_2O. Kalina cycle has already been tested in a few commercial applications using a low-temperature heat source, however, showed multiple technical problems connected with coolant's purity and corrosion [46]. Kalina cycle's most suitable temperature range is expected to be between 100 °C and 200 °C (this temperature range is also depicted in Figure 1.2) [50].

Kalina cycles and most of the other cycles using anorganic zeotropic mixtures fall into a category of so-called absorption cycles. Absorption cycles work on a principle of vapour desorption (a release of a substance from a mixture) and absorption (a receive of a substance by a liquid mixture) processes and thus generalize to a range

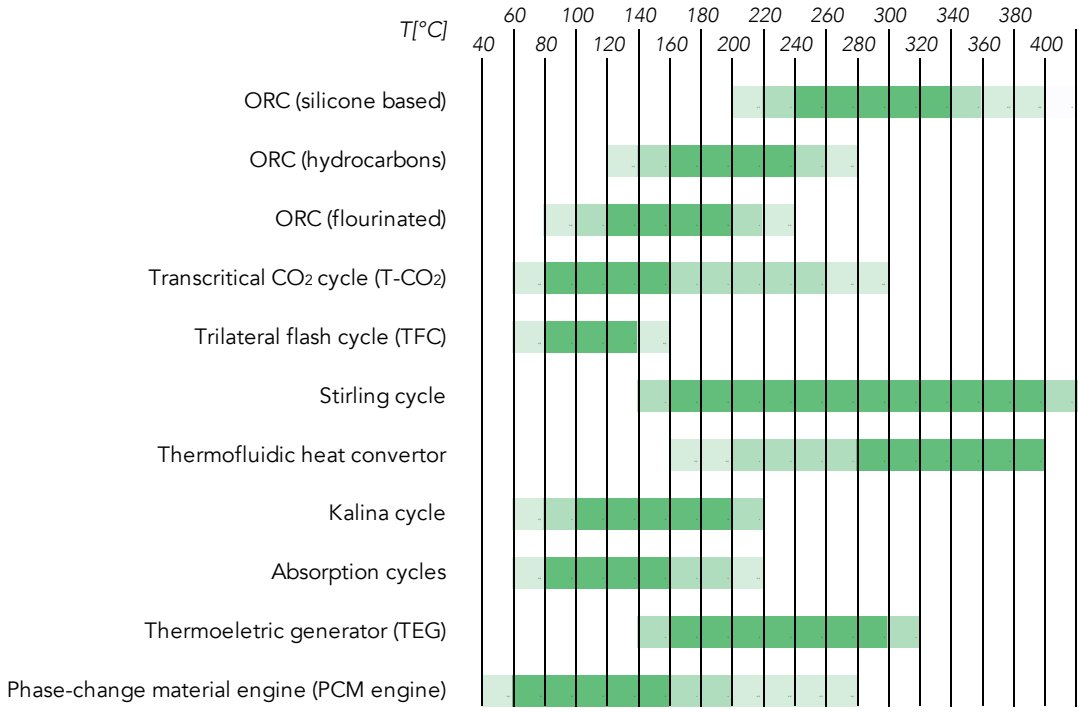

Figure 1.2: List of low-temperature power generation methods with their typical or theoretical range of possible inlet temperatures of the heat source (sources: [14, 50, 26, 4, 17, 41, 20, 19, 36])

of any possible working fluid, which is an absorbate-absorbent pair. These cycles are mostly known for its use in heat-induced cooling applications. Recent studies, however, have shown a possibility of using such a cycle in low-temperature power generation as well. Absorption cycle can work with a mixture of NH_3-H_2O and H_2O-LiBr that are the most common substances used; however, literature provides a variety of other theoretically possible aqueous salt solutions and other pairs. These cycles are theoretically most suitable for a heat source temperature range from 60 °C to 160 °C (range also marked in Figure 1.2) [26]. A detailed description of absorption cooling or power cycles is presented in Section 1.2.

Transcritical CO_2 cycle (T-CO_2) and trilateral flash cycle (TFC) are another low-enthalpy cycles that undergo a non-constant temperature heat addition. The advantage of good temperature match by non-constant temperature heat addition is created by supercritical heat addition in case of T-CO_2 cycle and sensible heat addition with flashing in case of TFC. TFC and T-CO_2 cycles are both only theoretically assumed cycles for low-temperature applications. TFC could be theoretically applied for heat sources of temperature between 80 °C to 140 °C [4, 17], while T-CO_2 cycle could be potentially used for higher temperatures as well [41].

Low-temperature Stirling engine is another discussed system in lower-enthalpy applications. Stirling engine has, on the other hand, already been known, constructed and used for some time; however, it has never spread worldwide due to its technical drawbacks resulting in significant losses. In the case of Stirling engine, the gas is intermittently compressed and expanded while heat is added to the system isothermally in an ideal case. Stirling engine supposedly requires a source of a higher temperature than TFC, T-CO_2, or absorption cycle, and its range of temperatures is somewhat similar to the ones of ORCs) [36].
Thermofluidic oscillators are working on a similar principle of a fluid intermittence between a cold and a hot end as in Stirling engines, however the fluid works in two phases (mostly liquid-vapour organic medium). Thermofluidic oscillators are being practically tested in low-temperature applications as self-sustained pumps; however, their application for power generation (thermofluidic heat converter) has been only theoretically discussed to be suitable in the high-temperature end of the ORC range [20]. Alternatively, also phase-change material (PCM) engines were theoretically discussed to be able to generate electricity from low-temperature source by expansion/compression during solidifying/liquifying of the material [19]. Temperature ranges of the heat source of all of these five power generation systems described in the paragraph are as well depicted in Figure 1.2.
In addition to all the thermal cycles mentioned, there are also systems that transform energy from heat to electricity directly. For low-temperature applications, it is a thermoelectric generator (TEG) that uses a Seebeck effect to generate electricity. TEGs can be applicable for heat source of the temperature of 150 °C or higher, and its typical range is also shown in Figure 1.2 [19, 23].
Absorption cycles seem to be applicable to one of the lowest temperature ranges. Although absorption cycles lack practical use in power generation, they have been already widely used in the cooling application. Thanks to this, the absorption principle and the associated technology are mature, tested and well functional. In order to progress in knowledge of this perspective option, this thesis is devoted to the study and application of an absorption power cycle (APC).

1.2 Utilization of absorption cycles

Absorption principle is mostly known for low-temperature applications in refrigeration and cooling. Absorption cooling cycles represent the main category of chillers known as thermally activated chillers. These cooling cycles have been already successfully used in full commercial applications recuperating low-temperature heat,

such as industrial waste heat, to cover various cooling needs. The maturity of the development and usage makes this cycle, with certain modifications, also promising for power generation. The ability to recover low-temperature heat makes this type of cycle ideal as the last stage bottoming cycle for energy efficiency enhancement and better overall fuel utilization.

1.2.1 Absorption cooling cycle

Absorption cooling principle has been used for decades, and it was even more widespread before the invention of the compression cooling systems. Compression cooling took the lead in the cooling industry, due to a higher coefficient of performance (COP). Nonetheless, absorption cooling systems have still its niche application as the cooling is thermally activated as opposed to mechanically powered compression systems. Absorption principle works on using the low-temperature heat to power the interaction of the substances of the zeotropic mixture that are is at different concentrations. The interaction is done between coolant and an absorbent that absorbs the coolant's vapours. NH_3-H_2O and H_2O-LiBr are the most known working pairs of the absorption systems. NH_3-H_2O is used mostly for refrigeration, while H_2O-LiBr is more suitable for cooling and air conditioning, as it uses water as a coolant.

Figure 1.3 represents a simplified scheme of an absorption chiller using a zeotropic mixture of NH_3-H_2O. Desorber, in this case, is powered by waste heat from an ORC topping cycle (states 11-12). Heat added in the desorber makes the more volatile substance of the mixture to evaporate, which is, in this case, NH_3. Nevertheless, the boiling point of water is not much lower than the of NH_3, and this fact makes some water to be carried away by NH_3 vapour. Because of this reason, a rectifier is installed downstream on the vapour side to remove most of the remaining water content (a distillation column is also sometimes added at to the desorber exit). After the NH_3 vapour is purified, it is condensed by an external source of cooling water. NH_3 almost pure liquid is then expanded at very low pressure that is maintained by an expansion valve. At very low pressure, evaporation takes places at very low temperature and the system collects the heat needed for the NH_3 to be evaporated from an external fluid (air, water, or other) which creates the desirable chilling/refrigeration effect. The vapour is then absorbed by an NH_3 weak solution that comes from the desorber (states 4-6). Similarly to condensation, absorption process needs to be supported by an external cooling as well in order to be successful. After the NH_3 vapour is absorbed, NH_3 strong solution is pumped back to the desorber where the cycle recommences. For higher efficiency and to subcool the liquid solution before

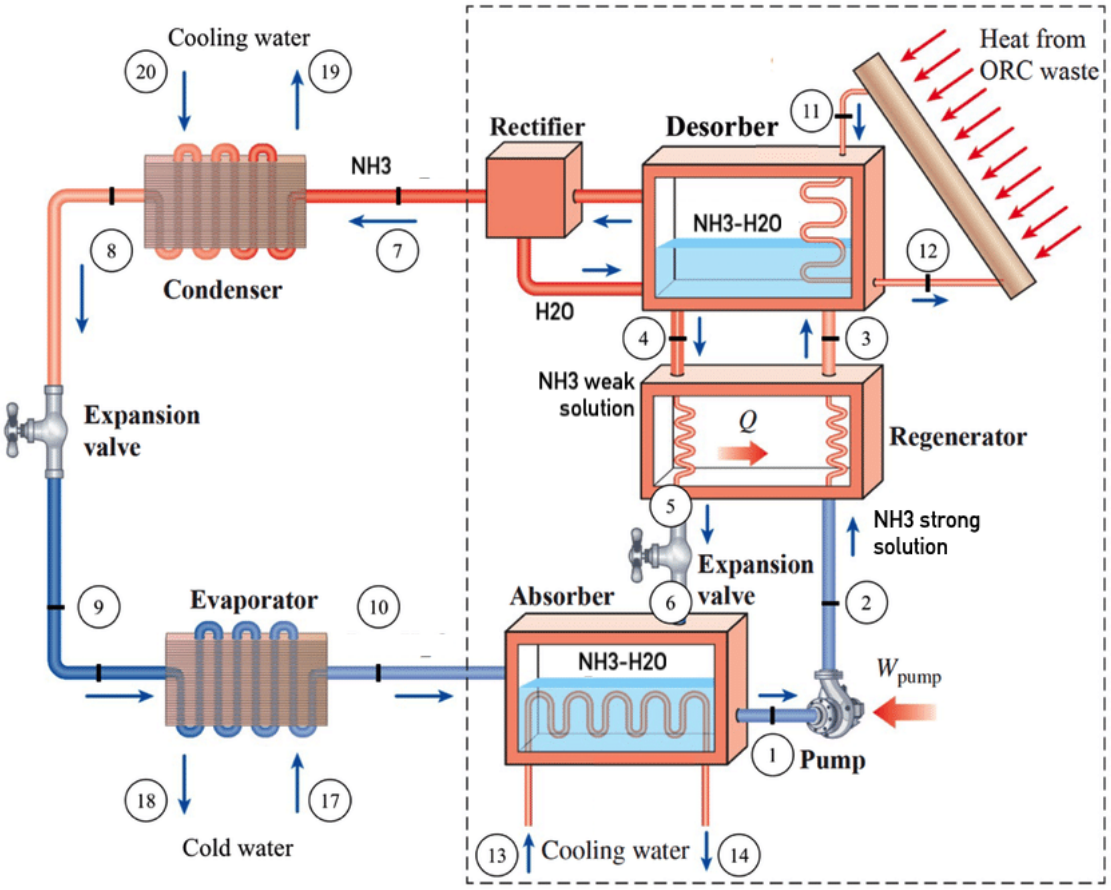

Figure 1.3: A schematic representation of a typical NH_3-H_2O absorption chiller [47]

throttling, a regenerator between a NH_3 weak and strong solution is added here. The cycle using H_2O-LiBr functions similarly to the one of NH_3-H_2O; however, it has an advantage that the rectifier is not in use as LiBr salt is not volatile, so there is no risk of vapour contamination. In case of H_2O-LiBr, where water steam is used as an absorbate (coolant), steam is at a higher temperature than it would be for pure water thanks to the thermodynamic equilibrium between the salt solution and the vapour; the vapour is then effectively superheated. Another advantage of H_2O-LiBr solution is in a greater environmental friendliness of the fluid in comparison to NH_3-H_2O. Additionally, the pressure levels of the H_2O-LiBr system are very low (typically $4 \div 20\,kPa$) so the airtightness might be of a more significant issue [26]. H_2O-LiBr cooling systems cannot be used for refrigeration (temperatures much below 0 °C) as the coolant (pure water) would freeze.

1.2.2 Absorption power cycle

Understanding the absorption system, the question of using the difference between the desorption and absorption pressure to generate power has risen over the years. There have been attempts for such a solution that would be done, in general, by replacing typical cooling components with an expander. The idea of considering absorption principles in power generation creates a category of so-called absorption power cycles (APCs). An APC thus uses a zeotropic solution of coolant and absorbent which interact throughout the process to recover the low-temperature heat. Interaction of the two fluids for power generation has already been studied by some researchers either by totally omitting the cooling effect generation, partially omitting the cooling effect generation or by having the cycle built on a separate principle. First known cycle for solely power generation was proposed by prof. Kalina and this cycle has been modified in various designs under a common name of Kalina cycles [34]. Kalina cycles use a working pair of NH_3-H_2O. Kalina cycles have already been extensively studied by different researchers and have been already employed in several pilot installations showing multiple practical problems in operation [46]. Many derived cycles from the work of prof. Kalina, or those using the same working pair of NH_3-H_2O but a similar approach, proposed absorption power cogeneration with cooling. The example of combined cooling and power cycle (CCP) was developed by Goswami [48], Ericsson et al. [10] or Wang et al. [43]. Working pair of H_2O-LiBr, known for its applications in absorption cooling cycles, has been studied in power generation systems as well, e.g. by Garcia-Hernando et al. [16], or in sole power production as an APC by Novotny at. [29, 26, 30]. APC using H_2O-LiBr is a promising option in low-temperature applications; such as low-enthalpy industrial waste heat, bottoming cycle in organic Rankine cycles (ORCs) or the last stage bottoming cycle in any cascaded thermal system.

2

Absorption Power Cycle Unit

This work presents an approach to a practical application of the extensive theoretical work in the field of APC by Novotny et al. [29, 30]. Following the theoretical introduction to low-temperature power generation possibilities, absorption power cycle using H_2O-LiBr as a working pair is chosen for an experimental proof-of-concept unit. APC using H_2O-LiBr seems to be a promising option in low-temperature applications, such as bottoming cycle in organic Rankine cycle (ORC). An APC unit presented here will be thus using heat from a topping ORC. The modelled unit of an APC will serve as a proof-of-concept device, as after completion, to the best knowledge of the author, it will be the first of its kind. The system is calculated and designed with care to provide the functionality, adaptability and flexibility. These features are especially important as the APC unit will serve as an experimental system with different working modes, or interchangeability of components; and unforeseen complications linked to the lack of previous operational experience of APCs can be expected. It is thus desired that the system is vigorous and resilient enough to cope with possible entanglements.

The APC unit is, at the time of writing the thesis, being constructed by the researchers of *Czech Technical University in Prague* (CTU) at the site of the *University Centre for Energy Efficient Buildings* (UCEEB) in Buštěhrad, Czech Republic. A working group of UCEEB, *Energy Systems of Buildings*, has been, since the commencement of the institute, in intensive research of technologies to provide more cost and fuel efficient, and sustainable energy systems for various decentralized applications. The working group has put a particular interest in the development of modular ORC plants. These ORC plants are designed as combined heat and power plants with a predominant generation of heat. This thesis is a part of the initiative to research and apply improvements on total power to fuel input ratio of such an ORC system.

This chapter, in its Section 2.1, presents a specification of the heat source used, while Section 2.2 summarizes the given and expected entry values to the APC system. A thermodynamic model is presented in Chapter 3 and design methodology of the

components with the resulting model of the apparatus is in Chapter 4.

2.1 Heat source of the unit

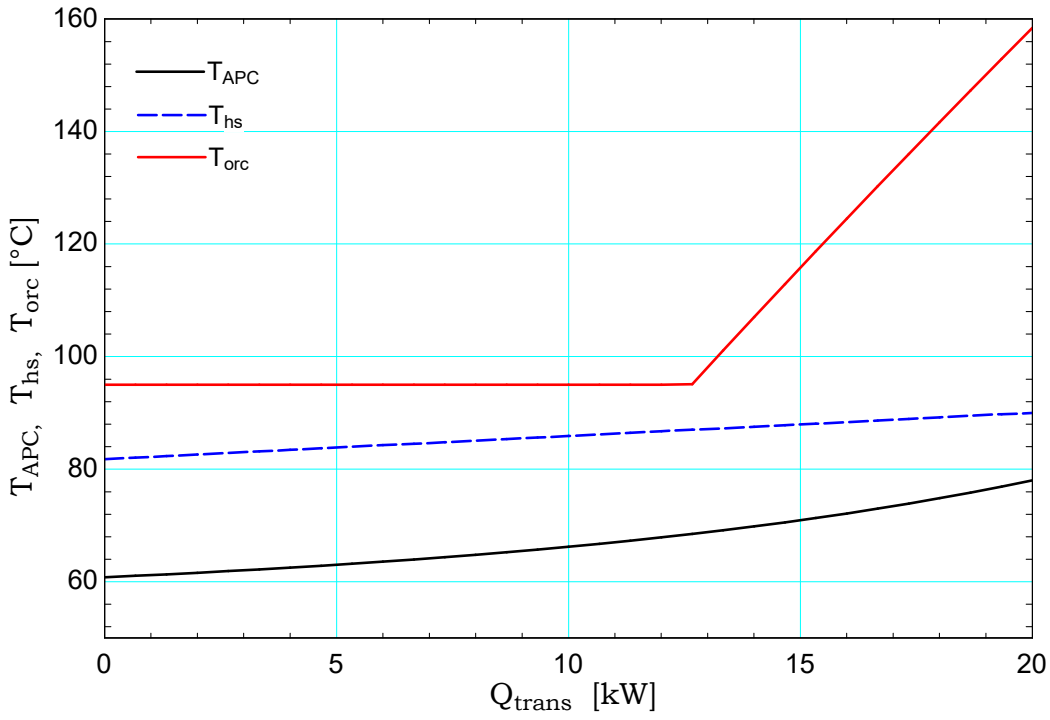

Figure 2.1: Q-T distribution along the heat exchangers in the ORC-APC system

Organic Rankine cycles (ORCs) are especially popular in modular decentralized power generation; however, the thermodynamic properties of most of the organic fluids do not allow turbine exit temperatures to be lowered to similar temperatures as in steam-based Rankine cycles at the same pressures. Due to this reason, desuperheating and condensing in ORCs provide a utilizable heat source for an APC system even in small decentralized units. This experimental unit is set to collect the heat in a condenser of a topping ORC unit operating with MM working fluid.
Figure 2.1 provides a Q-T diagram that represents temperature changes along the longitudinal dimension of the heat exchangers as the heat is transferred. The red line in Figure 2.1 represents a cooling and condensation of the organic fluid in the ORC. The Q-T diagram proves that the organic fluid is expanded to a relatively high expander outlet temperature. This is due to a steep character of isobars in the superheated vapour region. These isobars are fixed to the condensation temperature, which is set by the pinch point temperature limitation of the condenser.

The condensation temperature of the ORC unit Wave 50 is set high, as the heat from the ORC's condenser is used in space heating with an input temperature of 90 °C. The heat from the ORC's condenser is added to an intermediate water loop (blue line) A part of the heat from the hot water is then transported to the APC's desorber (black line) where the working fluid evaporation undergoes a non-constant temperature glide at constant pressure. Water loop was added to accommodate higher flexibility of the heat provided in the condenser and better control of the system, as not all of the ORC's heat rejected is utilized to run the APC, but most of it goes the building's space heating. The ORC cycle developed at the UCEEB has a commercial name Wave 50, as it has a heat output of 50 kW. Although the heat output of the ORC is significant, the heat input into the desorber of the APC unit is limited to 20 kW considering the device size for experimental purposes. Table 2.1 provides a basic specification of the topping ORC unit, such as energy input, energy output, fuel and cycle efficiencies. The overall input parameters of the APC unit are presented in Section 2.2. A picture of one of the modular ORC units Wave 50

Table 2.1: A product sheet of the topping ORC unit Wave 50 [8]

Fuel	Wooden chips (max. 40 % MC)	
Expected LHV of the fuel	11	MJ/kg
Energy in fuel	67	kW
Energy input to the ORC	55	kW
Boiler losses	12	kW
Turbine power output	3.1	kW
Energy in heating fluid	50	kW
Cooling fluid	Water of the heating circuit	
Cooling water exit temperature	90 ÷ 95	°C
Net power output	2.0	kW
Net electric efficiency	3.0	%
Net CHP efficiency	77.6	%

in the laboratories of UCEEB CTU is presented in Figure 2.2.

Figure 2.2: A picture of the 50 kW ORC unit, Wave 50 in laboratories of UCEEB, CTU [40]

2.2 Boundary conditions & performance expectations

A small scale experimental APC unit with an energy input of 20 kW is to be introduced. The APC unit will use and test the applicability of a plastic 3D printed turbine that was developed by the researchers of the UCEEB CTU [29, 37]. This turbine is, under experimental conditions, designed to produce approximately 0.4 kW of electrical power.

Concentrations of the solution in rich LiBr solution branch and weak LiBr solution branch were chosen to respect the recommended concentration difference in the literature as mentioned earlier. Design concentrations in LiBr rich solution and LiBr weak solution branch are 50 % and 65 % of water mass in total solution weight respectfully.

While absorption cooling/refrigeration cycle requires cooling of both absorber and the condenser, the cooling system in the APC is limited to absorber only. A cooling coil is, however, expected to be installed in the LiBr solution tank for additional cooling of the working fluid if needed. Heat rejection is done by a dry cooling tower

cooled by surrounded air with respect to the climate conditions valid for the location of Buštěhrad, Czech republic. Average humidity and average high temperature were evaluated to secure the functionality of the system in summer. The general requirements and expectation are summarized in Table 2.2.

Table 2.2: A summary of main parameters of the APC system

Heat source	Water circuit from topping ORC		
Inlet temperature of the heat source	T_{hs}	90	°C
Energy input to the APC unit	Q_{in}	20	kW
Working pair	H_2O-LiBr		
Mass concentration of lean solution	ξ_{lean}	35	%LiBr/solution
Mass concentration of rich solution	ξ_{rich}	50	%LiBr/solution
Desgined turbine power output	W_{gross}	0.3÷0.5	kW
Heat sink	Cooling water circuit with dry cooler		
Intet temperature of the cooling water	T_{rej}	30	°C
Max. inlet temperature of air in DC	T_{ext}	25	°C

3

Thermodynamic Model of APC

In this chapter of the thesis, a thermodynamic model of the APC unit is presented. Thermodynamic description of the cycle, methodology and results of energy balances, mass flows, solution concentrations, temperatures, pressures and enthalpies of all of the states are given. Thermodynamic model of the APC unit has been modified and built on the one introduced by Novotny et al. [29]. The thermodynamic model is then followed by the design methodology and the construction strategy presented in Chapter 4.

3.1 Cycle description

Figure 3.1 presents a schematic diagram of an absorption power cycle (APC) as assumed for the theoretical model and later for the construction.
The heat from the topping cycle (hot water intermediate circuit) is added to the system in a component called desorber (states 21 - 23). Desorber is a heat exchanger that functions on the desorption principle. On the working fluid side, LiBr weak solution (from now on "weak solution"), marked light green in Figure 3.1, enters the desorber at state 2 and as the heat is added, water vapour is generated, and the solution gets more concentrated in LiBr at the opposite side of the component. At this point, LiBr rich solution (from now on "rich solution") at state 7, marked dark green in Figure 3.1, and water vapour at state 5, marked blue in Figure 3.1, leave the desorber. The water vapour then flows to the turbine and expands to the lower pressure at state 6. The pressure at the turbine outlet is kept constantly low thanks to the continuous absorption process in a component called absorber. The rich solution from the desorber is led here through a recuperator, where it gives away some of the heat. The rich solution is sprayed through expansion nozzles (state 9) onto the absorber's cooling coils, and as it cools down, the low-pressure vapour is absorbed into the solution. At the end of the absorption process, the water content of the solution rises and liquid leaving the absorber is the lean solution (state 11) that is then pumped back to the desorber through a recuperator that serves as a

preheater.

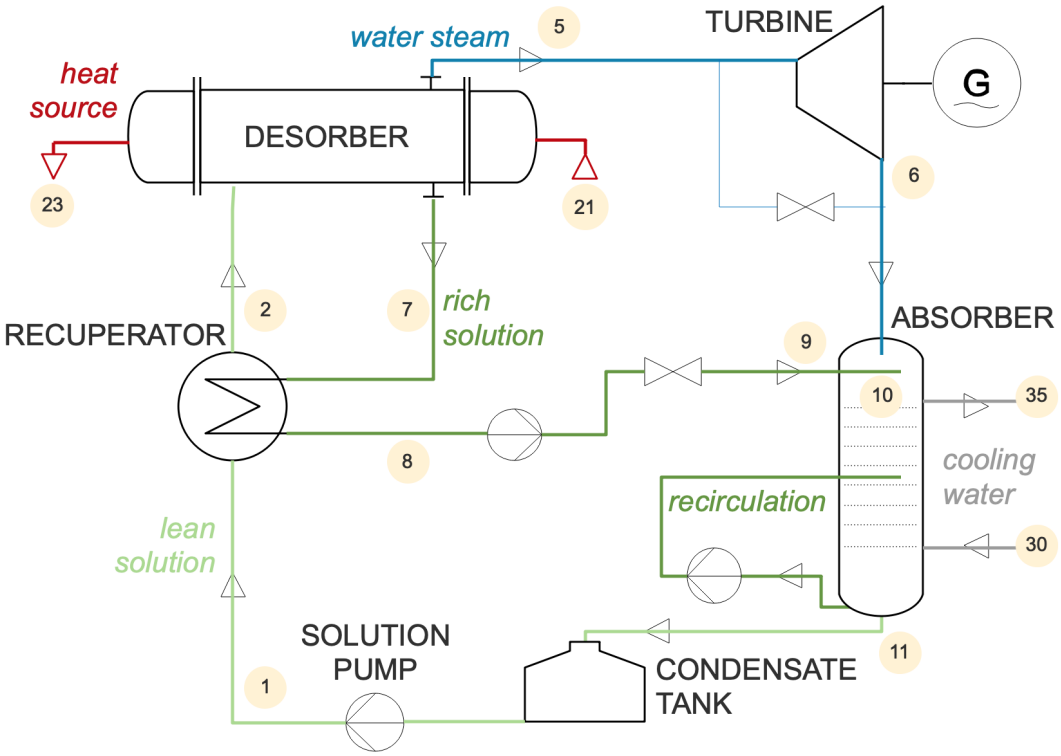

Figure 3.1: Schematic diagram of the APC unit with state numbers referring to the model program

Figure 3.1 also shows some of the additional arrangements to the basic absorption cycle, such as turbine by-pass, recirculation in the absorber, booster pump on rich solution, or the condensate tank. All of these complementary parts will be described in design methodology Section (Chapter 4) as these arrangements are a result of design & construction analysis, but do not play a direct role in the thermodynamic calculation.

Desorber in Figure 3.1 is demonstrated as a single component of a shell and tube arrangement, which is used in the APC unit. However, a plate heat exchanger was also initially considered. A diagram of the cycle with a plate heat exchanger as a desorber is shown in Figure 3.2. Because it is a two-phase mixture at the outlet of the desorber, in this case, a separator needs to be installed downstream. The change in the arrangement of the desorber has no effect on the thermodynamic model of the cycle, further description of the component is presented in chapter 4.

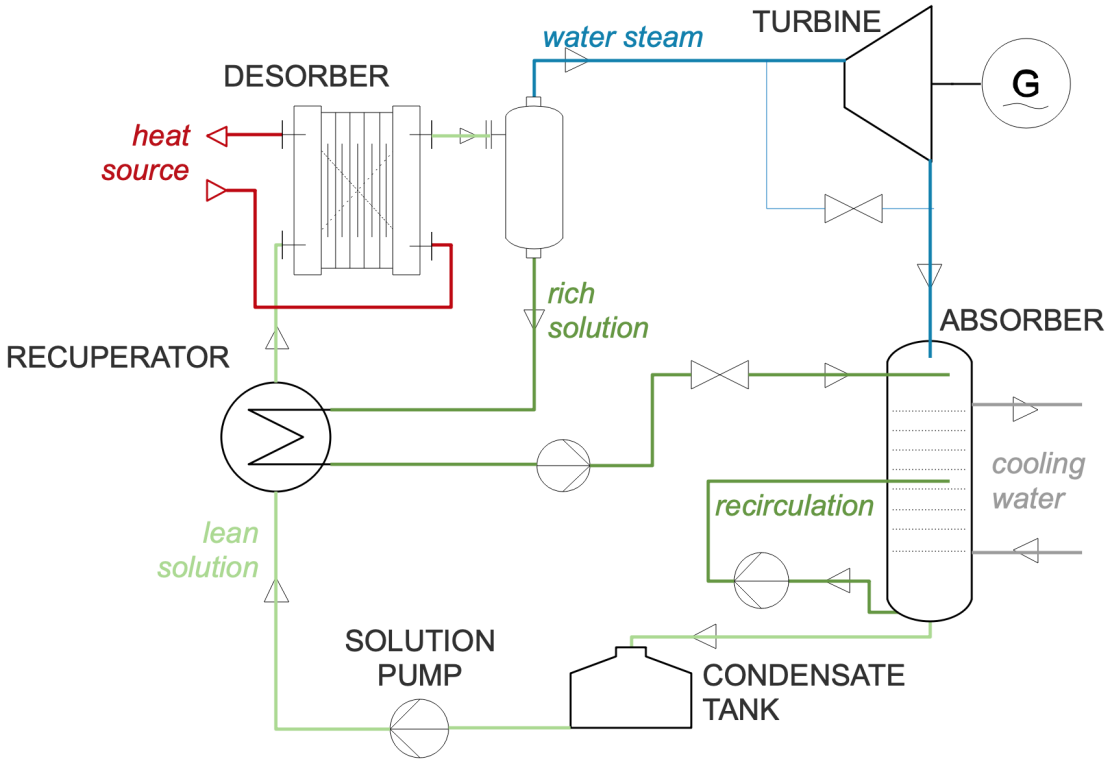

Figure 3.2: Schematic diagram of the APC unit of the plate HX desorber arrangement

3.2 Methods of thermodynamic calculations

3.2.1 Cycle and system assumptions

In the thermodynamic models, counter-flow HX with pinch points limiting the heat transfer are considered. Terminal temperature differences (TTD) are 10 K, 10 K and 5 K for desorber, absorber and recuperator respectively, where the minimum TTD is expected thanks to the suitable and well-optimized design. In case of the desorber and the absorber, where a non-constant temperature evaporation/condensation takes place, pinch point analysis of the temperature differences along the heat exchangers is recommended to properly set the TTD limitations. For this purpose desorber's and absorber's, heat input is divided into 30 elements of the same heat amount transferred. In case of the solution heat exchanger TTD is assumed to be at the cold end of as the cold stream has higher absolute heat capacity.

There are three main setting parameters of the thermodynamic model that had been a result of the cycle optimization. These are working fluid absorber exit temperature (at state 11) $T_{11} = 44.5°C$, LiBr weak solution concentration $\xi_{weak} = 0.65$ (mass

fraction of water in total solution) and LiBr rich solution concentration $\xi_{rich} = 0.5$. Isentropic efficiency of the expander and pump has been preliminarily selected on the conservative values of 40 % and 20 % respectively.

3.2.2 Thermodynamic calculations of components

For purposes of a general thermodynamic modelling, components are described by equations of heat, mass and species conservation. Equation (3.1) presents the most elementary mass balance of a component. Each stream i entering the component takes a positive value of the mass flow $\dot{m}$ while exiting stream takes the negative. Equation (3.1) can be extended to Equation (3.2) which also comprises LiBr mass concentrations of the solution ξ in stream i entering or exiting the component. This is especially required for components dealing with variable solution concentration. Equation (3.3) presents a heat balance of the component consisting of the energy entailed in the entering/exiting stream i, heat input/output j and work output/input k. This Equation follows the convention that heat input to the component is with a positive sign and work done by the component is negative.

$$\sum_i \dot{m}_i = 0 \tag{3.1}$$

$$\sum_i \xi_i \dot{m}_i = 0 \tag{3.2}$$

$$\sum_i h_i \dot{m}_i + \sum_j \dot{Q}_j + \sum_k \dot{W}_k = 0 \tag{3.3}$$

Equation (3.3) is a practical modification of the 1st law of thermodynamics. In components where direct heat exchange is not applicable, such as turbine, the heat flow element is omitted, and the Equation takes its typical form, as shown in Equation (3.4). In this case, only one work output, one stream input and one stream output are considered. The same approach can be applied to the situation of no work flow involved in a component. Equation (3.5) shows the modified version with the consideration of only one heat flow.

$$\dot{W} = \dot{m}_i(h_{i+1} - h_i) \tag{3.4}$$

$$\dot{Q} = \dot{m}_i(h_{i+1} - h_i) \tag{3.5}$$

The thermodynamic model was created in a mathematical modelling program Engineering Equation Solver (EES). EES also includes a property library of different fluids, of which water/steam library following IAPWS formulations were used. Property library of H_2O-LiBr mixture is not included in EES by default, it was, however,

implemented to EES by Hochschule Zittau/Görlitz as a commercial library under a name LibWaLi [21]. State properties, such as enthalpy h, temperature T, pressure p, entropy s, density ρ, Prandtl number Pr, dynamic viscosity μ for water; and additionally LiBr mass fraction ξ for H_2O-LiBr, are calculated using these libraries. An example of an entry enthalpy h_{H_2O} or $h_{\mathrm{H_2O\text{-}LiBr}}$ is demonstrated in Equations (3.6) and (3.7). Remaining state quantities are expressed by exchanging enthalpy in the formulas. If the calculation is done at a saturation state, one of the inputs becomes redundant and needs to be omitted.

$$h_{H_2O} = f(T; p) \tag{3.6}$$

$$h_{\mathrm{H_2O\text{-}LiBr}} = f(T; p; \xi) \tag{3.7}$$

Equation (3.5) is directly applicable to describe the heat transfer in all of the heat exchangers in the system between the fluids. In order for the heat transfer to work, it is necessary to set a reasonable terminal temperature difference (TTD) that reflects a result of a thermo-economical assessment; selected TTDs were described in Chapter 2. Localization of TTDs in the desorber and absorber should result from an analysis in the Q-T diagram of the component as the heat addition/rejection in the zeotropic mixture do not follow a constant-temperature isobaric phase change. For this purpose, heat transferred in these two components is discretized into 30 elements (each marked as i in the equations presented), with an elementary heat transferred $d\dot{Q}_i$ according to the Equation (3.8).

$$d\dot{Q}_i = \frac{\dot{Q}_{in}}{30} \tag{3.8}$$

State properties after each of the 30 elements in the heat exchanger are calculated according to the state function in Equations (3.6) and (3.7). This is especially necessary for the subsequent calculation of the temperatures along the heat addition/rejection process to locate the minimal temperature difference.
Isentropic efficiencies of the turbine (expander) and of the pumps mentioned before are used in first thermodynamic design for enthalpy calculations as stated in Equations (3.9) and (3.10).

$$\eta_{exp} = \frac{h_{exp;in} - h_{exp;out,ie}}{h_{exp;in} - h_{exp;out}} \tag{3.9}$$

$$\eta_p = \frac{h_{p;out} - h_{p;in}}{h_{p;out;ie} - h_{p;in}} \tag{3.10}$$

3.2.3 Methods of cycle evaluation

Both 1^{st} law and 2^{nd} law efficiency (exergetic) analysis are assumed for the cycle. Equations (3.11) and (3.12) present the calculations of gross and net 1^{st} law efficiency of the cycle respectively. While gross 1^{st} law efficiency considers the expected power output of the turbine without the losses on the generator and any own consumption, net 1^{st} law efficiency also takes the own consumption of the pumps and the cooling circuit fan.

$$\eta_{1^{st}law,brut} = \frac{\dot{W}_{turb}}{\dot{Q}_{in}} \tag{3.11}$$

$$\eta_{1^{st}law,net} = \frac{\dot{W}_{turb} - \dot{W}_{pump} - \dot{W}_{cw,pump} - \dot{W}_{fan}}{\dot{Q}_{in}} \tag{3.12}$$

Equation (3.13) states the total specific exergy of the heat source in regard to the dead state 0 (ambient conditions). Equation (3.14) then presents a calculation of net exergy efficiency of the cycle.

$$\Delta e_{hs} = (h_{hs,in} - h_0) - (T_0 + 273.15) \cdot (s_{hs,in} - s_0) \tag{3.13}$$

$$\eta_{ex,net} = \frac{\dot{W}_{turb} - \dot{W}_{pump} - \dot{W}_{cw,pump} - \dot{W}_{fan}}{\dot{m}_{hs} \cdot \Delta e_{hs}} \tag{3.14}$$

3.3 Thermodynamic results

Pursuant to the thermodynamic model of the APC in the EES sofware, the set of equations was solved yielding state parameters at each point of cycle (numbers corresponding to the diagram in Section 3.1). Table 3.1 provides temperature T_i, pressure p_i, mass fraction ξ_i of H_2O in H_2O-LiBr solution, mass flow $\dot{m}_i$, specific enthalpy h_i and specific entropy s_i of each state i. States 1-11 represent the cycle of the working fluid, while states 21-23, 30-35, 41-42 represent heat source fluid, cooling fluid and air in cooling tower respectively. State 3 is used to locate the liquid saturation point which is expected to be present somewhere close to the point 2 of the weak solution entry to the desorber. The sensible heat addition takes place at the beginning of the desorber as the point three is modelled to be slightly after the solution's entry to the desorber, although it might not always be the case and the solution can enter desorber already in two-phase state right after reaching saturation in the recuperator. In the base calculation presented, desorption process is assumed to be slightly shifted from the desorber entry condition, thus state 3 temperature reaches marginally higher value than the one of state 2.

Table 3.1: List of the main resulting states from the thermodynamic model

i	$T_i[°C]$	$p_i[bar]$	$\xi_i[-]$	$\dot{m}_i[kg\,s^{-1}]$	$h_i[kJ/kg]$	$s_i[kJ\,kg^{-1}\,K^{-1}]$
1	44.51	0.146	0.65	0.02603	100.1	0.4483
2	62.42	0.146	0.65	0.02603	147.3	0.5928
3	62.64	0.146	0.65	0.02603	147.9	0.5945
4	79.99	0.146	0.65	0.02603	915	2.836
5	79.99	0.146	1	0.007809	2649	8.167
6	36.14	0.05993	1	0.007809	2596	8.421
7	79.99	0.146	0.5	0.01822	172.1	0.5513
8	49.51	0.146	0.5	0.01822	104.7	0.5513
9	49.51	0.05993	0.5	0.01822	104.7	0.4267
10	59.79	0.05993	0.5058	0.02603	852	2.774
11	44.5	0.05993	0.65	0.02603	100.1	0.4482
21	90	2		0.7236	377.1	1.193
22	83.43	2		0.7236	349.5	1.116
23	83.42	2		0.7236	349.5	1.116
30	30	2		0.2616	125.9	0.4367
35	47.9	2		0.2616	200.7	0.6765
41	20	1		0.2854	46.09	
42	37.9	1.02		0.2854	114.7	

Having the states parameters presented, Table 3.2 summarizes main energy, power, efficiency parameters, as well as the overall compounds' mass flow and the two pressure levels. The sum of the LiBr and water mass flows represent a total mass flow in LiBr weak stream coming from the absorber. The two pressure levels at which the cycle is operating are the admission and emission pressures with respect to the turbine, or so-called high and low pressures with subscripts hp and lp respectively. Figures 3.3, 3.4 and 3.5 represent so-called Q-T diagrams of all of the heat exchanger in the APC that are in contact with the working fluid. Q-T diagrams show temperature changes to the fluid along the surface area of the exchanger as the heat is added. Q-T diagrams serve as an important indicator, especially in cycles with zeotropic mixtures, in analyzing the precision of the pinch point condition and the exergy destruction of the heat exchangers that is proportional to the area in between the temperature curves. The red line in Figure 3.3 displays the cooling of the heating source fluid in the desorber, the blue line in Figure 3.4 illustrates the heating of the cooling fluid in the absorber. The black curves in these Figures 3.3

Table 3.2: List of the main resulting parameters from the thermodynamic model

Total LiBr mass flow	$\dot{m}_{LiBr}$	0,0911	kg/s
Total water mass flow	$\dot{m}_{H_2O}$	0,0169	kg/s
High admission pressure	p_{hp}	14,6	kPa
Low emission pressure	p_{lp}	5,99	kPa
Heat source outlet temperature	$T_{hs,out}$	83,42	°C
Heat transferred in desorber	$\dot{Q}_{in}$	20	kW
Heat transferred in recuperator	$\dot{Q}_{rec}$	1,2	kW
Heat transferred in absorber	$\dot{Q}_{abs}$	19,57	kW
Turbine power output	$\dot{W}_{gross}$	0,4118	kW
Required solution pump power	$\dot{W}_{pump}$	0,86	W
Required cooling water pump power	$\dot{W}_{cw,pump}$	42	W
Required cooling fan power	$\dot{W}_{fan}$	73,3	W
Net Plant power output	$\dot{W}_{net}$	0,2965	kW
1st law efficiency of the cycle	$\eta_{1^{st}law,gross}$	2,06	%
Net 1st law efficiency of the plant	$\eta_{1^{st}law,net}$	1,48	%
Net exergy efficiency of the plant	$\eta_{ex,net}$	1,86	%

and 3.4 stand for the isobaric desorption/absorption process that corresponds to the vapour evaporation and condensation which undergo a constant-temperature heat addition/rejection in traditional single component Rankine cycles. Figure 3.5 shows the cooling of the rich solution (green line) preheating the weak solution (black line) recuperating some heat to higher the efficiency of the cycle and subcool rich solution before throttling.

Temperature entropy (T-s) diagrams are used in conventional pure fluid cycles to visually demonstrate basic energy ratios of the cycle, such as heat input and output, and temperature levels. Application of the second law of thermodynamics enables the heat transferred to/from the cycle to be directly calculated as an area under the curve representing the heat addition/rejection. In cycles using zeotropic mixtures, the heat flow cannot be directly visualized in such a diagram with specific entropy involved as there is different mass flow in each of the cycle's streams. A T-s diagram in absorption cycle can serve, however, as a comparison tool and as a tool to understand and review the absorption or desorption processes, temperature levels, steam quality and equilibrium points. Irreversibilities of the components, such as turbine or pumps, can also be seen in T-s diagrams; these are demonstrated as a rise in entropy in comparison to the ideal process.

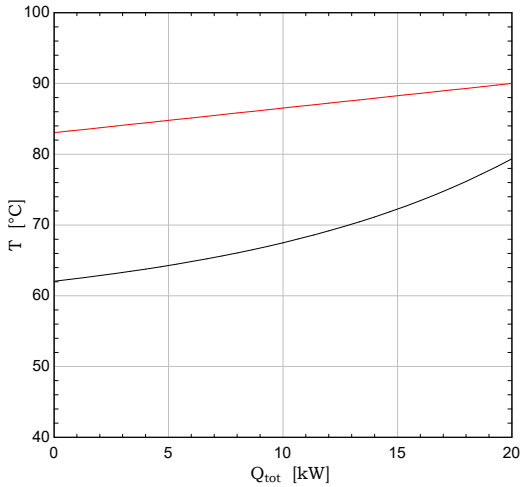

Figure 3.3: Q-T diagram of desorber (red line: heat source fluid, black line: working fluid)

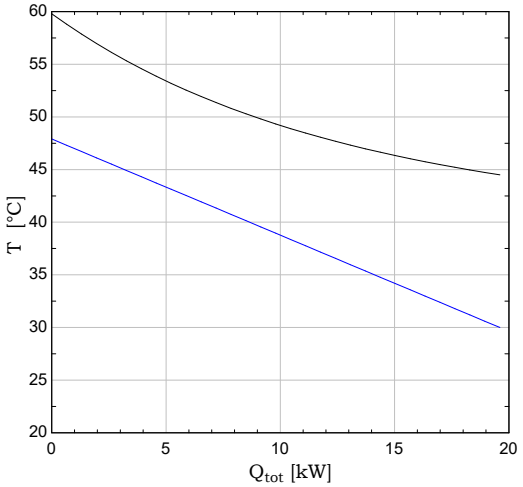

Figure 3.4: Q-T diagram of absorber (black line: working fluid, blue line: cooling fluid)

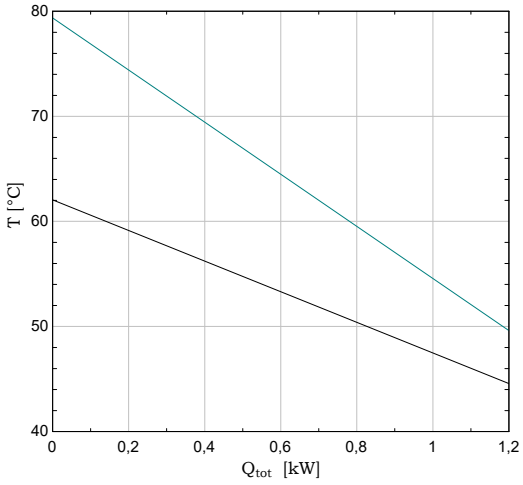

Figure 3.5: Q-T diagram of recuperator (green line: rich solution, black line: weak solution)

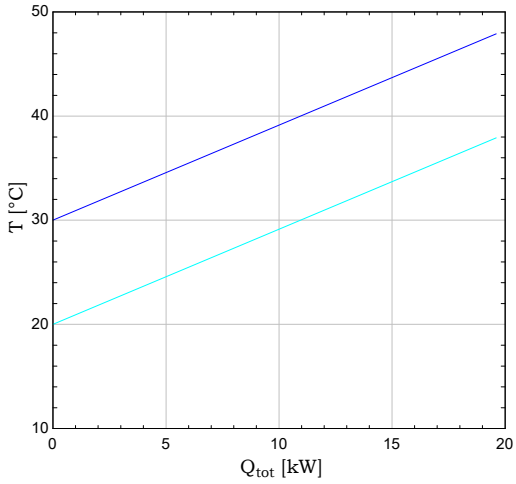

Figure 3.6: Q-T diagram of dry cooling tower (dark blue: cooling fluid, light blue: cooling air)

Figure 3.7 represents a T-s diagram of the modelled APC. Black densely dashed lines represent the saturation curves of pure steam (H_2O, x=0 and H_2O, x=1). Besides the saturation curves which are usually demonstrated in pure fluid cycles contouring the two-phase region, the diagram also shows the low and high-pressure isobars (p_H, p_L) representing the liquid-vapour equilibrium states of the solution. On the left side of the diagram, the isobars begin directly on the pure steam saturation curve, which represents a 100 % water content in H_2O-LiBr solution. Following the isobars, points further away from the steam saturation curve display the equilibrium for the solution of lower water mass fraction (higher LiBr concentration). State 11 is located

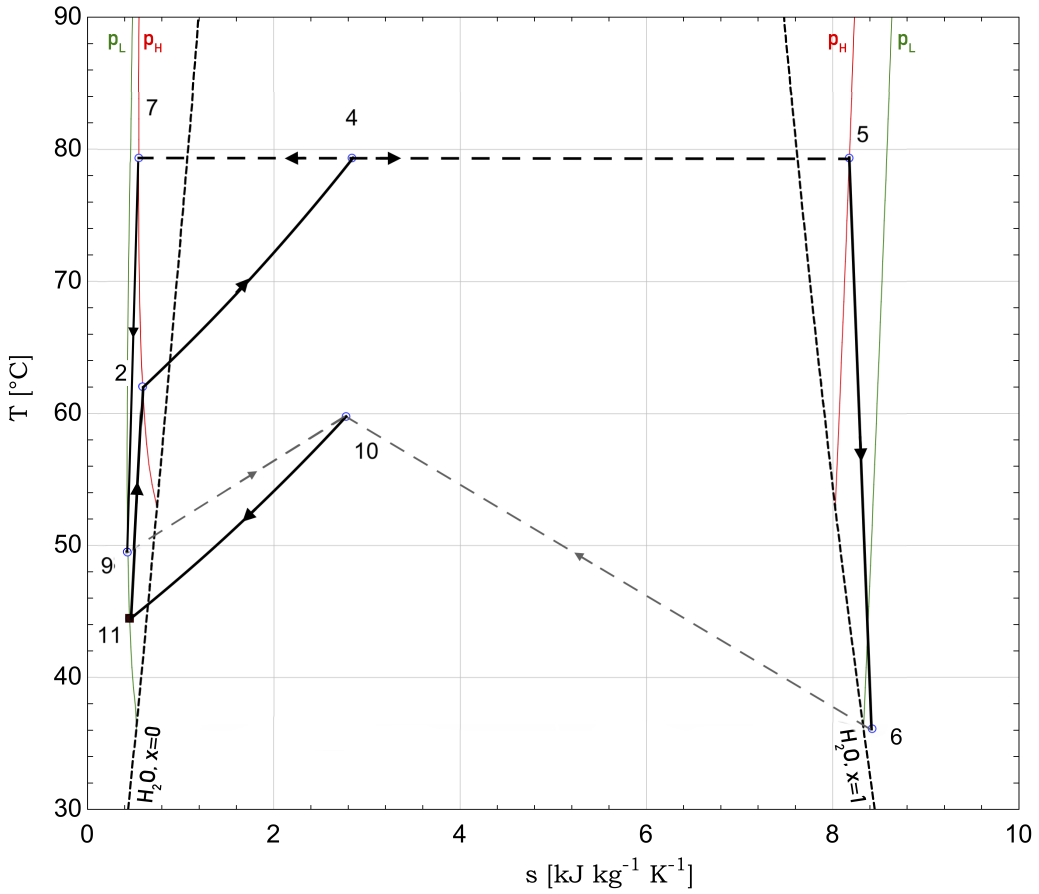

Figure 3.7: Extended T-s diagram of the APC

at low pressure at the end of the absorption process; the fluid's water mass fraction is here at 65 % (LiBr weak solution). The solution is then pumped and preheated to the high-pressure state 2, keeping the same concentration. Process 2-4 depicts an isobaric heat addition in the desorber, which is clearly not isothermic as it is the case in pure fluid cycles. State 4 represents the two-phase character of the fluid at the end of the desorption process. In case of a plate-and-frame desorber, the fluid leaves the desorber at state 4 characterized by a two-phase mixture. The plate heat exchanger would be followed by a separator where vapour (state 5) and liquid (state 7) would be separated. In case of the shell-and-tube desorber, vapour and liquid streams are already the outlets by the principle of process and state 4 presents only an abstract transition point. In any case, water released from the working fluid leaves a LiBr rich solution at the state 7 at the high-pressure liquid equilibrium curve. On the right side of the diagram, saturated vapour-solution equilibrium curves for high and low pressures can be similarly found. The character of the equilibrium curves leaves the vapour at the state 5, after the desorption process, in the superheated

state. This is one of the main differences in comparison to pure fluid cycles which would require an additional superheater for the vapour to get to this state. The superheated vapour is then to be expanded in a turbine to the low-pressure state 6 close to the saturation point keeping the steam in dry-steam conditions. Steam is then mixed (state 10) and absorbed by the LiBr strong solution coming from the desorber (state 9), and with the heat being rejected to the external heat sink (change 10-11), a resulted LiBr weak solution leaves the absorber at the state 11, from where the cycle recommences.

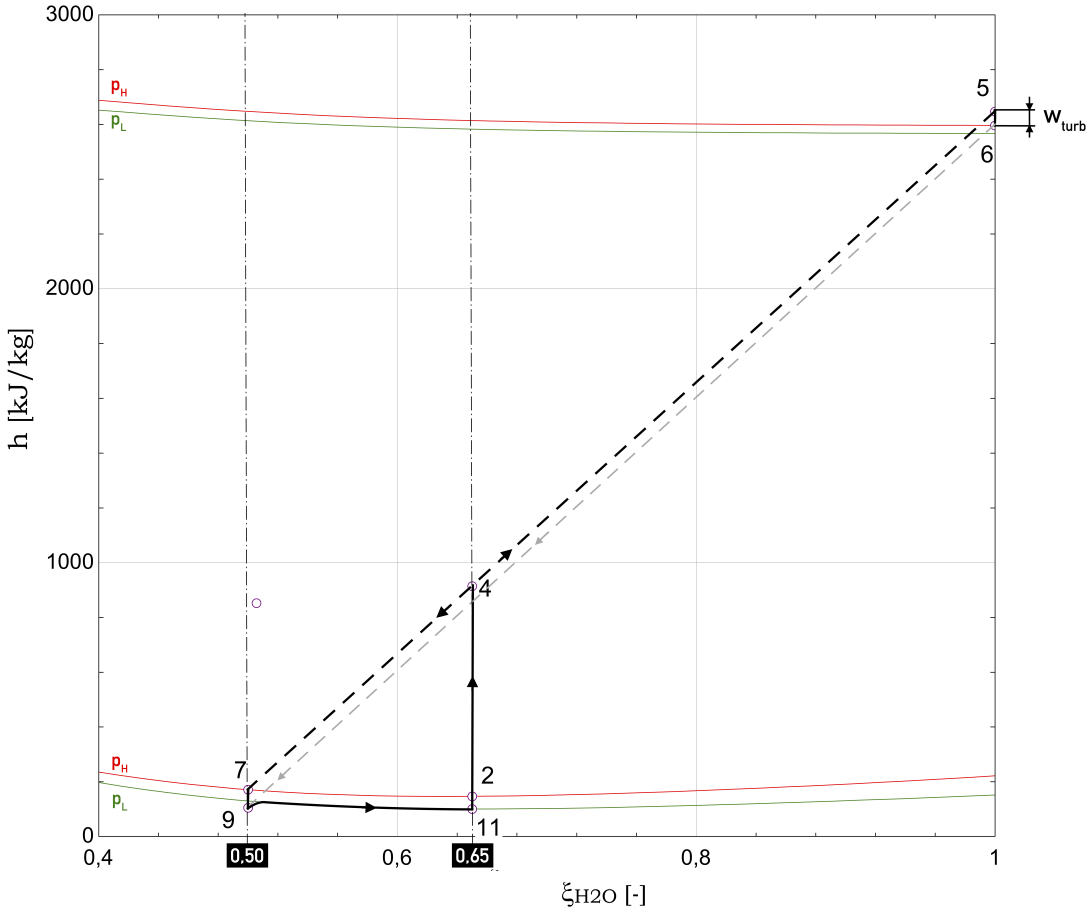

Figure 3.8: Enthalpy - mass fraction diagram of the APC

It is common to depict absorption cooling cycles in enthalpy mass fraction (h-ξ) diagrams to show better a visual understanding of the energy ratios, especially concerning the amount of heat removed from the surrounding to create the cooling effect. Figure 3.8 represent a such h-ξ diagram of the APC with a specific turbine power w_{turb} demonstrated on the left side of the diagram at $\xi = 1$ (100 % water mass fraction). The two other mass fraction levels are depicted by the vertical lines of ξ_{H_2O} of 0.50 (LiBr strong solution) and 0.65 (LiBr weak solution).

4

Design of Experimental APC Unit

This section describes a theoretical methodology and the strategy of the designing of each component and the device as a whole. A design methodology is based on the thermodynamic results of the cycle which serve as an input for sizing calculation and as a specifier of the boundary conditions. The methodology is followed by the design results, which represent a summary of the chosen construction accompanied with the technical drawings of the components in the appendices.

4.1 Design methodology of components

4.1.1 Heat exchangers

The best thermodynamic benefit for low-enthalpy heat recovery would be obtained with strictly counter-flow one-pass heat exchangers (typically flat plate exchangers, possibly membrane and mini/microchannel). A separator would then follow the heat exchanger. Such a system with a plate heat exchanger accompanied by a separator was already depicted in Figure 3.2. To minimize the risk of operation failure, an option of a shell & tube arrangement for two-phase flow heat exchangers is chosen for this project. The components are following a methodology of heat exchangers in standard absorption chillers, modified to fulfill the operating conditions of an experimental absorption power cycle unit. This shell & tube heat exchanger, in case of desorber, serves as separator and, in case of the absorber, as a mixing chamber, in addition to its heat transfer function. The following subsections describe a methodology of design and selections of heat exchangers of the cycle; these include: a desorber (in Subsection 4.1.1.1), absorber (in Section 4.1.1.2) and a recuperator (in Section 4.1.1.3).

4.1.1.1 Desorber

Originally two conceptual configurations were considered. The first one was a plate heat exchanger with a vapour separator downstream and the second one was a

single component heat exchanger of the shell & tube configuration (large volume, LiBr solution in the shell with specified liquid level), which is common to absorption chillers. Uncertainties linked to the actual operation of plate exchangers and the fact that the solution is only partly evaporated and an unknown regime of two-phase flow occurs in the heat exchanger has caused the latter concept to be adapted for this experimental unit. In the calculations, it is still expected that the exchanger will behave in a counter-flow configuration with the goal to gradually increase the concentration of the solution and its temperature from the inlet to outlet. In order to approach this behaviour, the conceptual design of a single passage of both fluids in the exchanger is adopted.

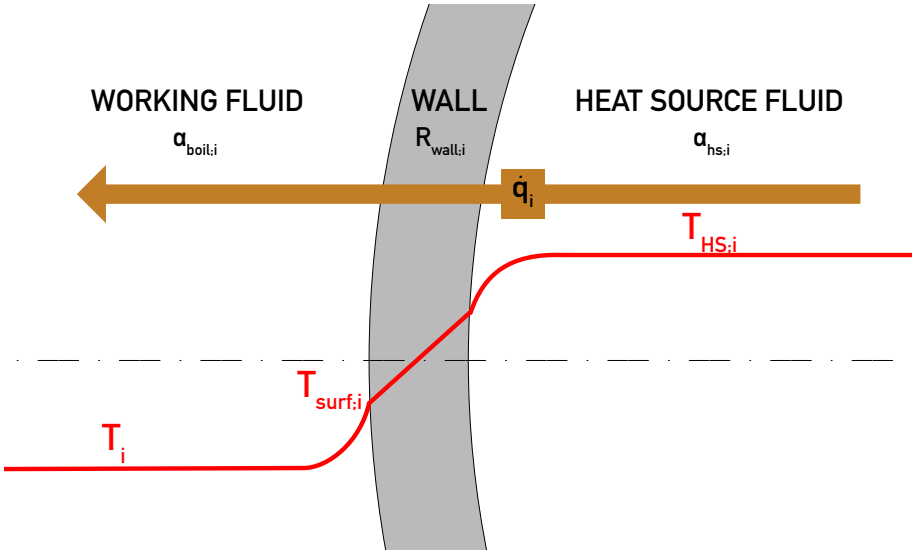

Figure 4.1: Schematic representation of the heat transfer from the heat source fluid into the working fluid in desorber

As described in Section 3.2.2, the exchanger is discretized into 30 elements (each marked as i in the equations presented) of identical elementary heat transferred $d\dot{q}_i$. For each of these elements, heat transfer is analyzed separately. Figure 4.1 represents a schematic temperature profile between the heat source fluid and the working fluid, along the pipe wall's cross-section. Total heat flux of the element is described in Equation (4.1).

$$\dot{q}_i = \frac{T_{hs;i} - T_i}{R_{boil;i} + R_{wall;i} + R_{hs;i}} \tag{4.1}$$

Heat flux $\dot{q}_i$ is defined as a heat flow per area and it is then, with regards to the

element i, presented in Equation (4.2).

$$\dot{q}_i = \frac{d\dot{Q}_i}{A_i} \tag{4.2}$$

In each of these elements, besides all the state properties mentioned in Section 3, the temperature difference between the heating water and the solution, additional properties concerning the fluid mechanics and the values of thermal resistance R_i (as shown in Equation (4.1)) are calculated. These additional parameters are necessary to determine the total heat flux in the element $\dot{Q}_i$ as formulated in Equation (4.1), and finally to calculate the necessary thermal surface area in the element A_i according to the Equation (4.2). This way, necessary thermal surface area is calculated from each of the element i and the sum of the areas yields a total surface area A_{des} of the desorber, expressed in Equation (4.3), needed for the heat transfer under the conditions stated.

$$A_{des} = \sum_{i=1}^{30} A_i \tag{4.3}$$

Heat flux $\dot{q}_i$ in the Equation (4.1) cannot be calculated before the thermal resistances R_i for each element i are determined. The thermal resistance of the tube wall (which is assumed to be stainless) $R_{wall,i}$ is calculated as a fraction of the wall's thickness t_{wall} and the thermal conductivity of the material k_{wall}, shown in Equation (4.5). Equations (4.4) and (4.6) represent calculations of thermal resistance on the side of working fluid and heating fluid, respectively; these are determined by the inverse values of convective heat transfer coefficients α. Heating fluid is located inside the tubes, thus, a basic heat transfer formula would be relative to the area on the inside diameter d_i. In order to have the overall heat transfer relative to the calculated outside surface area, the thermal resistance of the heating fluid in Equation (4.6) is modified by the ratio of outside and inside diameters d_o, d_i. The radial effect is neglected in the calculation of thermal resistance of the wall, as it is assumed to be very small.

$$R_{boil,i} = \frac{1}{\alpha_{boil,i}} \tag{4.4}$$

$$R_{wall,i} = \frac{t_{wall}}{k_{wall}} \tag{4.5}$$

$$R_{hs,i} = \frac{1}{\alpha_{hs,i}} \frac{d_o}{d_i} \tag{4.6}$$

The convective heat transfer coefficient α_{hs_i} on the heating fluid side is calculated from a definition of the Nusselt number presented in Equation (4.7). Here, d_h is a

characteristic length which, in this case, is equal to the inner diameter of the tube d_i.

$$Nu_{hs,i} = \frac{d_h \alpha_{hs,i}}{k_{hs,i}} \tag{4.7}$$

Gnielinski correlation (Equation (4.8)) is a common method of calculation the Nusselt number for turbulent flow, thus, it was chosen to determine the Nusselt number of the heating fluid. In Equation (4.8), $f_{coef;i}$ is called a Darcy friction factor and is obtained from the Petukhov correlation expressed in Equation (4.9). Friction factor could be alternatively obtained from the Moody diagram. Reynolds number $Re_{hs,i}$ in the Equations (4.8) (4.9) is expressed by a common formula modified by the division of the heating fluid mass flow by a number of parallel tubes n_tube in the desorber (Equation (4.10)). Characteristic length d_h is similarly equal to the inner diameter of the tube d_i.

$$Nu_{hs,i} = \frac{f_{coef,i}}{8}(Re_{hs,i} - 1000)\frac{Pr_{hs,i}}{1 + 12.7\left(\frac{f_{coef,i}}{8}\right)^{0,5}\left(Pr_{hs,i}^{0.67} - 1\right)} \tag{4.8}$$

$$f_{coef,i} = \left[0.79\, ln(Re_{hs,i}) - 1.64\right]^{-2} \tag{4.9}$$

$$Re_{hs,i} = \frac{\dot{m}_{hs}}{n_{tube}\frac{\pi d_i^2}{4}}\frac{d_h}{\mu_{hs,i}} \tag{4.10}$$

As it is more complex to determine direct Nusselt number on the side of the H_2O-LiBr solution, heat transfer coefficient $\alpha_{boil,i}$ is derived from a formula of convective heat transfer expressed in Equation (4.11).

$$\dot{q}_i = \alpha_{boil,i}\left(T_{surf,i} - T_i\right) \tag{4.11}$$

By presenting the Equation (4.11), another unknown variable, surface temperature $T_{surf,i}$, is added to the system. Boiling mechanism on the side of the working fluid needs to be described by an additional equation. Working fluid is at a saturated and nearly quiescent (minimal velocity of flow) state along the entire exchanger and boiling and evaporation take place at the submerged conditions in the liquid. Pool boiling correlation shown in Equation (4.12) is, thus, adopted from Charters et al. to obtain the heat flux $\dot{q}_i$ iteratively with respect to the temperature difference between a hot wall surface and working fluid and then used to obtain the boiling heat transfer coefficient $\alpha_{boil;i}$ [6].

$$\frac{c_{p,l,i}}{h_{fg,i}}(T_{surf,i} - T_i) = 0.0136\left\{\frac{\dot{q}_i \cdot 10^{-3}}{\mu_{l,i} h_{fg,i}}\left[\frac{\sigma_{\mathrm{H_2O\text{-}LiBr}}}{9.81(\rho_{l,i} - \rho_{v,i})}\right]^{0.5}\right\}^{0.34} Pr_{l,i}^{0,85} \tag{4.12}$$

Here, $c_{p,l}$ is specific heat capacity of the saturated liquid, h_{fg} is latent heat of evaporation, $\sigma_{\mathrm{H_2O\text{-}LiBr}}$ is surface tension of the solution's liquid-vapour interface and $(\rho_l - \rho_v)$ is a density difference between the liquid and vapour phase (the rest of the more common variables are described in list of abbreviations and acronyms of the document).

After the total area needed for the desorption is calculated, it is divided into a number of tubes selected. Thanks to the design model created, the number of tubes is possible to be selected according to the best thermo-economical optimization. This multi-criteria analysis encompasses the number of tubes and the diameter of the tubes, which both affect the overall length of the exchanger, and thus on the price.

Desorption processes are prevalent not only in the cooling systems but mostly in different industrial and chemical processing utilities. In such industrial processes, kettle reboilers are usually used for desorption of vapours. Kettle reboilers are a type of shell-and-tube heat exchangers, of which the diameter of the shell is multiplied by a certain factor while keeping the original diameter of the tube bundle. Large shell diameter creates enough space for vapour to be developed. An example of kettle reboiler is presented in Figure 4.2.

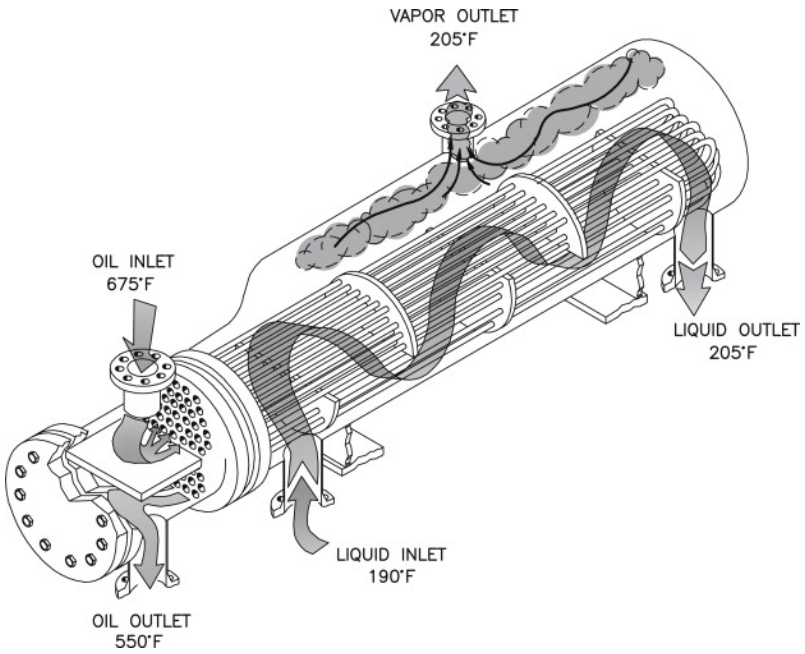

Figure 4.2: Example of a typical kettle reboiler set up [31]

Kettle reboilers are large, complex and, relatively to other alternatives, expensive components. For the application in the APC, some arrangements would need to be necessary to provide a counter-current flow of the fluids and functioning outflow

of the LiBr rich solution. As an alternative to kettle reboiler, simplified version resembling common one-pass shell-and-tube heat exchanger is proposed to reduce the cost and to omit the obstacles of kettle reboilers. Such a shell-and-tube heat exchanger is expected to have the top layers of the tubes omitted to create the space necessary for vapour generation and development. To calculate a necessary free space above the tube bundle, Jacimovic et al. proposed a formula for calculation of a recommended shell to bundle ratio as a function of the heat flux $\dot{q}$ in kW/m^2 (Equation (4.13)) [18].

$$\frac{D_{shell}}{D_{bundle}} = 1 + (0.015 \div 0.025)\,\dot{q} \tag{4.13}$$

4.1.1.2 Absorber

In the case of the absorber, heat and mass analysis is conducted to calculate the size of the absorber. Absorber considered is to be of a shell-and-tube arrangement with cooling water the tubes and the working fluid on the side of the shell. As large surface area is expected for the absorption process, a helical cooling coil with a vertical axis is assumed in order to save as much of the space as possible, to keep a continuous flow of the falling film and to maintain a counter-current set-up of the exchanger for the most efficient heat transfer.
There are two approaches in calculating vapour mass absorbed by a liquid solution which comes from a general mass transfer theory. The first approach is derived from the first Fick's law (Equation (4.14)).

$$j_A = -\rho \mathfrak{D}_{AB} \nabla c \tag{4.14}$$

Where j_A is mass flux $[kg\ s^{-1}\ m^{-1}]$, ρ is density of the liquid, $\mathfrak{D}_{AB}$ is diffusivity of a component A to the solution B and ∇c is concentration gradient.
Two more inputs are added to the Equation (4.14) to reflect the effect of the concentration distribution and contribution of the bulk motion. Implementation and further simplifying of the equation yield the general Equation (4.15) of a H_2O-LiBr falling film. The process of obtaining the formula is described in a publication from García Rivera [15].

$$d\dot{m}_{abs} = -\frac{\mathfrak{D}_l \rho_l}{c_{if}} \nabla c \cdot \vec{n}\ dA \tag{4.15}$$

Where $\dot{m}_{abs}$ is a vapour mass absorbed by the liquid solution, c_{if} is a concentration of the gas near the gas-liquid interface, $\vec{n}$ is the normal vector respecting the geometry of the corresponding falling film system and A is a respected area.

Hafsia et al. presented a calculation model for a falling film absorption process with an introduction of a precise geometry of horizontal cooling water tubes. The model expects three separate subsystems of mass transfer: (i) falling film, (ii) droplet formation and (iii) falling droplet. The most dominant falling film subsystem is described by modifying the Equation (4.16) by introduction of the geometry as shown in Figure 4.3 [3].

$$\dot{m}_{v,\Theta} = -\frac{\mathfrak{D}_l \rho_l}{c} \left.\frac{\partial c}{\partial y}\right|_{y=\delta} (r_e + \delta)\, \Delta\Theta \tag{4.16}$$

Where r_e is outside radius of the cooling tube, δ is the thickness of the film at certain angle Θ. The second approach to describe the vapour absorption is by

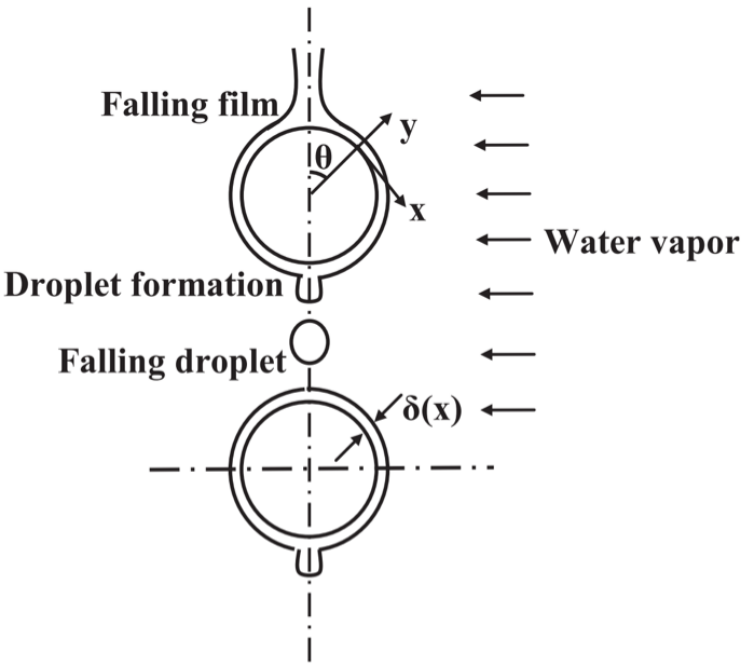

Figure 4.3: The represantation of the basic geometry of the falling film system presented in Hafsia et al. [3]

a simplification defined by a convective mass transfer. This reduction method is described by the Equation (4.17) of the convective transfer that presents an analogy to the Newton's convective heat transfer. In Equation (4.17), k_l is a mass transfer coefficient and ρ_l is liquid density, Δc_{H_2O} is difference in concentration between saturated solution at given temperature and pressure and actual concentration of subcooled solution in the liquid film. Mass transfer coefficient k_l of H_2O-LiBr can vary from $1 \cdot 10^{-5} \div 5 \cdot 10^{-5} m/s$. This mass transfer coefficient is dependant on the solution flow rate per unit of length Γ, which can be calculated additionally in Equation (4.25) [49]. It is assumed, however, that flow rate per unit of lenght will

be in our case a relatively small number a due to this a mass transfer coefficient is chosen from a lower end of the interval.

$$d\dot{m}_{H_2O} = k_l \rho_l \Delta c_{H_2O} dA \tag{4.17}$$

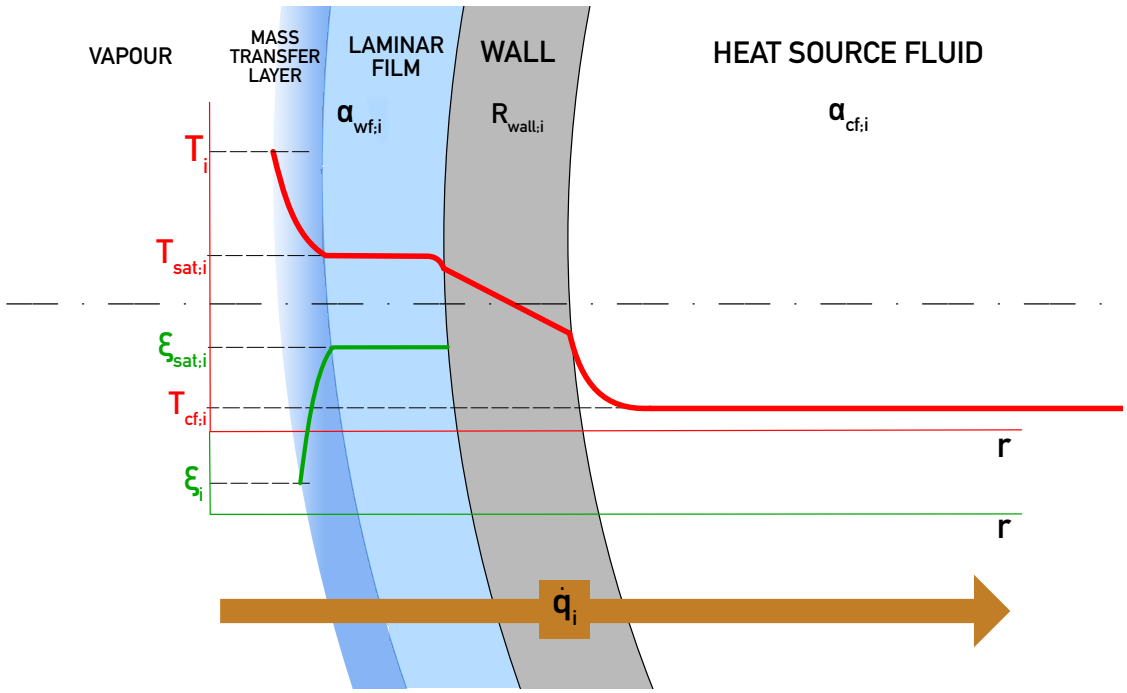

Figure 4.4: Schematic representation of the heat transfer from the falling film into the cooling fluid in the absorber

Experimental works have shown considerable uncertainty in the absorption rate in comparison with the theoretical assumptions. Furthermore, the theoretical analyses of the mass absorption presented have been mostly adapted to the processes typical for the absorption chillers which operate at generally different conditions than the designed APC. APC is expected to work at higher absorption pressure, higher temperatures and altered concentrations than absorption cooling cycle. Therefore a rather simple methodology with subsequent oversizing is chosen. This simplified approach is used in multiple articles, proving practical applicability of the basic mass diffusion principle omitting the necessity of complex and uncertain geometrical transfer models [7, 42, 49, 22]. The design is then based on a convective mass transfer coefficient between the vapour and the liquid solution, as described in equation (4.17). The differential elements of the Equation (4.17) are replaced with a discretized element of a total of 30 elements along the absorber. The modified formula is presented in Equation (4.18) with parameters calculated for each of the

elements, similar to the mentioned calculation method of the desorber process.

$$\dot{m}_{abs,i} = k_l \rho_{l,i} (\xi_{l,sat,i} - \xi_{l,i}) A_i \tag{4.18}$$

The driving force of the absorption process, as described in (4.18), is the difference in water mass fraction at the saturation conditions in the liquid-vapour interface $\xi_{l,i}$ and in the subcooled liquid film $\xi_{l,sat,i}$. Mass fraction of the film $\xi_{l,sat,i}$ is a function of bulk saturation temperature $T_{sat,i}$ which is a result of the heat transfer analysis of the absorption system. Once the required state parameters (liquid density ρ_l, and the mass ratio of the saturated liquid $\xi_{l,sat}$ and of the actual solution in the liquid film ξ_l) are derived from the heat transfer analysis that needs to be run alongside the mass transfer calculation, the Equation (4.18) yields the surface area A_i needed for the design of the absorber. For the ease of the calculation, the heat and mass transfer model in Figure 4.4 is simplified to a mathematical model that expects a uniform temperature along the dimension perpendicular to the surface area for the entire falling film. It is expected that the liquid film that is participating in the mass transfer is spread on all the computed heat transfer area. Equation (4.19) presents an overall formula for calculating an overall heat flux $\dot{q}_i$ between the film and the cooling fluid, from which bulk saturation temperature $T_{l,sat,i}$ can be calculated.

$$\dot{q}_i = \frac{T_{l,sat,i} - T_{cf,i}}{R_{wf,i} + R_{wall,i} + R_{cf,i}} \tag{4.19}$$

Heat flux $\dot{q}_i$ in the absorber is determined the same way as it was in case of the desorber, presented in Equation (4.2) as a discretized heat rejected per area calculated. Thermal resistance of the working fluid $R_{wf,i}$, the tube wall $R_{wall,i}$, and of the cooling fluid $R_{cf,i}$ are calculated similarly as in case of the desorber and are presented in Equations (4.20), (4.21) and (4.22).

$$R_{wf,i} = \frac{1}{\alpha_{wf,i}} \tag{4.20}$$

$$R_{wall,i} = \frac{t_{wall}}{k_{wall}} \tag{4.21}$$

$$R_{cf,i} = \frac{1}{\alpha_{cf,i}} \frac{d_o}{d_i} \tag{4.22}$$

The thermal resistance calculation on the side of the working fluid is very complex and experimental data have found large uncertainty and inconsistency of the theoretical models. These models are highly dependant on the geometry of the specific absorber's exchanger, and thus subsequent arrangements covering these un-

certainties need to be applied. One of the correlations to calculate a convective heat transfer coefficient of the falling film of the H_2O-LiBr solution was stated by Shi et al. based on the experimental data of a falling film generator [35]. The correlation is presented in Equation (4.23), where q_i is the element's heat flux, and Re_i is the Reynolds number of the falling film expressed in Equation (4.24). Γ_i is mass flow of the working fluid per circumference of the coil O_{coil}, as shown in (4.25), and $\mu_{l,i}$ is dynamic viscosity of the liquid film.

$$\alpha_{wf,i} = 129.7712\, \xi_{l,i}^{-0.8058}\, q_i^{0.2422}\, Re_i^{-0.0856} \tag{4.23}$$

$$Re_i = \frac{4\Gamma_i}{\mu_{l,i}} \tag{4.24}$$

$$\Gamma_i = \frac{\dot{m}_{l,i}}{2\, O_{coil}} \tag{4.25}$$

Due to the large uncertainties in the distribution of the mass flow, calculation of the mass flow and the condensing vapour, direct calculation of the convection heat transfer coefficient via the correlation in Equation (4.23) can be replaced by an indirect approach. Indirect calculation of the convective heat transfer coefficient $\alpha_{wf,i}$ is done from the overall heat transfer coefficient U_i with known conduction and convection coefficients on the side of the tube and the cooling fluid respectively. Overall heat transfer coefficient is deducted from measurements of temperature differences and mass flows of the cooling and working fluids. This indirect experimental method is used and subsequent resulting convection heat transfer coefficient of the absorbing film $\alpha_{wf,i}$ is taken from the literature and it is assumed to be 2000 W/m^2K [42, 49]. Thermal resistance of the cooling fluid, according to the Equation (4.22), is the inverse of the convective heat transfer coefficient $\alpha_{cf,i}$ that is calculated the same way as in case of the heating water flow inside the tubes of the desorber. Calculation is then done from the formula of the Nusselt number in Equation (4.7), and from the Gnielinski correlation in Equation (4.8). As the cooling tubes of the absorber are in the arrangement of helical coils, the effect of the radial movement of the cooling fluid on the heat transfer can be alternatively considered. Researchers considered modified Gnielinski or Rohsenow correlation and one, used by Yoon et al., is presented in equation (4.26) (the equation is adapted for calculation in each of element i of the absorption process) [49]. In Equation (4.26), $k_{cf,i}$ is a thermal conductivity of the cooling fluid, d_{cf} is the inner diameter of the cooling tubes, while $d_{coil,j}$ is the diameter It is expected that the convective heat transfer deducted from Equation (4.26) would give a slightly greater number than one from Gnielinski correlation, as the radial movement enhances the turbulent flow [32]. Although the latter cor-

relation is presented with an expected better heat transfer coefficient, Gnielinski correlation is used in the calculation, as it has been proven experimentally, and it adds on safety due to its more conservative assumption.

$$\alpha_{cf,i} = 0.023 \frac{k_{cf,i}}{d_{cf}} Re_{cf,i}^{0.8} Pr_{cf,i}^{0.4} \left[1 + 82.4 \left(\frac{d_{cf}}{d_{coil,j}}\right)^3\right] \tag{4.26}$$

As it was described in the heat and mass transfer analysis of the absorber, experimental works demonstrated considerable uncertainty in the absorption process. In order to ensure operation in the case of lower absorption rate or insufficient heat transfer, the surface area is oversized, and a supplementary recirculation of the solution is added. In order to keep as much of the counter-flow principle as possible, to be able to assess the operation of this part as well as to what extent the recirculation improves the process, a second (lower) segment of the cooling coils is added underneath. The second segment is identical in size to the first one designed. Recirculation nozzles are placed into the middle of the entire absorber in between the two cooling coil segments of the same surface area. This modification multiplies the total surface area of the cooling coils needed by a factor of two approximately in comparison to the theoretical model. This enlargement of the area does not only secure the uncertainty of the theoretical mass and heat transfer model, but it also covers the possible conditions of an off-design operation that is present in experimental use.

4.1.1.3 Solution heat exchanger

Solution heat exchanger or so-called recuperator is used to recuperate some of the heat from the rich solution and to preheat the weak solution coming into the desorber. There are no special requirements for the recuperator, only that the pressure drop of the chosen heat exchanger on both sides needs to be considered in pump design. It is assumed that for a small scale one-phase operation, a plate heat exchanger is the most suitable option. Many manufacturers provide a heat exchanger selection tool that for the input values of inlet and outlet temperatures, and heat load, returns a list of the recommended options ordered according to the suitability. Such an interface of an SSP program from SWEP is presented in an example in Figure 4.5 [38].

4.1.2 Expander

A progressive approach is followed as well in the selection and designing of the APC. The APC unit, for a component of such a low power output expected, utilizes an

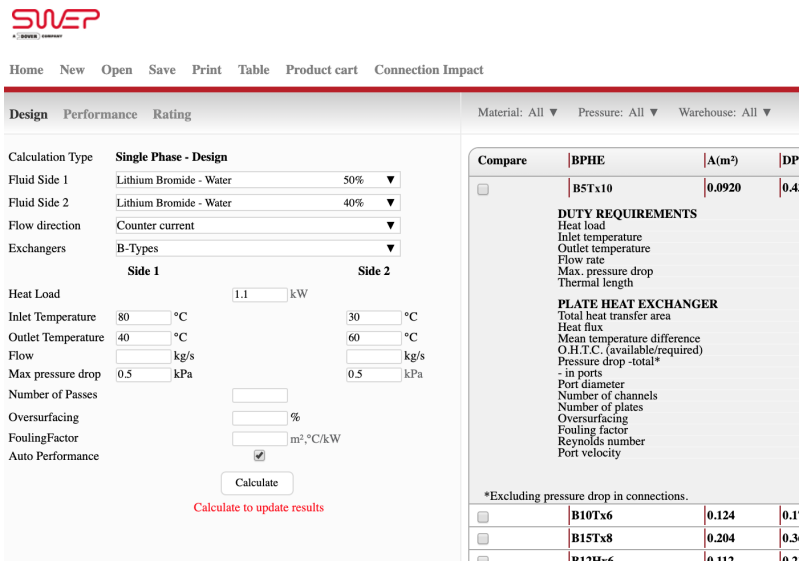

Figure 4.5: Example of the SWEP P interface for plate heat exchanger selection and performance analysis

experimental turboexpander that has been researched and designed by the team at the Faculty of mechanical engineering at CTU in Prague, as well as at UCEEB CTU. The turbine is to be manufactured by a commercial plastic 3D printing technology. The project has a goal to prove and add on the possibility and applicability of such a turboexpander in low power and low-end parameters. The thesis is linked to the works and design of author's colleagues V. Novotný [27, 28], J. Špale [28], D. Suchna [37] and others.

The problem of utilization the expander machines in low power applications is mostly their price that occupies a relatively high portion in cost analysis. The objective of the utilization of 3D printed turboexpanders is to find and implement a low cost, light and reliable alternative that would benefit from a fast manufacturing process and more effortless interchangeability.

An axial-flow turboexpander is assumed to be used as large steam volumetric flows are expected. Rotational speed and mean diameter of the rotor are selected regarding the highest efficiency and to the limitations of the generator. Design and a more thorough description of the turboexpander used are located in the design result section of the document (Section 4.3.4).

4.1.3 Pumps

The main solution pump, crucial for the functioning of the cycle, is to be located at the lowest level of the apparatus. This solution pump enables the liquid solution to be transported from the absorber and the condensate tank up to the desorber,

and at the same time, the pump raises the pressure of the liquid to its desorption operation level. The solution pump needs to provide enough power to overcome the height differences and the pressure loss of the pipelines and the utility components between the absorber and the desorber. The overall pressure difference needed to be overcome by the pump, also known as manometric head, is then calculating as a sum of the differences of pressure caused by friction and local losses Δp_{loss}, total height difference Δp_{head}, and by the difference in operational pressures Δp on both sides of the lean liquid solution (the calculation is presented in Equation (4.27)).

$$\Delta p_{total} = \Delta p_{loss} + \Delta p_{head} + \Delta p \tag{4.27}$$

Total pressure differences caused the losses Δp_{loss} is calculated according to the Equation (4.28) as a sum of the pressure loss due to pipe friction Δp_f and due to local disturbances Δp_{loc}. Equations (4.29) and (4.30) present a calculation of these friction and local pressures losses.

$$\Delta p_{loss} = \Delta p_f + \Delta p_{loc} \tag{4.28}$$

$$\Delta p_f = \lambda \frac{l}{d} \frac{w^2}{2} \rho \tag{4.29}$$

$$\Delta p_{loc} = \sum_{i=1}^{n} \zeta_i \frac{w^2}{2} \rho \tag{4.30}$$

In the Equations (4.29) and (4.30), w represents the velocity of the fluid calculated from the mass flow and the diameter of the pipe, l is the length of the pipe concerned, and d is the inner diameter of the pipe. Parameter λ is another symbol for the Darcy friction factor and it can calculated using the Equation (4.31) in case of laminar flow, or as a result of the Blasius formula (Equation (4.32)) for turbulent flow.

$$\lambda = \frac{64}{Re} \tag{4.31}$$

$$\lambda = 0.3164\, Re^{-0.25} \tag{4.32}$$

In Equation (4.30), ζ_i presents a coefficient of local losses that is set for a specific component or a local disturbance in the flow. Table 4.1 delivers a list of the components that are present on the pipeline of the liquid LiBr lean solution with either a coefficient of local loss or a direct pressure loss.
The next variable in the total manometric pressure head calculation is a difference in hydrostatic pressure Δp_h on both sides of the pump. This pressure head is a result of different heights of the liquid level in the system, calculated in Equation

Table 4.1: List of the minor local loss coefficients or direct pressure losses of components

Component	Local loss coefficient ζ_i	Source
Elbows (90°, welded)	0.25	[9]
Tees (90°, line flow)	0.05	[9]
Pipe reduction	$0.1 \div 0.3$	[9]
Ball valves (fully opened)	0.05	[9]
	Local pressure loss $[kPa]$	
Flow meter LVB vortex LVB-06	0.34	[5]
Needle valves (ARMAT 487 - 3/8")	0.85	[2]
Plate HX SWEP 5BT-8	0.35	[38]

(4.33). h in Equation (4.33) is a height difference between the pump and the liquid level, where state 1 is the pump's outflow and state 11 the pump's inflow.

$$\Delta p_h = h_1 \rho_1 g - h_{11} \rho_{11} g \tag{4.33}$$

Once the total pressure difference Δp_{total} is calculated, total pumping power P_{pump} needed can be determined according to the Equation (4.34), as a pressure difference Δp_{total} multiplied by the volumetric flow of the liquid solution $\dot{V}$.

$$P_{pump} = \Delta p_{total} \dot{V} \tag{4.34}$$

From the thermodynamic analysis in Chapter 3, the volumetric flow of the solution was calculated to be very small, but denser and more corrosive than water. These flow parameters expect the use of a micro gear pump with reliable operation in chemical processes being able to transport a wide range of liquids. Requirements for the pump are also a hermetic design, low required NPSH, corrosion resistance and minimal volumetric flow rates in the order of a few dozen $ml\,s^{-1}$.
Once the the total pumping power required is determined it is necessary to check the selected micro pumps whether the pumping power calculated in Equation (4.34) is within the range of the power output possibilities and whether the calculated operation point in Equation (4.33) is on or under the maximum pressure head for the given volumetric flow in the characteristic pump performance curve.
Another pump is required to be placed in the recirculation of the solution, added to the lower part of the absorber (as described in Section 4.1.1.2). The same approach can be adapted for the selection of this recirculation pump as well; however,

similarities in the flow character and lower requirements, in this case, expect to use the same pump selection as for the primary solution pump, if suitable. Another booster pump is expected to be placed and used in the LiBr rich solution branch to ensure the continuous flow to the absorber, in the situation of the system initiation, experimental operational conditions, or of the pressure loss in the absorber nozzles too high.

4.2 Auxiliary devices and system's interconnection

Since the proposed apparatus is an experimental unit, it is equipped with additional components. These include temperature (pressure) and volumetric flow measuring devices on most of the branches downstream and upstream the crucial components. In case of the desorber and absorber, the thermometers are placed directly in the component with a goal to have an overview of the temperature glides within the mass transfer process as well as of the other parameters that are a function of temperature. The desorber contains six thermometers places inside the liquid and the absorber has eight thermometers that are rather placed in the vapour zone close to the inner diameter of the shell. The desorber is also equipped with a sigh glass crossing the desirable level of the liquid. This arrangement will serve as visual feedback on the desorber's solution level. All of the measuring devices, as well as the more detailed interconnection of the components, is pictures in the piping & instrumentation diagram (P&ID) in Appendix A.

A solution tank is added downstream from the absorber, mainly to provide storage of the solution for both maintenance and operation with the varying volumetric flow of the solution at different experimental regimes. The solution tank is equipped with an additional cooling coil in case of insufficient NPSH and sight glass. Both cooling sections and the condensate tank are all connected to the same dry cooler (DC) that is already installed at UCEEB CTU. An ambient air temperature of 20 °C is used in the DC calculations.

The functionality of the absorption process relies entirely on the working pair interaction in between the designed components and on maintaining the critical conditions at the operational levels. One of these crucial conditions is to preserve very low pressure of the system. For such complex and experimental device, that works under these low pressures (5÷15 kPa), it can be challenging to keep the airtightness of the whole system. Due to this fact, comprehensive care needs to be taken in designing the interconnection of the components and the pipeline system itself.

Different dimensions of connectors, multiple measuring points, valves from different manufacturers and the length of the pipes and components demand precise and more expensive manufacturing. The diameter of the pipes of the APC was designed according to a range of recommended velocities for liquid/vapour flow under certain conditions with consideration of a reasonable technological solution. In order to keep the low pressure in the whole system, also high-quality sealing is necessary, such as Teflon or silicone based for flanges and NPT threads were used on other piping connections. Another reason that raised the importance of a well-sealed system is a high risk of corrosion in case of oxygen intrusion. The H_2O-LiBr solution is highly corrosive if in contact with oxygen. For this reason, stainless steel was chosen as a material for all of the components and their interconnection. Although copper or carbon steel is standard in absorption devices, it is not recommended for an experimental unit as oxygen intrusion and improper inhibitor choice might occur in higher frequency. Inhibitors that are added to the solution are lithium salts of chrome, molybdates and nitrates [44]. Molybdate inhibitor is considered to be used in this work.

4.3 Design results & construction

The methodology of the thermodynamic cycle and of the components design was interconnected in a one set of equations creating one large model in Engineering Equation Solver (EES). After having completed all the calculations based on the boundary conditions, necessary outputs were collected from the EES's solution window and from from the result table of parameters, so-called arrays table, for each state of the cycle. The whole model in the form of EES formatted equations is located in Appendix A. The print of the main design and thermodynamic results that are not "arrays" is in Appendix B. All the necessary data for specific design requirements (such as total area necessary for the heat transfer, the pitch in between the absorber coils or the character of the fluid at certain state) was then forwarded either to the designers at UCEEB CTU or to the external design and manufacturing firm. The design of the desorber, absorber and the condensate tank was prepared in cooperation with a design firm, CERBET. The expander was designed by Ing. Suchna and Ing. Novotný and the piping & supporting structure was drawn by Ing. Pavličko. All the pictures from the drawings are published with their consent.

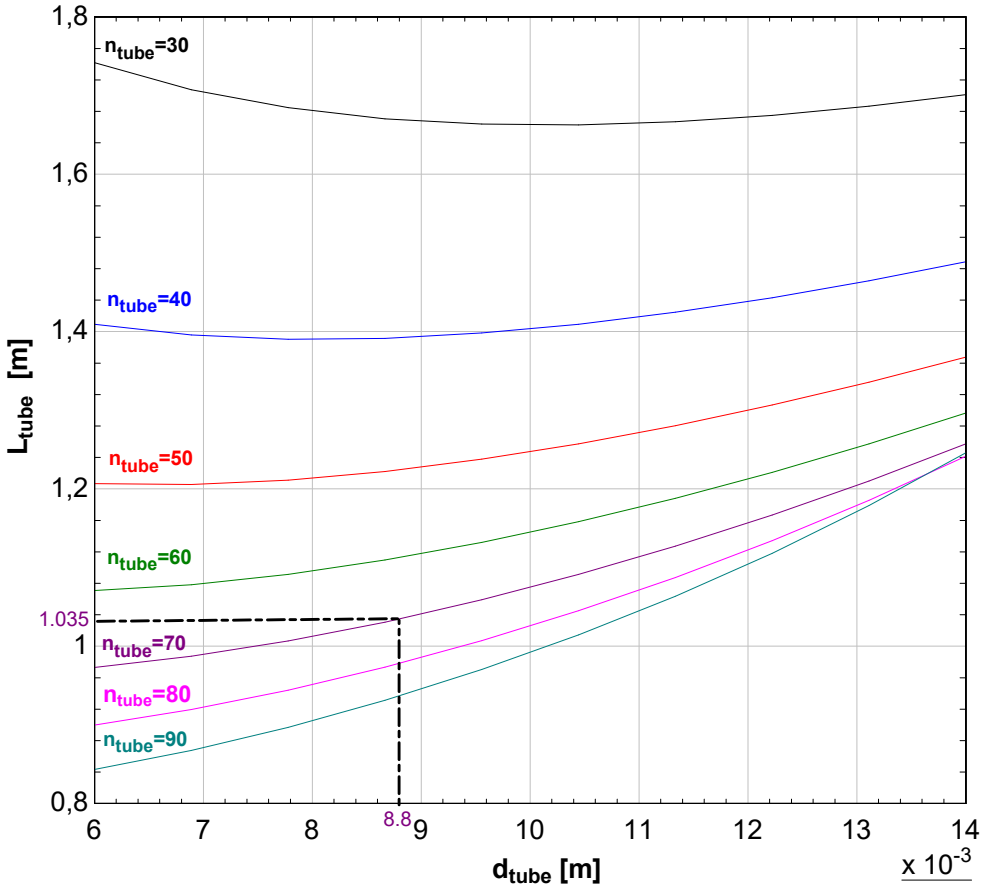

Figure 4.6: Graph of optimization of the total length of tubes in the desorber as a function of the inner diameter of tubes d_{tube} and number of tubes n_{tube}

4.3.1 Desorber

A model of heat and mass transfer according to the formulae in Section 4.1.1.1 was created for the desorber as specified by the boundary conditions. As it was stated before, the main purpose of the theoretical methodology was to calculate the functional heat transfer area, which was then directly used in the design of the component. As the total area is to be spread over several tubes of certain dimensions, an iteration problem of the model arises. With the number of tubes and the inner diameter of the tubes, the fluid properties of the heat source water change, which has a direct effect on the shift in overall heat transfer area calculated. Thanks to the design model created, thermo-economical optimization can be done via multivariable plot (Figure 4.6) of total tubes length L_{des} as a function of tube inner diameter d_{tube} and of the number of tubes n_{tube} (depicted as contour lines in Figure 4.6). In Figure 4.6, a chosen optimization point is presented. To minimize the resulting length of the pipes, a number of 70 stainless pipes was chosen with a reasonable nominal diameter

of DN8 (13.5 x 2.35 mm). Following the described methodology, the resulting heat exchanger has a heat transfer surface area of 3.07 m^2 and tubes of the theoretical functional length $L_{tube,th}$ of 1.04 m and final constructional length $L_{tube,r}$ of 1.15 m.

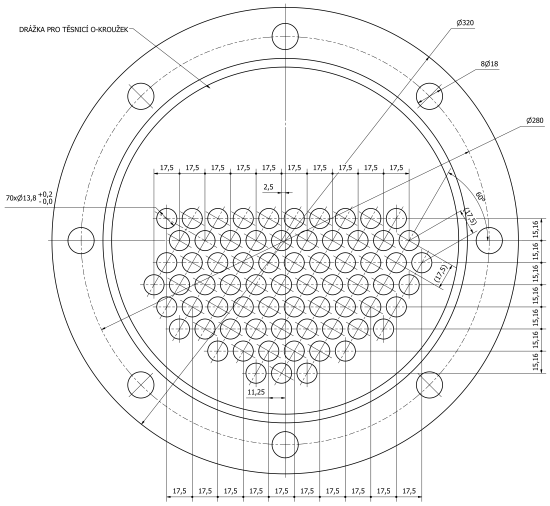

Figure 4.7: Tubes arrangement demonstrated on the flange cap of the desorber (by CERBET)

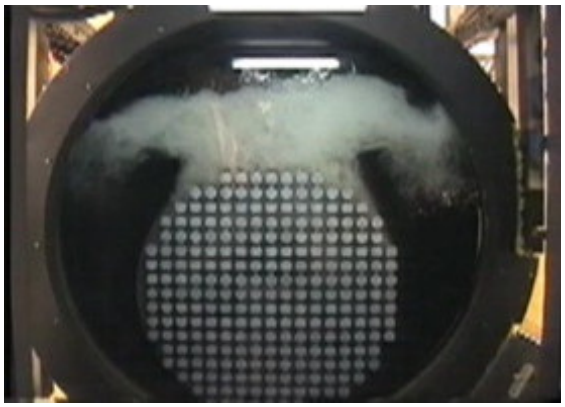

Figure 4.8: Example of tests on boiling pattern in a kettle reboiler with a refrigerant R113 at a heat flux of 10 kW/m^2 [25]

Altered shell-and-tube heat exchanger arrangement of the desorber was chosen. Kettle reboiler arrangement was abandoned due to uncertain operation for the APC conditions. According to the formula from Jacimovic et al. stated in Equation (4.13), with a maximum heat flux of 10.9 kW/m^2, required minimal shell diameter should be 1.22 times larger the bundle diameter. Enlargement of the shell diameter of the typical kettle reboilers in not necessary and proposed simplified shell-and-tube arrangement with a reduced number of tubes are used. Tubes with a triangular layout of 60 degrees provide a good density of tubes and do not require the diameter of the shell to be too large. This layout and the chosen shell inner diameter of 213.9 mm results in approximately 1.5 of the shell diameter to bundle height ratio and it gives enough of the free space above the solution level for the vapour to develop. Figure 4.7 presents the chosen and an actual tube and shell layout constructed for the APC. The experiments of the actual pool boiling of the H_2O-LiBr solution during the desorption process are only to be done, but Figure 4.8 gives a good example of how a heat flux of 10 kW/m^2 of a fluid with a similar density a viscosity looks like [25]. A maximal heat flux of approximately 10 kW/m^2 will be present, in the case of the designed APC unit, only at the beginning of the desorption process. This fact can be seen in the graphs of Figure 4.9, where the significantly larger temperature difference between the heating and the working fluid at the beginning of the desorption results in great heat flux then it is at the end of the process. The

Figure 4.9 shows the front view on the designed APC unit, and it can be seen that the vapour outlet is placed closer to the end of the process, where the heat flux and the subsequent liquid level variation is significantly lower. This position of the vapour outlet is thus more secure in preventing any liquid to be raised and torn by the vapour to the vapour branch.
The three graphs in Figure 4.9 present the variable of temperatures T_i, $T_{hs,i}$ and their difference ΔT_i in the first one, mass flows of the liquid $\dot{m}_{l,i}$, of the vapour being generated $\dot{m}_{v,i}$ and mass fraction of the liquid solution ξ_l in the second one, and heat transfer parameters (convective heat transfer coefficients α_i, $\alpha_{hs,i}$ and heat flux $\dot{q}$), all as a function of the total surface area from the beginning of the absorption process. Some of these variables are summarized in numbers, alongside with general design parameters, in Table 4.2.

Table 4.2: Design results for the desorber arrangement and construction

Heat input	$\dot{Q}_{in}$	20	kW
Average heat flux	$\dot{q}_{ave,des}$	6.512	kW/m^2
Maximal heat flux	$\dot{q}_{max,des}$	10.855	kW/m^2
Minimal heat flux	$\dot{q}_{min,des}$	2.344	kW/m^2
Reynolds number range of HS fluid	$Re_{hs,des}$	4414÷4756	
Heat transfer coeff. range of HS fluid	$\alpha_{hs,des}$	1.745÷1.838	$kW/(m^2K)$
Heat transfer coeff. range of WF	$\alpha_{wf,des}$	0.306÷1.149	$kW/(m^2K)$
Overall heat transfer area	A_{des}	3.071	m^2
Number of tubes	n_{tube}	70	
Nominal diameter of the tubes		DN8	
Theoretical lenght of one tube	$L_{tube,th}$	1.035	m
Actual designed lenght of one tube	$L_{tube,r}$	1.150	m
Number of passes of the HS fluid		1	
Material of the tubes and shell		EN 1.4404 / AISI 316L	
Shell to tube bundle diameter ratio	D_{sh}/D_{bu}	1.550	

Besides the front view on desorber drawing, it is also depicted as a model from a CAD program in Figure 4.10 in a orthographic projection. Right next to the CAD model of the desorber a photograph of the actual constructed desorber of the APC unit is shown (Figure 4.11). In Figures 4.10 and 4.11, additional elements, not evident from the previous figures, can be seen. Temperature sensors along the shell length are incorporated to provide information on the real temperature glide during the operation. Another element that provides a visual feedback of the boiling

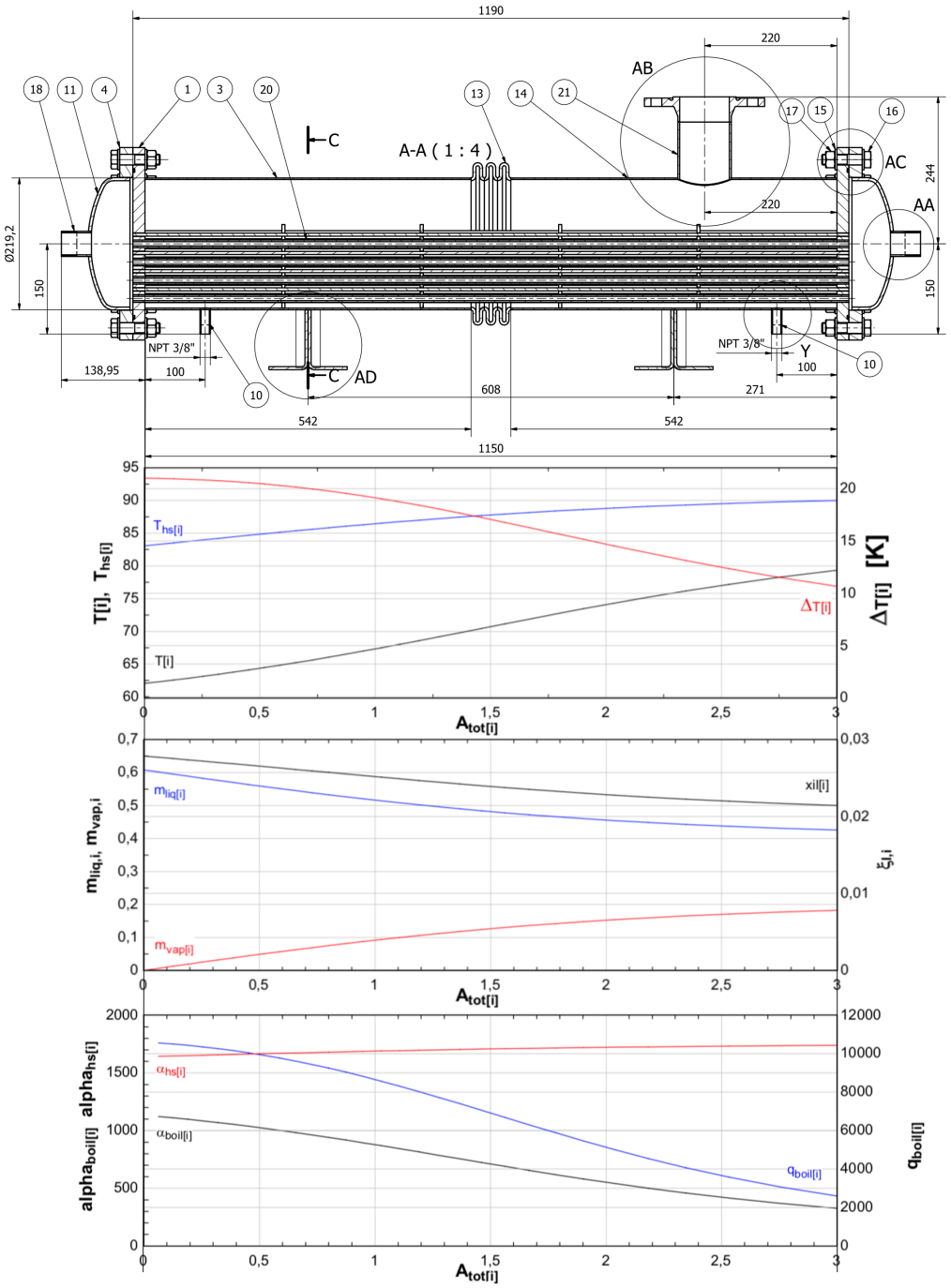

Figure 4.9: Front view on the drawing of the desorber assembly with graph of the changing properties along the longitudinal dimension of the heat transfer area (drawing by CERBET)

process and liquid level of the solution is a sight glass. The sight glass is attached at the height corresponding to the designed liquid level. The entire drawing of the desorber assembly is attached in the appendices of the document.

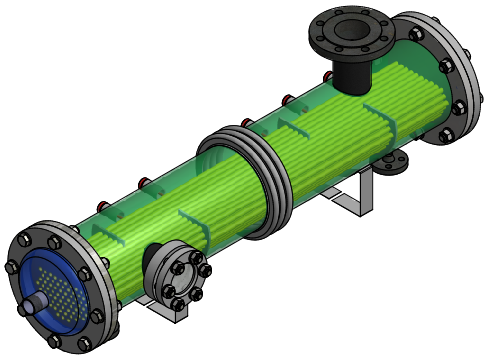

Figure 4.10: A perspective view on the desorber modeled in CAD software (by CERBET)

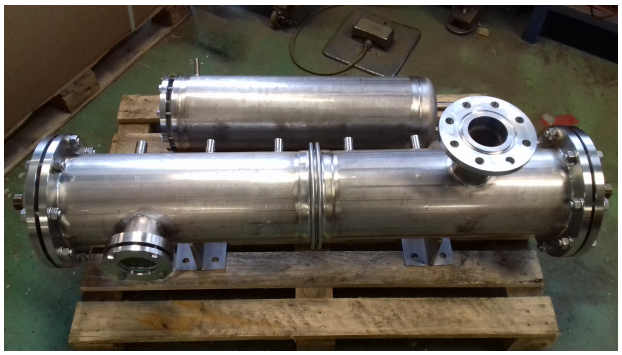

Figure 4.11: A photograph of the fabricated desorber (front) and of the solution tank (back)

4.3.2 Absorber

Reliable heat and mass transfer model of the absorption process is crucial in optimization and designing of the component. This theoretical model was created according to the set of equations presented in Section 4.1.1.2 with the set boundary conditions. As it was stated before, the main purpose of the theoretical methodology was to calculate the necessary surface area of the liquid film to absorb the present vapour. Heat transfer analysis adds on to the calculation by determining the fluid properties along the absorption process, respecting the necessity of the heat rejection to keep the solution in subcooled condition and thus to keep the driving force of the mass transfer of vapour into the liquid.

The creation of the sufficient surface area of the arriving rich solution to the free space of the absorber and its distribution is an essential and the first design step. The rich solution is expected to form a falling film on the surface of cooling helical coils, as described in the methodology part of the document (Section 4.1.1.2). A similar problem of the multi-criteria optimization, as in the case of the desorber, arises for the absorber as well as the heat transfer coefficient of the cooling fluid is dependent on the diameter, length and the disposition of the cooling tubes. Change in heat transfer coefficient has a following effect on the total area, or the temperature ratios, as well as on the mass transfer coefficient and thus on the overall size of the component. As a result of thermo-economical optimization, four concentric cooling coils of the same length with nominal diameter DN15 (21.3 x 2.0 mm) were chosen. Total surface area A_{abs} of 5.695 m^2 calculated for one section yields, with respect to the selected number of tubes and their diameter, a total length of one tube $L_{coil,abs}$ of 21.3 m in one section. Setting a reasonable pinch distance between the turns of the coil gives a total height of one coil section of 0.56 m. All the remaining performance

Table 4.3: Design results for the absorber arrangement and construction

Heat rejected	$\dot{Q}_{rej}$	19.5	kW
Average heat flux	$\dot{q}_{ave,abs}$	3.437	$kW/m2$
Maximal heat flux	$\dot{q}_{max,abs}$	6.236	$kW/m2$
Minimal heat flux	$\dot{q}_{min,abs}$	2.703	$kW/m2$
Reynolds number range of CF	$Re_{cf,abs}$	6037÷8495	
Reynolds number range of WF	$Re_{wf,abs}$	6.74÷14.02	
Heat transfer coeff. range of CF	$\alpha_{cf,abs}$	1.585÷1.977	$kW/(m^2K)$
Heat transfer coeff. range of WF	$\alpha_{wf,abs}$	1.318÷1.986	$kW/(m^2K)$
Overall heat transfer area of a section	A_{abs}	5.695	m^2
Nominal diameter of the tubes		DN15	
Total lenght of tubes needed	$L_{the,abs}$	85.11	m
Number of concentric coils	n_{coil}	4	
Lenght of one tube per section	$L_{coil,abs}$	21.28	m
Height of one section	$H_{coil,abs}$	0.562	m
Number of sections	n_{sec}	2	
Material of tubes and the shell		EN 1.4404 / AISI 316L	

and design parameters are summarized in Table 4.3.

As it was described in the methodology (4.1.1.2), uncertainties linked to the behaviour of the falling film and the overall vapour absorption process, the coiled section is duplicated and added underneath with the solution recirculation in between. The modelled absorber thus consists of two coil sections with parallel connection of external cooling water. Temperature sensors are further added along the height to measure the temperature; it is, however, expected to measure the temperature of the bulk vapour, but the one of the film. The drawing of the designed absorber assembly from a front view is presented in Figure 4.12. It can be seen in the drawing in Figure 4.12 that the vapour inlet (N1) is located in the uppermost part of the absorber, from where it is directed to the annular space confined by the inner diameter of the absorber's shell and by the outer diameter of the central column. In this annular space, upper-floor rich solution nozzles, upper-floor coil section, lower-floor recirculation nozzles and lower-floor coil section are located alongside with four temperature sensors per each section close to the outermost cooling coil.

Similarly to the desorber's methodology, properties along the absorption process were calculated in 30 discretized elements. This approach enables to create a graphical representation of changing properties relative to the vertical dimension of the

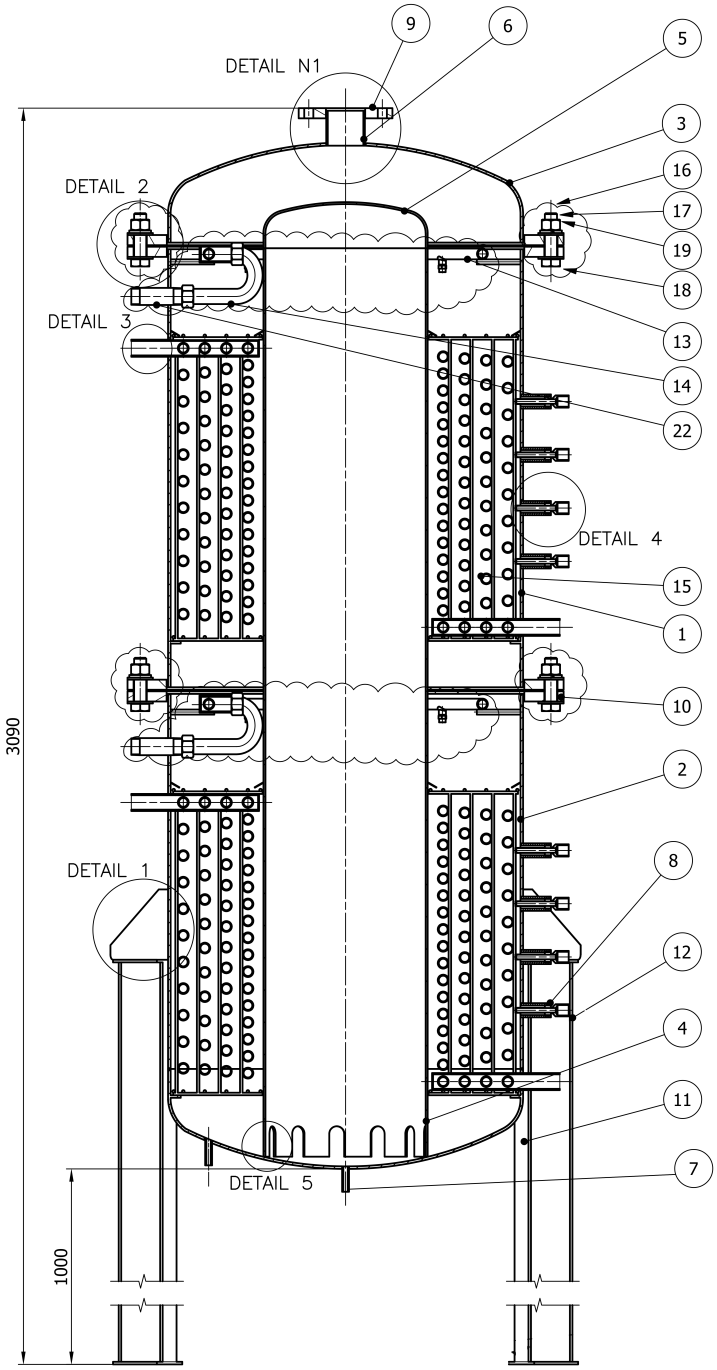

Figure 4.12: Front view on the drawing of absorber assembly (by CERBET)

coil section, and thus total cumulative surface area $A_{tot,i}$. Figure 4.13 demonstrates these graphs relative to the total surface area from the beginning of the absorption process alongside with the drawing of a cooling coils section.

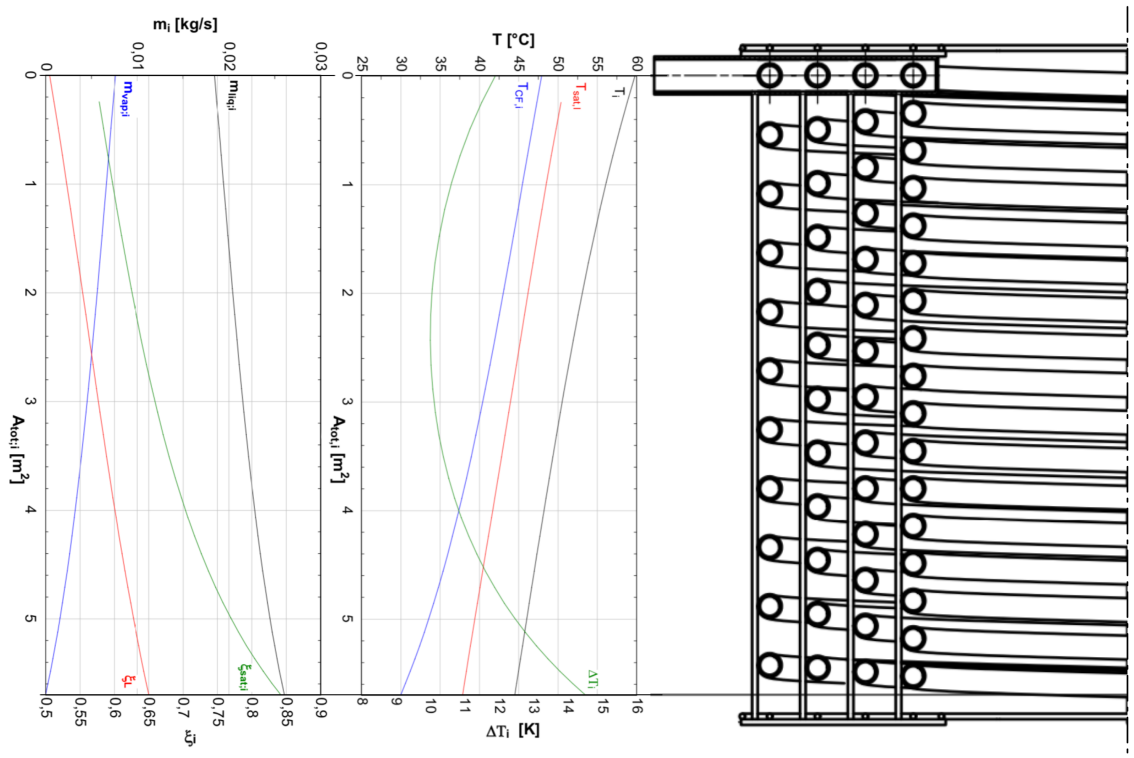

Figure 4.13: Front view on a half cut cooling coils bundle alongside with the graphs of temperature and mass flow properties relative to the total surface area

4.3.2.1 Condensate tank

A condensate tank is located downstream from the absorber, mostly to provide storage of the solution for both maintenance and operation with varying solution volumetric flow at different experimental regimes. The solution tank is equipped with an additional cooling coil in case of insufficient NPSH and a sight glass. The solution tank can be seen in a model of the overall APC assembly in Figure 4.19.

4.3.3 Solution heat exchanger

Designed recuperator work with liquid solutions on both side of the exchanger and thus, there is no special requirement. A plate heat exchanger is chosen due to its compactness and reliability. The pressure loss is not a major issue as a booster pump is installed on the side of the LiBr rich solution. A flat plate exchanger chosen for this purpose is SWEP heat exchanger B5T with ten plates, which is suitable for application with small flows and efficient in variable conditions [38]. The selection and the size was consulted with manufacturer-provided sizing tool based on heat transfer calculation and their own proprietary correlations. An exemplary visualization of the selected plate heat exchanger is in Figure 4.14. Heat load expected

Figure 4.14: Product visualization of a chosen plate heat exchanger SWEP 5BT [38]

for this recuperator is from 1.00 to 1.15 kW. Pressure drop on the side of the rich solution is expected to be 0.35 kPa with four channels per pass and 0.27 kPa with five channels on the side of the weak solution.

4.3.4 Expander

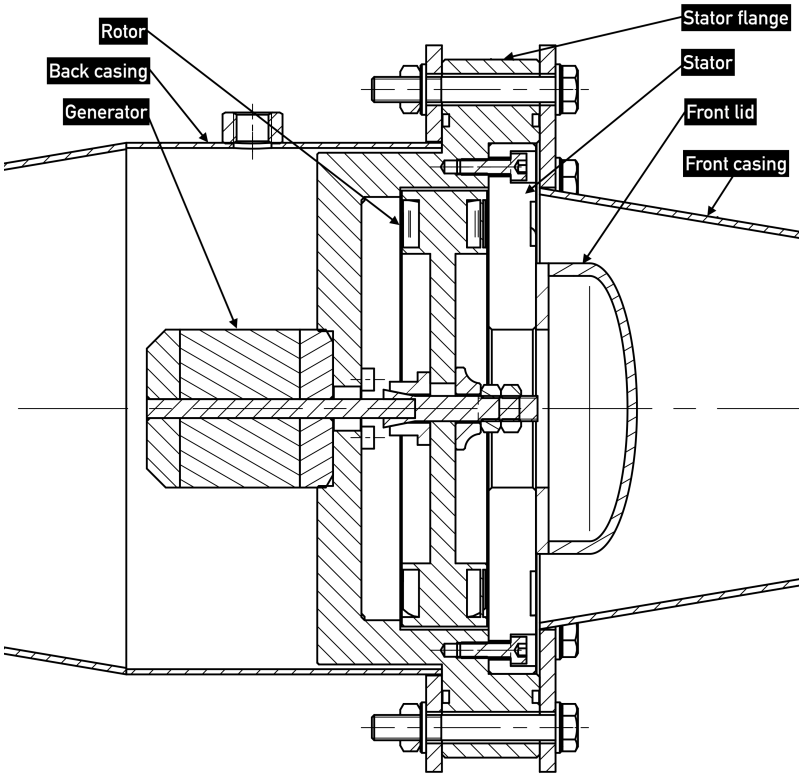

Figure 4.15: Part of the turbine assembly (by Ing. Suchna)

Because generated steam in the APC unit is at very low pressures, which results in significant volumetric flow rates, this turboexpander concept is chosen. An axial impulse turbine with partial admission was selected for this application following suggestions of Weiß [45]. The design is based on a one-dimensional mean line model with chosen maximal rotational speed suitable for the generator and its bearings of 15 000 rpm (this number also encompass the safety margin). Mean rotor diameter was selected to be 120 mm to ensure technological manufacturability within the expected tolerances. The technology of the fabrication of the turboexpander is chosen to be the selective laser sintering (SLS) of polyamide powder. Design is identical as in the joint project of Novotny et al. [28].

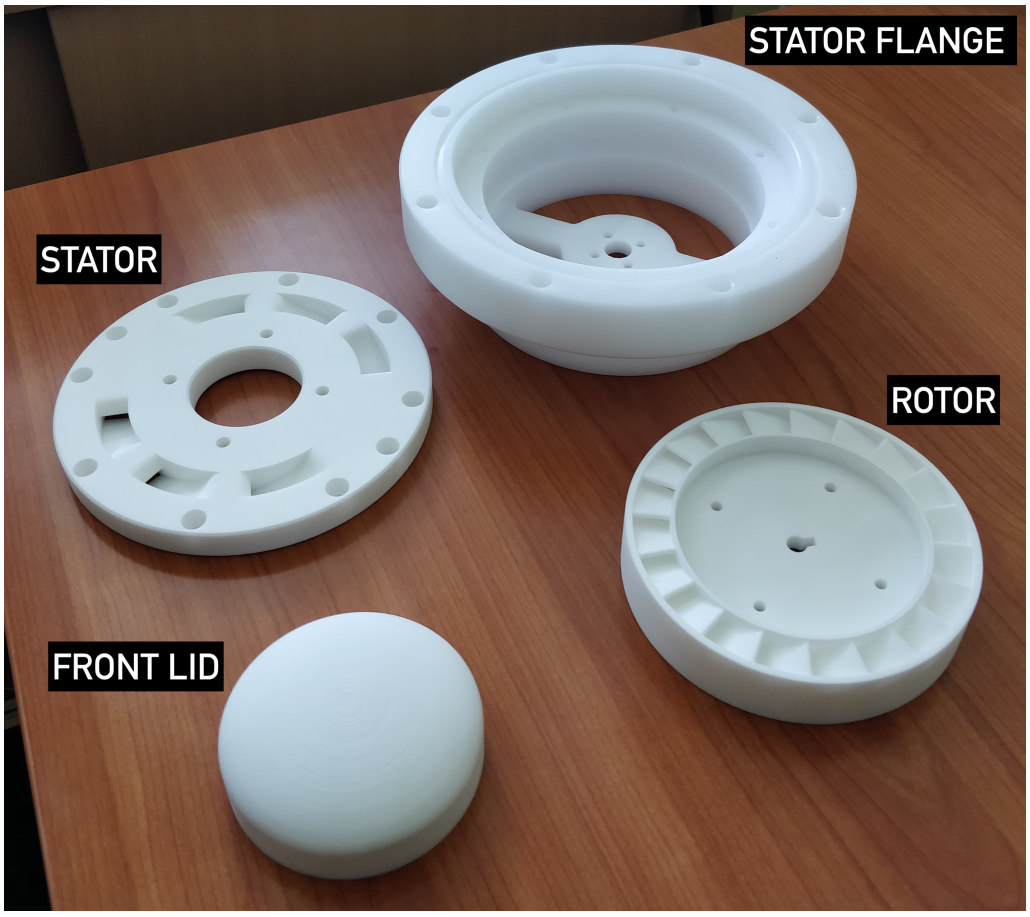

Figure 4.16: Platic parts of the turboexpanders

Following the design model of the turbine, the isentropic velocity is corrected by velocity coefficients which are, together with correlations for complimentary secondary losses (partial admission, secondary flow - horseshoe vortex loss, passage vortex loss, disc friction-ventilation loss and profile loss) and flow coefficients, acquired from the publication of Ambrož [1]. Nozzle angle and degree of partial admission are optimized to the maximal efficiency. Due to the constraints in both rotating speed and

diameter, however, the efficiency is not reaching its optimal values, and its designed nominal value of isentropic efficiency is 44 %. For experimental purposes and as proof of concept device, it is considered to be acceptable with space available for further improvement (for example, by adjusting the rotational speed).
Thanks to the low operating temperatures and stage loadings, plastic, which can be well 3D printed, is used as a material suitable for nozzles and rotor buckets. The resulting concept is a turboexpander with stator nozzles ring and rotor buckets wheel manufactured each in a single piece with the rotor directly mounted to a permanent magnet generator. The generator used is converted from a typical aeromodelling BLDC motor. The case of the expander consists of two conical pipe extensions made of stainless steel that are attached to the stator flange from both sides. The design is shown in Figure 4.15. All of the components that were manufactured from plastic are shown in Figure 4.16. Rotor, stator and the front cover lid were 3D printed using the SLS method, while the stator flange is manufactured by machine turning with additional adjustment. The stator flange serves a structural base fixing the stator and holding the generator that contains the bearing on which the rotor is allowed to rotate via a collet.

4.3.5 Pumps & Piping

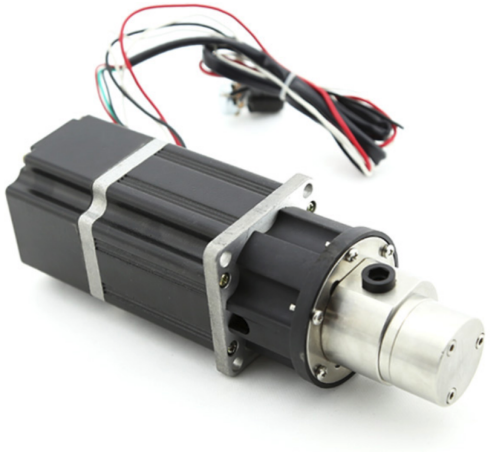

Figure 4.17: Picture of a chosen micropump MG213XK/DC24WI [39]

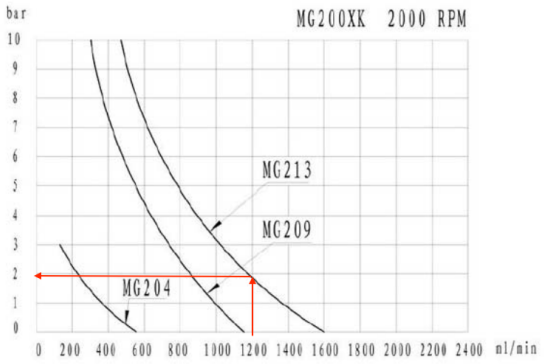

Figure 4.18: Pump performance curve of the selected model with a maximum working point for the volumetric flow in weak solution branch

A micro gear pump, Topsflo MG213XK/DC24WI, driven via a magnetic coupling has was chosen as it seems to fulfill all of the necessary requirements for the low volumetric flow and working fluid compatibility. In the name of unity, the same micro gear pump was chosen for both the booster pump on the rich solution and as

well as the absorber recirculation pump. This micro gear pump is shown in Figure 4.17.

Pressure drop and total pressure head calculation were done for the main solution pump following the methodology described. Total pressure difference for the pump to overcome is 0.3392 bar, which corresponds to energy flow required of 0.675 W. For the volumetric flow of 1195 ml/min in weak solution branch, performance curve in Figure 4.18 of the selected pump yields a maximum pressure head of $1.9 \div 2$ bar, which confirms that the working point is within the operating conditions of the pump [39].

4.3.6 Entire unit interconnection and design summary

The resulting main dimensions and parameters of the components are summarized in Table 4.4. Design of the overall system is then depicted in Figure 4.19. Figure 4.19 is missing some of the structural features due to visibility turned off for the purpose of the image presentation. It is apparent that the whole system is very large for the heat input of 20 kW and gross power generated of 0.5 kW. The massiveness of the APC is evidently due to the oversized absorber, where maximal counter-flow temperature profile and covering the possible malfunction is intended. Absorber, besides having its coil surface area almost doubles, it was also required to have the component lifted with regards to the net positive suction head (NPSH) of the pump. The expander is placed upstream, right above the absorber's inlet. This placing supposedly increases the expander's power output, but it also increases the highest point of the whole system, which is then 4.3 m above the ground. A second floor has been added to reach of the components easily; it is just not visible due to the explanation stated before.

Design methods theoretically described in available literature mainly for desorber and absorber yield physically large components for this low-temperature heat source of 90 °C. This is due to low operating pressures that accounts for large volumetric flows, small mass flow rates, and also due to the factor of design safety margin. This character can be seen in Figure 4.19 where the red vapour part and both absorber and desorber where the vapour is located are massively larger than the parts on the solution side. The mass flow of the rich and weak solution is so low and recommends the pipes' nominal diameter to be DN6 in some sections. The yellow, also not visible, pipe connects the micro gear pump and the desorber on the weak solution side through a recuperator of a similarly smaller size. Green pipes represent LiBr rich solution and blue interconnection on desorber, absorber and condensate tank are for the external fluids (heating source fluid or cooling fluid).

Out of 20 kW of thermal heat input in the heating source fluid, it is now 0.37 kW expected to be converted to power with the rest being rejected in the absorber. Net power respecting the own power consumption in the system is 0.26 kW. This yields a 1^{st} law efficiency of the system of 1.3 %. Although the system is thermodynamically partly optimized, this number could be reduced due to further loses unforeseen or omitted in the calculation due to process and design uncertainties.

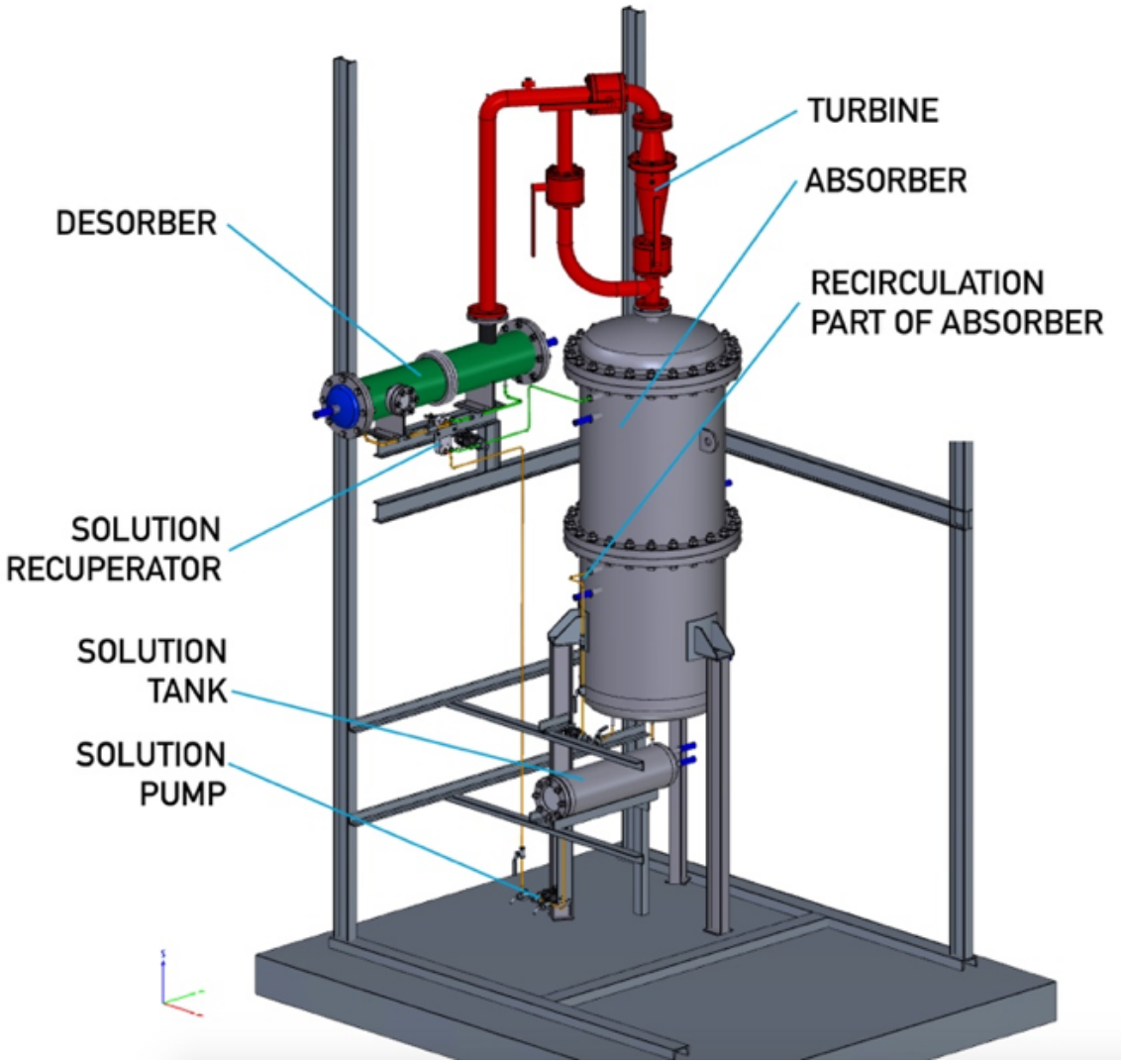

Figure 4.19: Overall design of the experimental APC unit (Red coloured components are for vapour branch, green for LiBr rich solution and light brown colour for LiBr lean solution) (models of the components by CERBET, structure & piping by Ing. Pavličko)

Table 4.4: Design summary of each of the main component

Component	Design	Dimensions	Performance
Desorber	Single pass shell & tube, LiBr in shell and heating water in tubes	70 pipes of DN8 (13.5 x 2.35) with a length of 1.15 m; liquid volume of 14.4 l	Heat load: 20 kW, $TTD = 10K$, $\dot{m}_{HS} = 0.724kg/s$, $\dot{m}_{vap} = 0.0078kg/s$
Absorber	Spiral tube heat exchanger of two sections of cooling coils with distribution nozzles and packing; cooling fluid in tubes	4 concentric spiral pipes of 21 m in length each in one coil section; section height: 0.55 m;	Heat rejection: 19.5 kW, $TTD = 10K$, $\dot{m}_{cf} = 0.261kg/s$
Recuperator	Flat plate SWEP B5Tx10	Specified by manufacturer [38]	Heat load: 1.2 kW
Expander	3D printed (SLS, Polyamide PA 2200) axial single stage turbine with permanent magnet generator, designed in stainless housing	$D_{mean} = 120mm$, $D_{overall} = 230mm$	Nominal power: 360 W, $\eta_{is} = 44\%$, 15 000 rpm
Pumps	Three identical pumps Topsflo MG213XK/DC24WI on weak solution branch, on absorber recirculation and on rich solution branch	Specified by manufacturer [39]	Flow range: 300÷3500 ml/min; power: 70 W

5

Conclusion

Among multiple possibilities of utilization of low-to-medium temperature heat sources in power generation, ORC systems exhibit the most promising fitting, especially in small scale applications, thanks to their exclusive thermodynamic advantages. ORC systems, however, loose rapidly on their advantage when the temperature of the heat source decreases and approached approximately 150 °C (depending on the organic fluid used). Usability of this very-low temperature heat source in power generation is significantly narrowed beyond this point. From the theoretical introduction describing different power-generating systems supposedly applicable to very-low temperature heat source, the Kalina cycle has gotten applications closest to the commercial usage. Despite the good thermodynamic results of the Kalina cycles in comparison to conventional Rankine cycles, the operation of very few power plants has demonstrated many drawbacks of usage of NH_3-H_2O linked to the substance health danger, decomposition of NH_3, corrosion and to the overall complexity of the system. Absorption power cycles using a mixture of H_2O-LiBr have been theoretically introduced after a reliable operation of the substance in commercial absorption chillers. A H_2O-LiBr solution is a promising mixture to cover some of the flaws of the NH_3-H_2O. LiBr as salt is a non-volatile substance, eliminating the need of a rectifier, it has a relatively high specific heat of vaporization, and the equilibrium with solution generates vapour directly at its superheated state which simplifies the operation of the expanders and avoids possible corrosion problems.

On the other hand, H_2O-LiBr requires very low operating pressures making the construction more complicated and also the corrosion seems to be an issue in case of any minor air intake. To the author's knowledge, no APC unit is used or has been successfully constructed at the moment. With a goal of testing the absorption principle for low-temperature applications, a work team of UCEEB CTU is, at the time of publishing this thesis, constructed a proof-of-concept APC unit using H_2O-LiBr solution as a working fluid.

This work, thus, presents a detailed methodology for the practical design of an absorption power machine for waste heat recovery. The system has a nominal heat

source temperature of 90°C, heat input of 20 kW (to receive from a topping ORC unit) and gross electrical output of 410 W. Design was based on the optimized thermodynamic model of an APC and heat and mass transfer formulae presented in the methodology section. A few of the theoretical correlations used in mass and heat transfer analysis have only a limited experimental evaluation or have only been used in solely cooling applications. For this reason, a proportional over-sizing of the components was taken into account with a goal to cover uncertainty in the model, unforeseen operational complications, or to give more versatility in case of experimental off-design tests.

Design and construction of an APC that followed the results of a created mathematical model are also presented and described. The resulted dimensions of the whole system are rather large, due to a very tall absorber respecting the NPSH of the pump and an expander located on top of the absorber. It is, however, made in order to have a working experimental system based on which possibilities for further performance improvement will be investigated. For future work, experiments on the constructed device need to be held. After having proved and functional absorption process in power generation, these experimental results will determine if and how the size can be reduced, and design simplified. Then careful feasibility study, further performance improvement and subsequent thermo-economical optimization need to be conducted in order to provide a potentially competitive technology for the intended low-temperature applications, in, e.g. commercial last stage waste-heat recovery.

Bibliography

[1] Jaroslav Ambroz. *Parní turbíny a kondenzace (Steam turbines and condensation.* 1984.

[2] Armat. "Stainless Steel Needle Valce PN 400 F/F". 2019. URL: https://www.armat.cz/pdf/nerezovy-jehlovy-ventil-zavitovy-bsp-npt-model-481-487.pdf.

[3] Nabil Ben Hafsia, Bechir Chaouachi, and Slimane Gabsi. "Surface tension effects on the absorption process in a spiral tubular absorber working with LiBr–H2O couple". In: *International Journal of Thermal Sciences* 94 (Aug. 2015), pp. 79–89. ISSN: 1290-0729. DOI: 10.1016/J.IJTHERMALSCI.2015.02.009. URL: https://www.sciencedirect.com/science/article/pii/S1290072915000678.

[4] Giuseppe Bianchi et al. "Development and analysis of a packaged Trilateral Flash Cycle system for low grade heat to power conversion applications". In: *Thermal Science and Engineering Progress* 4 (Dec. 2017), pp. 113–121. ISSN: 2451-9049. DOI: 10.1016/J.TSEP.2017.09.009. URL: https://www.sciencedirect.com/science/article/pii/S2451904917302731.

[5] Bronkhorst. *Liqui View Base brochure.* Tech. rep. Mass Flow Online B.V., 2019. URL: https://www.bronkhorst.com/getmedia/42c3235f-4d9d-4c44-93f6-4a2b9e708a51/LIQUI-VIEW-Base-brochure.

[6] W.W.S Charters et al. "Atmospheric and sub-atmospheric boiling of H2O and LiBr/H2O solutions". In: *International Journal of Refrigeration* 5.2 (Mar. 1982), pp. 107–114. ISSN: 01407007. DOI: 10.1016/0140-7007(82)90085-8. URL: http://linkinghub.elsevier.com/retrieve/pii/0140700782900858.

[7] E. L. Cussler. *Diffusion : mass transfer in fluid systems.* Cambridge University Press, 2009, p. 631. ISBN: 9780511805134.

[8] DAMGAARD Consulting. *ORC WAVE 50 - Produktový lost.* Tech. rep. Buštěhrad: UCEEB CVUT. URL: http://www.damgaardsolutions.com/wave-50/.

[9] Dubbel. "Odpory v potrubí a armaturách". In: *Inženýrská příručka pro stavbu strojů I.* Praha: SNTL, 1961, pp. 333–342.

[10] Donald C. Erickson, G. Anand, and Icksoo Kyung. "Heat-Activated Dual-Function Absorption Cycle". In: *ASHRAE Transactions: Symposia* 110.1 (2004), pp. 515–524.

[11] European Commission. *2018 assessment of the progress made by Member States towards the national energy efficiency targets for 2020 and towards the implementation of the Energy Efficiency Directive as required by Article 24(3) of the Energy Efficiency Directive 2012/27/EU*. Tech. rep. Brussels: EU, 2019. URL: https://ec.europa.eu/commission/sites/beta-political/files/report-2018-assessment-progress-energy-efficiency-targets-april2019_en.pdf.

[12] European Commission. *EUROPE 2020: A strategy for smart, sustainable and inclusive growth*. Tech. rep. Brussels: European Commission, 2010. URL: http://eur-lex.europa.eu/LexUriServ/LexUriServ.do?uri=COM:2010:2020:FIN:EN:PDF.

[13] European Commission. *Good practice in energy efficiency - Clean energy for all Europeans*. 2017. ISBN: 9789279653322. DOI: 10.2833/75367. URL: http://mejoresedificios.com/wp-content/uploads/2017/04/good_practice_in_ee_-web.pdf.

[14] Daniele Forni et al. "Heat recovery for electricity generation in industry". In: *ECEE summer study on energy efficiency in industry*. March (2012), pp. 523–534. URL: http://www.hreii.eu/public/2012%20ECEEE.pdf.

[15] E. García Rivera. "Modelling and Experimental Validation of Water Vapor Absorption by Falling Films of LiBr Aqueous Solution Under Wave Regimes Conditions and Presence of Non-Absorbable Gases". PhD thesis. Universidad Politecnica de Catalunya, 2015.

[16] Néstor Garcia-Hernando et al. "Energy and exergy analysis of an absorption power cycle". In: *Applied Thermal Engineering* 55.1-2 (2013), pp. 69–77. DOI: 10.1016/j.applthermaleng.2013.02.044. URL: http://dx.doi.org/10.1016/j.applthermaleng.2013.02.044.

[17] Md Arbab Iqbal et al. "Trilateral Flash Cycle (TFC): a promising thermodynamic cycle for low grade heat to power generation". In: *Energy Procedia* 160 (Feb. 2019), pp. 208–214. ISSN: 1876-6102. DOI: 10.1016/J.EGYPRO.2019.02.138. URL: https://www.sciencedirect.com/science/article/pii/S187661021931224X.

[18] Branislav Milenko Jacimovic, Srbislav Genic, and Nikola J Budimir. "Criteria for the Vapor Space Design in Kettle Reboilers". In: April 2015 (2008).

[19] Maria T. Johansson and Mats Söderström. "Electricity generation from low-temperature industrial excess heat-an opportunity for the steel industry". In: *Energy Efficiency* 7.2 (2014), pp. 203–215. ISSN: 15706478. DOI: 10.1007/s12053-013-9218-6.

[20] Christoph Kirmse et al. "Comparison of a Novel Organic-Fluid Thermofluidic Heat Converter and an Organic Rankine Cycle Heat Engine". In: *Energies* 9.7 (June 2016), p. 479. ISSN: 1996-1073. DOI: 10.3390/en9070479. URL: http://www.mdpi.com/1996-1073/9/7/479.

[21] Matthias Kunick and S Hasch. "Property Library for Mixtures of Water / Lithium Bromide FluidLAB with LibWaLi". In: (2011).

[22] Sangsoo Lee et al. "Measurement of absorption rates in horizontal-tube falling-film ammonia-water absorbers". In: *International Journal of Refrigeration* 35.3 (May 2012), pp. 613–632. ISSN: 0140-7007. DOI: 10.1016/J.IJREFRIG.2011.08.011. URL: https://www.sciencedirect.com/science/article/pii/S0140700711002131.

[23] Mingxi Liu, Yang Shi, and Fang Fang. "Combined cooling, heating and power systems: A survey". In: *Renewable and Sustainable Energy Reviews* 35 (July 2014), pp. 1–22. ISSN: 13640321. DOI: 10.1016/j.rser.2014.03.054. URL: http://www.sciencedirect.com/science/article/pii/S1364032114002263.

[24] Ennio Macchi and Marco Astolfi. *Organic Rankine Cycle (ORC) Power Systems: Technologies and Applications*. Woodhead Publishing, 2016, p. 698. ISBN: 9780081005118.

[25] David A. McNeil et al. "Investigation of flow phenomena in a kettle reboiler". In: *International Journal of Heat and Mass Transfer* 53.5-6 (Feb. 2010), pp. 836–848. ISSN: 0017-9310. DOI: 10.1016/J.IJHEATMASSTRANSFER.2009.11.041. URL: https://www.sciencedirect.com/science/article/pii/S0017931009006413.

[26] Vaclav Novotny and Michal Kolovratnik. "Absorption power cycles for low-temperature heat sources using aqueous salt solutions as working fluids". In: *International Journal of Energy Research* 41.7 (2017), pp. 952–975. ISSN: 1099114X. DOI: 10.1002/er.3671.

[27] Vaclav Novotny and Petr Zikmund. "3D Printed Parts for Power Industry". In: *Technological forum 2018* August (2018).

[28] Vaclav Novotny et al. "3D Printing for Low-Cost Low-Parameters and Rapidly Developed Turboexpanders for Decentralized Micro-Power Systems". In: *ASME Turboexpo 2018 (poster)*. Oslo, 2018.

[29] Vaclav Novotny et al. *Analysis and Design of Novel Absorption Power Cycle Plants*. 2016. URL: http://dx.doi.org/10.1115/ES2016-59272.

[30] Vaclav Novotny et al. "Design of Experimental Rig for Validation of Absorption Power Cycle Concept". In: *Energy Procedia* 105 (2017), pp. 4990–4996. ISSN: 18766102. DOI: 10.1016/j.egypro.2017.03.998. URL: http://dx.doi.org/10.1016/j.egypro.2017.03.998.

[31] Roy A. Parisher et al. "Mechanical Equipment". In: *Pipe Drafting and Design* (Jan. 2012), pp. 112–133. DOI: 10.1016/B978-0-12-384700-3.00006-2. URL: https://www.sciencedirect.com/science/article/pii/B9780123847003000062.

[32] S. S. Pawar and Vivek K. Sunnapwar. "Studies on convective heat transfer through helical coils". In: *Heat and Mass Transfer* 49.12 (Dec. 2013), pp. 1741–1754. ISSN: 0947-7411. DOI: 10.1007/s00231-013-1210-3. URL: http://link.springer.com/10.1007/s00231-013-1210-3.

[33] Sylvain Quoilin et al. "Techno-economic survey of Organic Rankine Cycle (ORC) systems". In: *Renewable and Sustainable Energy Reviews* 22 (June 2013), pp. 168–186. ISSN: 1364-0321. DOI: 10.1016/J.RSER.2013.01.028. URL: https://www.sciencedirect.com/science/article/pii/S1364032113000592.

[34] Emmanouil Rogdakis and Periklis Lolos. "Kalina Cycles for Power Generation". In: *Handbook of Clean Energy Systems*. Chichester, UK: John Wiley & Sons, Ltd, July 2015, pp. 1–25. DOI: 10.1002/9781118991978.hces014. URL: http://doi.wiley.com/10.1002/9781118991978.hces014.

[35] Chengming Shi et al. "Heat transfer performance of lithium bromide solution in falling film generator". In: *International Journal of Heat and Mass Transfer* 53 (2010), pp. 3372–3376. DOI: 10.1016/j.ijheatmasstransfer.2010.02.051. URL: https://core.ac.uk/download/pdf/54188831.pdf.

[36] Lee Smith et al. "25 kW Low-Temperature Stirling Engine for Heat Recovery, Solar, and Biomass Applications". In: *Cool Energy* (2017), p. 20. URL: https://www.ohio.edu/mechanical/stirling/ISEC_2016_papers/ISEC2016-CoolEnergy.pdf.

[37] Daniel Suchna. "Návrh komponent pro experimentální smyčku LiBr absorpčního oběhu." PhD thesis. Prague: ČVUT, 2018. URL: https://dspace.cvut.cz/bitstream/handle/10467/80562/F2-DP-2018-Suchna-Daniel-SUCHNA%20DP%202018.pdf?sequence=-1&isAllowed=y.

[38] SWEP. "B15T Product Sheet". 2018. URL: https://www.swep.net/products/b5t/.

[39] TOPSFLO. *MG200XK&DC24WI Product List*. 2019. URL: http://www.topsflo.com/micro-gear-pump/mg200xk-dc24wi.html#Curve.

[40] UCEEB. *Jak je to nyní s mikroelektrárnou WAVE? Několik postřehů z jejího vývoje | UCEEB*. 2018. URL: https://www.uceeb.cz/aktuality/jak-je-nyni-s-mikroelektrarnou-wave-nekolik-postrehu-z-jejiho-vyvoje.

[41] Fredy Vélez et al. "Low temperature heat source for power generation: Exhaustive analysis of a carbon dioxide transcritical power cycle". In: *Energy* 36.9 (Sept. 2011), pp. 5497–5507. ISSN: 0360-5442. DOI: 10.1016/J.ENERGY.2011.07.027. URL: https://www.sciencedirect.com/science/article/pii/S0360544211004750.

[42] Gary C. Vliet, Michael B. Lawson, and Rudolfo Lithgow. *Water-Lithium Bromide Double-Effect Absorption Cooling Analysis*. Tech. rep. Center for Energy Studies, Univeristy of Texass, 1980. URL: https://www.osti.gov/servlets/purl/6727822/.

[43] Jiangfeng Wang, Yiping Dai, and Lin Gao. "Parametric analysis and optimization for a combined power and refrigeration cycle". In: *Applied Energy* 85.11 (Nov. 2008), pp. 1071–1085. ISSN: 03062619. DOI: 10.1016/j.apenergy.2008.02.014. URL: http://www.sciencedirect.com/science/article/pii/S0306261908000536.

[44] Xiaolin Wang and Hui T. Chua. "Absorption Cooling: A Review of Lithium Bromide-Water Chiller Technologies". In: *Recent Patents on Mechanical Engineering* 2.3 (Jan. 2010), pp. 193–213. ISSN: 1874477X. DOI: 10.2174/1874477X10902030193. URL: http://www.scopus.com/inward/record.url?eid=2-s2.0-77951632768&partnerID=tZOtx3y1.

[45] Andreas P Weiß. "Volumetric expander versus turbine – which is the better choice for small ORC plants". In: *3rd ASME ORC Conference, Brussels (Belgium)*. 2015, pp. 1–10.

[46] Peter Whittaker. "Corrosion in the Kalina cycle". PhD thesis. The School of Renewable Energy Science, 2009, p. 79. URL: http://skemman.is/stream/get/1946/7042/17795/1/Peter_Whittaker.pdf.

[47] Edward Xu. "Green Energy Island Integration and Operation Optimization Research". PhD thesis. 2018. URL: https://www.researchgate.net/publication/326912104_Green_Energy_Island_Integration_and_Operation_Optimization_Research_lusenengyuandaojichengyuyouhuayunxingyanjiu.

[48] Feng Xu, D Yogi Goswami, and Sunil S. Bhagwat. "A combined power/cooling cycle". In: *Energy* 25.3 (Mar. 2000), pp. 233–246. ISSN: 03605442. DOI: 10.

1016/S0360-5442(99)00071-7. URL: http://www.sciencedirect.com/science/article/pii/S0360544299000717.

[49] Jung-In Yoon et al. "Heat and mass transfer characteristics of a small helical absorber". In: *Applied Thermal Engineering* 26.2-3 (Feb. 2006), pp. 186–192. ISSN: 1359-4311. DOI: 10.1016/J.APPLTHERMALENG.2005.05.009. URL: https://www.sciencedirect.com/science/article/pii/S1359431105001742.

[50] CuiZhen Zhang et al. "2012 International Conference on Medical Physics and Biomedical Engineering Thermal Economic Analysis on LiBr Refrigeration -Heat Pump System Applied in CCHP System". In: *Physics Procedia* 33 (2012), pp. 672–677. ISSN: 18753892. DOI: 10.1016/j.phpro.2012.05.119. URL: http://www.sciencedirect.com/science/article/pii/S1875389212014320.

Appendices

A

P&ID of the APC unit

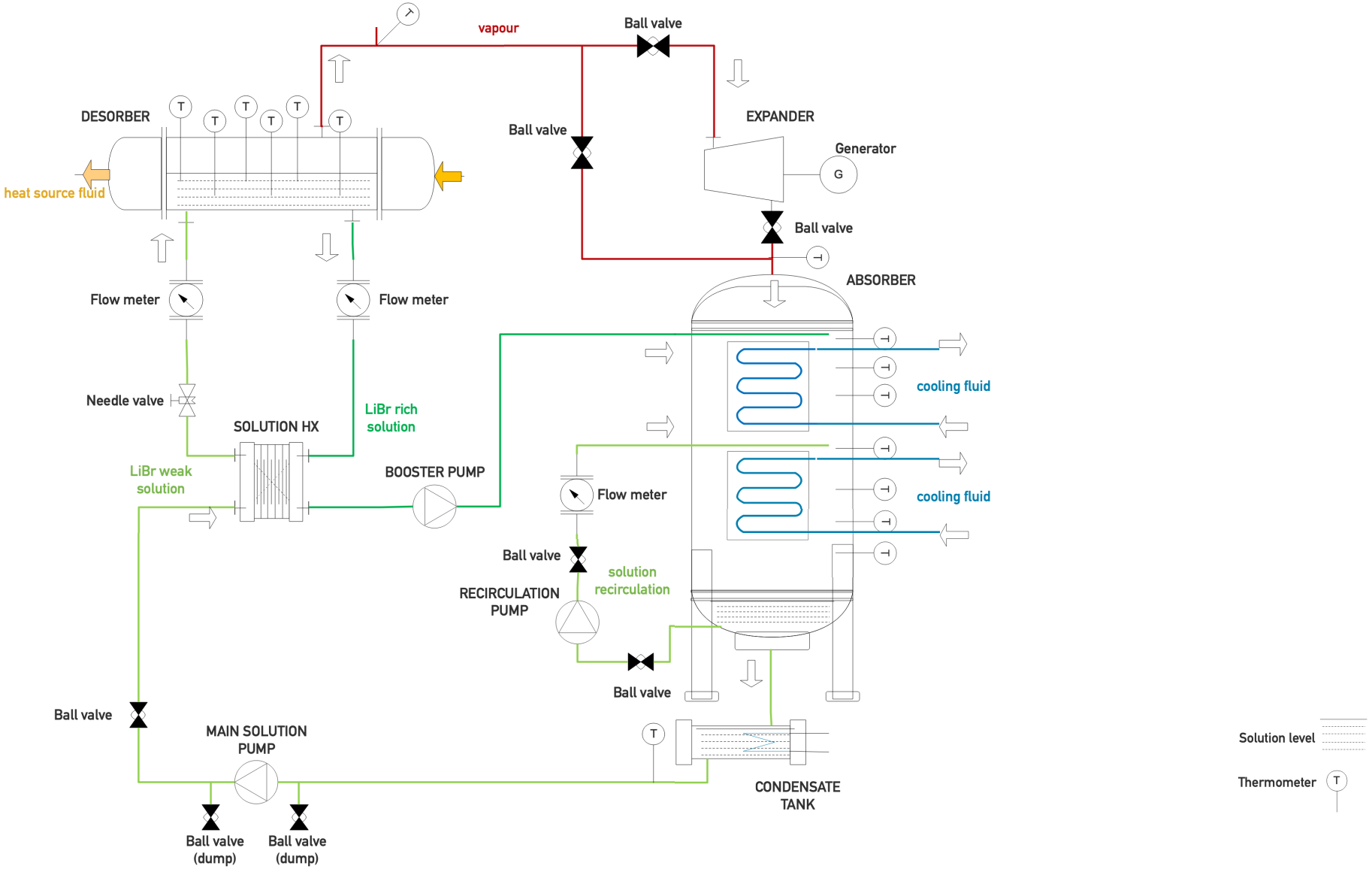

P&ID APC

1.6.2019
D. J. Szucs

B

Computational model of the APC in a from of formatted equations in EES

Generated in EES program based on the model from Ing. Novotný.

$t_e = 20$ *ambient temperature*

$T_{21} = 90$ *heat source temperature set*

$p_{21} = 2$ *heat source pressure set*

$Q_{in} = 20$ *kW*

$p_{31} = 2$ *cooling water pressure in [bar]*

Li-Br Novotny-Kolovratnik novel termodynamic cycle

units - deg C, bar

hot source definition

m_{21}=0,3

$m_{21} = m_{19}$ *heat source mass flow set r*

$h_{21} = \mathbf{h}(\text{steam}_{\text{iapws}}; T = T_{21}; P = p_{21})$ *enthalpy of entering heat source stream*

$s_{21} = \mathbf{s}(\text{steam}_{\text{iapws}}; T = T_{21}; P = p_{21})$

Controlling parameters

$T_{11} = 44{,}5$

setting of final absorber temperature (value is result of optimization)

$w_1 = 0{,}65$

setting of weak solution concentration (value is result of optimization)

$w_7 = 0{,}5$

setting of rich solution concentration (value is result of optimization)

$T_{21} = \text{AoptT}_{21}$

$T_{11} = \text{AoptT}_{11}$

$w_1 = \text{AoptW}_1$

$w_7 = \text{AoptW}_7$

pressure and concentration levels

$p_2 = p_1$

$p_3 = p_1$

$p_4 = p_1$

$p_5 = p_1$

$p_7 = p_1$

$w_2 = 1 - \left[\frac{m_{libr}}{m_w + m_{libr}}\right]$ *m_{libr} je celkové mnozství cirkulujícího LiBr, m_w je mnozství cirkulující vody*

$w_3 = w_2$

$w_5 = 1$

$w_6 = 1$

$w_{11} = w_2$

$w_1 = w_2$

$w_4 = w_2$

HEAT INPUT

Heating up to boiling point

$\Delta\text{Tmin}_{\text{hot}} = 10$ *Minimal temperature difference in HX on hot side ---Sem asi dám neco mezi 10 a 11 aby vychazel bol tri v desorberu*

dTse = 21

$\Delta_{T;100} = \text{dTse}$

$Q_{in} = Q_{FWH} + Q_{eva}$

$Q_{FWH} = m_2 \cdot (h_3 - h_2)$ *Mnozství tepla dodaného pri ohrevu prac. látky pred zacátkem varu*

$Q_{FWH} = m_{21} \cdot (h_{22} - h_{23})$ *Mnozství tepla dodaného pri ohrevu prac. látky pred zacátkem varu urcuje i entalpii výstupu zdroje tepla*

Call $\mathbf{s}_{\text{ptxi;WaLi;EES}}('';\ p_2;\ T_2;\ w_3 : s_2)$ *Z tlaku, T a w je urcena entropie na pocátku privodu externího tepla*

$T_{23} = \mathbf{T}(\text{steam}_{\text{iapws}}; h = h_{23}; P = p_{21})$ *teplota výstupu zdroje tepla*

$s_{23} = \mathbf{s}(\text{steam}_{\text{iapws}}; h = h_{23}; P = p_{21})$ *jenom dodatek do T-s*

Boiling

$m_3 = m_2$

Call $\mathbf{ps}_{\text{tsxil;WaLi;EES}}('';\ T_3;\ w_3 : p_3)$ *bod 3 je na mezní krivce - pocátek varu*

Call $\mathbf{hl}_{\text{pstsxil;WaLi;EES}}('';\ -1;\ T_3;\ w_3 : h_3)$ *Z teploty (urcené z chlazení zdroje tepla) a koncentrace je ur*

Call $\mathbf{sl}_{\text{pstsxil;WaLi;EES}}('';\ -1;\ T_3;\ w_3 : s_3)$ *Z teploty (urcené z chlazení zdroje tepla) a koncentrace je ur*

entalpie na pocátku varu

entropie na pocátku varu

$m_4 = m_3$

Call $\mathbf{ps}_{\text{tsxil;WaLi;EES}}('';\ T_4;\ w_7 : p_4)$ *v bode 4 je urcena teplota a koncentrace kapalné fáze ->tlak*

$Q_{eva} = h_4 \cdot m_4 - h_2 \cdot m_2$ *teplo predané pri varu*

$Q_{eva} = m_{21} \cdot (h_{21} - h_{22})$ *teplo predané pri varu - urcuje entalpii v bode 23*

$T_{22} = \mathbf{T}(\text{steam}_{\text{iapws}}; h = h_{22}; P = p_{21})$ *teplota v bode 23*

$s_{22} = \mathbf{s}(\text{steam}_{\text{iapws}}; h = h_{22}; P = p_{21})$ *dodatek do T-s*

Separator

$w_7 = \frac{m_{w;separ}}{m_{w;separ} + m_{libr}}$ *z rovnic je ur*

mé množství separované z odvodněném stavu a celkové páry (5) a roztoku (7)

mé množství separované z odvodněném stavu a celkové páry (5) a roztoku (7)

Tyé množství separované z odvodněném stavu a celkové páry (5) a roztoku (7)

$T_7 = T_4$ *pYi isobarické separaci by mě la být zachována rovnost teplot vsech slozek*

$h_4 \cdot m_4 = m_5 \cdot h_5 + m_7 \cdot h_7$ *energy balance*

$s_4 \cdot m_4 = m_5 \cdot s_5 + m_7 \cdot s_7$ *entropy balance*

Call $\mathbf{hv}_{pstsxil;WaLi;EES}$ ('' ; p_5 ; – 1 ; w_7 : h_5)

$s_5 = \mathbf{s}$ (steam$_{iapws}$; P = p_5 ; T = T_5) *entropy of vapour stream*

Call $\mathbf{hl}_{pstsxil;WaLi;EES}$ ('' ; – 1 ; T_7 ; w_7 : h_7) *enthalpy of liquid stream*

Call $\mathbf{sl}_{pstsxil;WaLi;EES}$ ('' ; – 1 ; T_7 ; w_7 : s_7) *entropy of liquid stream*

$x_{sep} = \frac{m_w - m_{w;separ}}{m_{libr} + m_w}$

TURBINE

$\eta_{turb} = 0{,}4$ *defines turbine efficiency*

$m_6 = m_5$

$p_6 = \mathbf{P}$ (steam$_{iapws}$; x = 0 ; T = T_6) *returns pressure for given outlet temperature (expansion ends in wet steam)*

$h_{e;ad} = \mathbf{h}$ (steam$_{iapws}$; s = s_5 ; P = p_6) *isentropic outlet enthalpy*

$h_6 = h_5 - (h_5 - h_{e;ad}) \cdot \eta_{turb}$ *real outlet enthalpy*

$s_6 = \mathbf{s}$ (steam$_{iapws}$; h = h_6 ; P = p_6) *outlet entropy*

$x_{steam;e} = \mathbf{x}$ (steam$_{iapws}$; h = h_6 ; P = p_6) *outlet steam quality*

$W_{turb} = m_5 \cdot (h_5 - h_6)$ *produced power*

$\rho_{v;6} = \rho$ (steam$_{iapws}$; h = h_6 ; P = p_6)

Recuperator

$m_2 = m_1$

$m_8 = m_7$

$w_8 = w_7$

$p_8 = p_7$

TTD = 5 *definition of recuperator HX minimal terminal temperature difference*

$T_8 - T_1 = TTD$ *recuperator HX minimal terminal temperature difference applied*

Call $\mathbf{h}_{ptxi;WaLi;EES}$ ('' ; p_8 ; T_8 ; w_7 : h_8) *entropy calculation after regeneration of rich solution*

$Q_{reg} = m_7 \cdot (h_7 - h_8)$ *energy balance*

$Q_{reg} = m_1 \cdot (h_2 - h_1)$ *energy balance*

Call $\mathbf{t}_{phxi;WaLi;EES}$ ('' ; p_2 ; h_2 ; w_2 : T_2) *returns T after recuperator*

Call $\mathbf{sl}_{pstsxil;WaLi;EES}$ ('' ; p_8 ; – 1 ; w_8 : s_8)

Call $\mathbf{sl}_{pstsxil;WaLi;EES}$ ('' ; p_9 ; – 1 ; w_9 : s_9)

Call $\mathbf{t}_{phxi;WaLi;EES}$ ('' ; p_9 ; h_9 ; w_9 : T_9)

Call $\mathbf{v}_{ptxi;WaLi;EES}$ ('' ; p_8 ; T_8 ; w_8 : v_8)

$Vol_8 = m_8 \cdot v_8$

QT diagram recuperator

$T_{hs;137} = T_7$

$T_{137} = T_2$

$Q_{tot;137} = 0$

$T_{hs;138} = T_8$

$T_{138} = T_1$

$Q_{tot;138} = Q_{reg}$

MIXING (beginning of absorber - condenser)

$m_{10} = m_{libr} + m_w$ *total mass flow*

$p_{10} = p_6$

$m_6 \cdot h_6 + m_8 \cdot h_8 = m_{10} \cdot h_{10}$ *energy balance*

CONDENSER - ABSORBER

$m_{11} = m_{10}$

$p_{11} = p_{10}$

Call $\mathbf{t}_{phxi;WaLi;EES}$ ('' ; p_{10} ; h_{10} ; w_{11} : T_{10}) *vypocet teploty na zacatku absorbce*

Call $\mathbf{xil}_{psts;WaLi;EES}$ ('' ; p_{10} ; T_{10} : w_{10})

$m_{cl} \cdot (1 - w_{10}) = m_{libr}$

$m_8 + m_6 = m_{cl} + m_{cv}$ *mass balance for the same*

$h_{cv} = \mathbf{h}$ (steam$_{iapws}$; T = T_{10} ; P = p_{10})

enthalpy of vapour phase

Call $\mathbf{sl}_{pstsxil;WaLi;EES}$ ('' ; -1 ; T_{10} ; w_{10} : $s_{10;l}$) *liquid phase entropy*

Call $\mathbf{s}_{ptxi;WaLi;EES}$ ('' ; p_{10} ; T_{10} ; w_{11} : s_{10}) *overall entropy*

Call $\mathbf{ps}_{tsxil;WaLi;EES}$ ('' ; T_{11} ; w_{11} : p_{11}) *this function actually defines the condensing pressure from given weak solution concentration and set temperature(also for functions backward)*

Call $\mathbf{hl}_{pstsxil;WaLi;EES}$ ('' ; -1 ; T_{11} ; w_{11} : h_{11}) *gives enthalpy at the end of absorption*

Call $\mathbf{sl}_{pstsxil;WaLi;EES}$ ('' ; -1 ; T_{11} ; w_{11} : s_{11}) *gives entropy at the end of absorption*

$Q_{rej} = m_{10} \cdot (h_{10} - h_{11})$ *energy balance*

$Q_{rej} = m_{31} \cdot (h_{35} - h_{31})$ *energy balance*

PUMP

$\eta_p = 0{,}2$ *pump efficiency*

$m_1 = m_{11}$

Call $\mathbf{t}_{psxi;WaLi;EES}$ ('' ; p_1 ; s_{11} ; w_1 : $t_{1;ad}$) *isentropic temperature*

Call $\mathbf{h}_{ptxi;WaLi;EES}$ ('' ; p_1 ; $t_{1;ad}$; w_1 : $h_{1;ad}$) *isentropic enthalpy via temperature (wasn't direct function with entropy)*

$$h_1 = h_{11} + \frac{h_{1;ad} - h_{11}}{\eta_p}$$ *real outlet enthalpy*

Call $\mathbf{t}_{phxi;WaLi;EES}$ ('' ; p_1 ; h_1 ; w_1 : T_1) *outlet temperature*

Call $\mathbf{s}_{ptxi;WaLi;EES}$ ('' ; p_1 ; T_1 ; w_1 : s_1) *outlet entropy*

$W_{pump} = m_1 \cdot (h_1 - h_{11})$ *pump power*

Call $\mathbf{v}_{ptxi;WaLi;EES}$ ('' ; p_{11} ; T_{11} ; w_{11} : v_{11})

$$\rho_{l;11} = \frac{1}{v_{11}}$$

$Vol_{11} = m_{11} \cdot v_{11}$

$$veloc_{1;11} = \frac{Vol_{11}}{\pi \cdot \frac{(6{,}8 \cdot 10^{-3})^2}{4}}$$

Call $\mathbf{eta}_{ptxi;WaLi;EES}$ ('' ; p_1 ; T_1 ; w_1 : $\mu_{l;1}$)

Throttling

$p_9 = p_{10}$

$m_9 = m_8$

$h_9 = h_8$

$w_9 = w_8$

Call $\mathbf{vl}_{pstsxil;WaLi;EES}$ ('' ; p_{11} ; -1 ; w_{11} : v_2)

$Vol_2 = m_{11} \cdot v_2$

Overal

$W_{plant} = W_{turb} - W_{pump}$ *power output (gross, excluding heat rejection fan)*

Q-T and parameter Distribution

Desorber

start

$n = 30$

$start_{eva} = 100$

$end_{eva} = 100 + n$

$T_{100} = T_2$

$h_{100} = h_2$

$h_{fluid;100} = h_{23}$

$T_{hs;100} = T_{23}$

$h_{orc;100} = \mathbf{h}(mm ; T = T_{orc;100} ; x = 0)$

$T_{orc;100} = 95$

$p_{orc} = \mathbf{P}(mm ; T = T_{orc;100} ; x = 0)$

m_{orc}=0,1

$T_{orc;eva} = 180$

$p_{orc;eva} = \mathbf{P}(mm ; T = T_{orc;eva} ; x = 1)$

$h_{orc;turb} = \mathbf{h}(mm ; P = p_{orc;eva} ; x = 1)$

$s_{orc} = \mathbf{s}(mm ; T = T_{orc;eva} ; x = 1)$

$h_{orc;end;ie} = \mathbf{h}(mm ; P = p_{orc} ; s = s_{orc})$

$$0{,}5 = \frac{h_{orc;turb} - h_{orc;real}}{h_{orc;turb} - h_{orc;end;ie}}$$

$Q_{in} = m_{orc} \cdot (h_{orc;real} - h_{orc;100})$

$m_{vap;100} = 0$

$w_{100} = w_3$

$Q_{tot;100} = 0$

$\Delta T_{;100} = T_{23} - T_2$

two phase flow parameters

$m_{10} = m_{wf}$

$\sigma_{LiBr} = 0,06$ *N/m, meni se s teplotou a koncentraci, ale ne moc a nemame na to funkci tady*

$C_{sf} = 0,0136$ *koeficienty do Rohsenow pool boiling (surface-fluid combination)*

$n_{coef} = 0,85$

$k_{Cu} = \mathbf{k}(\text{Copper}; T = 90)$

$l_{trubky} = 0,001$ *tloustka steny trubky*

$R_{trubky} = \frac{l_{trubky}}{k_{Cu}}$ *nikde nepouzito*

$aux_{q;avg} = \frac{Q_{in}}{A_{des}}$

Call $\mathbf{xil}_{psts;WaLi;EES}('';\ p_1;\ T_{100}:\ xil_{100})$

$xil_{100} = \frac{m_{liq;w;100}}{m_{liq;w;100} + m_{libr}}$

$m_{liq;100} = m_{liq;w;100} + m_{libr}$

$x_{steam;100} = \frac{m_{libr} + m_w - m_{liq;100}}{m_{libr} + m_w}$

Call $\mathbf{vl}_{pstsxil;WaLi;EES}('';\ p_1;\ -1;\ xil_{100}:\ v_{l;100})$

Call $\mathbf{vv}_{pstsxil;WaLi;EES}('';\ p_1;\ -1;\ xil_{100}:\ v_{v;100})$

$\rho_{l;100} = \frac{1}{v_{l;100}}$ *density of liq*

$\rho_{v;100} = \frac{1}{v_{v;100}}$ *density of vap*

$A_{tot;100} = 0$

$dh_{eva} = \frac{h_4 - h_2}{n}$

$h_i = h_{i-1} + dh_{eva}$ (for $i = start_{eva}+1$ to end_{eva})

$dQ_{eva;i} = m_1 \cdot dh_{eva}$ (for $i = start_{eva}+1$ to end_{eva})

$Q_{tot;i} = Q_{tot;i-1} + dQ_{eva;i}$ (for $i = start_{eva}+1$ to end_{eva})

Call $\mathbf{t}_{phxi;WaLi;EES}('';\ p_1;\ h_i;\ w_1:\ T_i)$ (for $i = start_{eva}+1$ to end_{eva})

$h_{fluid;i} - h_{fluid;i-1} = \frac{dQ_{eva;i}}{m_{21}}$ (for $i = start_{eva}+1$ to end_{eva})

$h_{fluid;i} = \mathbf{h}(steam_{iapws}; T = T_{hs;i}; P = p_{21})$ (for $i = start_{eva}+1$ to end_{eva})

$h_{orc;i} - h_{orc;i-1} = \frac{dQ_{eva;i}}{m_{orc}}$ (for $i = start_{eva}+1$ to end_{eva})

$T_{orc;i} = \mathbf{T}(mm;\ h = h_{orc;i};\ P = p_{orc})$ (for $i = start_{eva}+1$ to end_{eva}) *urceni teploty*

$\Delta_{T;i} = T_{hs;i} - T_i$ (for $i = start_{eva}+1$ to end_{eva})

two phase flow

Call $\mathbf{xil}_{psts;WaLi;EES}('';\ p_1;\ T_i:\ xil_i)$ (for $i = start_{eva}+1$ to end_{eva})

$xil_i = \frac{m_{liq;w;i}}{m_{liq;w;i} + m_{libr}}$ (for $i = start_{eva}+1$ to end_{eva})

$m_{liq;i} = m_{liq;w;i} + m_{libr}$ (for $i = start_{eva}+1$ to end_{eva})

$m_{vap;i} = m_{wf} - m_{liq;i}$ (for $i = start_{eva}+1$ to end_{eva})

$x_{steam;i} = \frac{m_{libr} + m_w - m_{liq;i}}{m_{libr} + m_w}$ (for $i = start_{eva}+1$ to end_{eva})

Call $\mathbf{vl}_{pstsxil;WaLi;EES}('';\ p_1;\ -1;\ xil_i:\ v_{l;i})$ (for $i = start_{eva}+1$ to end_{eva})

Call $\mathbf{vv}_{pstsxil;WaLi;EES}('';\ p_1;\ -1;\ xil_i:\ v_{v;i})$ (for $i = start_{eva}+1$ to end_{eva})

$Vol_{l;i} = m_{liq;i} \cdot v_{l;i}$ (for $i = start_{eva}+1$ to end_{eva})

$Vol_{v;i} = m_{vap;i} \cdot v_{v;i}$ (for $i = start_{eva}+1$ to end_{eva})

$Vol_i = Vol_{l;i} + Vol_{v;i}$ (for $i = start_{eva}+1$ to end_{eva})

$veloc_{l;i} = \frac{Vol_{l;i}}{des_{S;LiBr}}$ (for $i = start_{eva}+1$ to end_{eva})

$h_{steam;i} = \mathbf{h}(steam_{iapws}; T = T_i; P = p_1)$ (for $i = start_{eva}+1$ to end_{eva})

Call $\mathbf{hl}_{pstsxil;WaLi;EES}('';\ p_1;\ -1;\ xil_i:\ h_{sol;i})$ (for $i = start_{eva}+1$ to end_{eva})

parameters for HX design

$\rho_{L;i} = \frac{1}{v_{l;i}}$ (for $i = start_{eva}+1$ to end_{eva})

$\rho_{v;i} = \frac{1}{v_{v;i}}$ (for $i = start_{eva}+1$ to end_{eva})

Call $\mathbf{v}_{ptxi;WaLi;EES}('';\ p_1;\ T_i;\ w_1:\ )$ (for $i = start_{eva}+1$ to end_{eva})

Call $\mathbf{etal}_{pstsxil;WaLi;EES}('';\ p_1;\ T_i;\ -1:\ etal_i)$ (for $i = start_{eva}+1$ to end_{eva}) *dynamic viscosity of liquid in [Pas]*

pool boiling heat transfer

$h_{fg;i} = h_{steam;i} - h_{sol;i}$ (for $i = start_{eva}+1$ to end_{eva}) *latent heat*

Call $\mathbf{cpl}_{pstsxil;WaLi;EES}('';\ p_1;\ T_i;\ -1:\ cp_{l;i})$ (for $i = start_{eva}+1$ to end_{eva}) *c_p of liq*

Call $\mathbf{Prl}_{pstsxil;WaLi;EES}('';\ p_1;\ T_i;\ -1:\ Pr_{l;i})$ (for $i = start_{eva}+1$ to end_{eva}) *Prandtl of liq*

$$\frac{cp_{l;i}}{h_{fg;i}} \cdot (T_{surf;i} - T_i) = 0,0136 \cdot \left[\frac{\frac{q_{nucl;i}}{1000}}{etal_i \cdot h_{fg;i}} \cdot \left[\frac{\sigma_{LiBr}}{9,81 \cdot (\rho_{L;i} - \rho_{v;i})}\right]^{0,5}\right]^{0,34} \cdot Pr_{l;i}^{0,85}$$ (for $i = start_{eva}+1$ to end_{eva})

Charters et al.

$q_{nucl;i} = \alpha_{boil;i} \cdot (T_{surf;i} - T_i)$ (for i = $start_{eva}$+1 to end_{eva}) *jo, alfa vychazi nejak mala, prosim kontrolu*

$R_{water;i} = \frac{1}{\alpha_{hs;i} \cdot dD_{ratio}}$ (for i = $start_{eva}$+1 to end_{eva}) *replacement of commented alpha -> dle korelace*

$R_{boil;i} = \frac{1}{\alpha_{boil;i}}$ (for i = $start_{eva}$+1 to end_{eva}) *thermal resistance for working medium boiling*

$q_{boil;i} = \frac{T_{hs;i} - T_i}{R_{water;i} + R_{wall;des} + R_{boil;i}}$ (for i = $start_{eva}$+1 to end_{eva}) *doplneni o kondukci ve stěně ...*

$q_{boil;i} = q_{nucl;i}$ (for i = $start_{eva}$+1 to end_{eva}) *místo zakomentovane natvrdo urcene teploty povrchu pro prvni odhad*

$dQ_{eva;i} \cdot 1000 = A_{des;i} \cdot q_{boil;i}$ (for i = $start_{eva}$+1 to end_{eva}) *jednotky W*

$\rho_{hs;i} = \rho(steam_{iapws}; T = T_{hs;i}; P = p_{21})$ (for i = $start_{eva}$+1 to end_{eva})

$v_{hs;i} = \frac{1}{\rho_{hs;i}}$ (for i = $start_{eva}$+1 to end_{eva})

$Vol_{hs;i} = v_{hs;i} \cdot m_{21} \cdot 3600$ (for i = $start_{eva}$+1 to end_{eva}) *overall volume flow in [m^3/h]*

$Vol_{hs;tube;i} = \frac{Vol_{hs;i}}{nr_{tube}}$ (for i = $start_{eva}$+1 to end_{eva}) *in [m^3/h]*

$veloc_{hs;i} = Vol_{hs;i} \cdot \frac{\frac{1}{3600}}{nr_{tube} \cdot \frac{\pi \cdot d_{tube;i}^2}{4}}$ (for i = $start_{eva}$+1 to end_{eva})

$Pr_{hs;i} = \mathbf{Pr}(steam_{iapws}; T = T_{hs;i}; P = p_{21})$ (for i = $start_{eva}$+1 to end_{eva})

$\mu_{hs;i} = \mathbf{Visc}(steam_{iapws}; T = T_{hs;i}; P = p_{21})$ (for i = $start_{eva}$+1 to end_{eva})

$Re_{hs;i} = \frac{m_{21}}{nr_{tube} \cdot \frac{\pi \cdot d_{tube;i}^2}{4}} \cdot \frac{d_{h;des}}{\mu_{hs;i}}$ (for i = $start_{eva}$+1 to end_{eva})

$f_{coef;i} = (0{,}79 \cdot \mathbf{ln}(Re_{hs;i}) - 1{,}64)^{-2}$ (for i = $start_{eva}$+1 to end_{eva})

$Nuss_{hs;i} = \frac{f_{coef;i}}{8} \cdot (Re_{hs;i} - 1000) \cdot \left[\frac{Pr_{hs;i}}{1 + 12{,}7 \cdot \left[\frac{f_{coef;i}}{8}\right]^{(1/2)} \cdot (Pr_{hs;i}^{(2/3)} - 1)}\right]$ (for i = $start_{eva}$+1 to end_{eva})

Gnielinski correlation: Re(3000-5000000)

$k_{hs;i} = \mathbf{k}(steam_{iapws}; T = T_{hs;i}; P = p_{21})$ (for i = $start_{eva}$+1 to end_{eva})

$Nuss_{hs;i} = d_{h;des} \cdot \frac{\alpha_{hs;i}}{k_{hs;i}}$ (for i = $start_{eva}$+1 to end_{eva}) *from here, alpha$_{hs,i}$ of the cooling water*

$A_{tot;i} = A_{tot;i-1} + A_{des;i}$ (for i = $start_{eva}$+1 to end_{eva})

$PP_{hot} = \mathbf{Min}(\Delta_{T;start;eva..end;eva})$

$PP_{hot} = \Delta Tmin_{hot}$ ----------

$A_{des} = \mathbf{Sum}(A_{des;101..end;eva})$

$Q_{flux;des} = \frac{Q_{in}}{A_{des}}$

$\alpha_{hs;des;aver} = \frac{\mathbf{Sum}(\alpha_{hs;101..end;eva})}{n - 1}$

$\alpha_{boil;des;aver} = \frac{\mathbf{Sum}(\alpha_{boil;101..end;eva})}{n - 1}$

$Re_{hs;des;aver} = \frac{\mathbf{Sum}(Re_{hs;101..end;eva})}{n - 1}$

design of Shell and Tube desorber

$nr_{tube} = 70$

$A_{des} = nr_{tube} \cdot \pi \cdot d_{tube;o} \cdot L_{tube;need}$ *vypocet potrene delky trubek*

$d_{tube;o} = d_{tube;i} + 2 \cdot thick_{des}$

$d_{tube;i} = \frac{8{,}8}{1000}$ *DN8* ----------

$thick_{des} = \frac{2{,}35}{1000}$ *DN8 tlouska trubek v m*

$d_{h;des} = d_{tube;i}$ *charakteristicky rozmer totozny vnitrnimu prumeru trubky*

$k_{wall;des} = \mathbf{k}(Stainless_{AISI316}; T = T_{21})$

$R_{wall;des} = \frac{thick_{des}}{k_{wall;des}}$

$dD_{ratio} = \frac{d_{tube;i}}{d_{tube;o}}$

$S_{shell} = 3{,}14159 \cdot \frac{0{,}18^2}{4 \cdot 2}$

$S_{pipes} = 3{,}142 \cdot \frac{d_{tube;o}^2}{4} \cdot nr_{tube}$

$des_{S;LiBr} = S_{shell} - S_{pipes}$

$Dratio_{sh;bu;the;max} = 1 + 0{,}02 \cdot \frac{q_{boil;101}}{1000}$ *theoretical shell to bundle height ratio*

$Dratio_{sh;bu;actual} = \frac{213{,}9}{138}$

Condenser - Absorber

n2 = 30 *number of HX elements*

$start_{cond} = 150$ *array positions for HX elements*

$end_{cond} = 150 + n2$ *array positions for HX elements*

definition of properties at HX end

$T_{150} = T_{10}$

$w_{start,cond}=w_{10}$

$Q_{tot;150} = 0$

$h_{150} = h_{10}$

$h_{fluid;180} = h_{31}$

$T_{hs;150} = \mathbf{T}(steam_{iapws}; h = h_{35}; P = p_{31})$ *water inlet temperaure*

$\Delta_{T;150} = T_{10} - T_{35}$

$\mu_{l;150} = \mathbf{Visc}(steam_{iapws}; T = T_{hs;150}; P = p_{21})$

$Pr_{hs;150} = \mathbf{Pr}(steam_{iapws}; T = T_{hs;150}; P = p_{21})$

$$Re_{hs;150} = \frac{m_{31}}{Circles_{cw;abs} \cdot S_{cw;inner}} \cdot \frac{d_{cw}}{\mu_{l;150}}$$

$$Nuss_{hs;150} = \frac{f_{coef;150}}{8} \cdot (Re_{hs;150} - 1000) \cdot \left[\frac{Pr_{hs;150}}{1 + 12{,}7 \cdot \left[\frac{f_{coef;150}}{8}\right]^{(1/2)} \cdot (Pr_{hs;150}^{(2/3)} - 1)}\right]$$

$$f_{coef;150} = (0{,}79 \cdot \ln(Re_{hs;150}) - 1{,}64)^{-2}$$

$k_{hs;150} = \mathbf{k}(steam_{iapws}; T = T_{hs;150}; P = p_{21})$

$$Nuss_{hs;150} = d_{cw} \cdot \frac{\alpha_{hs;150}}{k_{hs;150}}$$

$$R_{cf;abs;150} = \frac{1}{\alpha_{hs;150}}$$

xi a x na pocatku

Call $\mathbf{xil}_{psts;WaLi;EES}('';\ p_{11};\ T_{150} : xil_{150})$

$$xil_{150} = \frac{m_{liq;w;150}}{m_{liq;w;150} + m_{libr}}$$

$m_{liq;150} = m_{liq;w;150} + m_{libr}$

$m_{vap;150} = m_{wf} - m_{liq;150}$

$$x_{steam;150} = \frac{m_{libr} + m_w - m_{liq;150}}{m_{libr} + m_w}$$ *muze vyjit spatne kvuli chybe z podchlazeni pod var ciste vody*

$A_{tot;150} = 0$

prestup tepla -> abs

$T_{L,0}=T_{10}$-1,5

$K_L = 0{,}00001$ *3e-5 m/s*

$alpha_{vl}$=0,005

$\alpha_{wf;abs} = 2000$ *convection coefficient in [W/m^2 K] - working fluid side (2000 W/m^2 K)*

$$R_{wall;abs} = \frac{thick_{abs}}{k_{wall;abs}}$$ *jeden z clenu v menovateli pro energy balance (dQ)*

$k_{wall;abs} = \mathbf{k}(Stainless_{AISI304}; T = T_{35})$

$$R_{wf;abs} = \frac{1}{\alpha_{wf;abs}}$$

$$dh_{cond} = \frac{h_{10} - h_{11}}{n}$$

loop of equations for the HX elements

$h_i = h_{i-1} - dh_{cond}$ (for $i = start_{cond}+1$ to end_{cond})

Call $\mathbf{t}_{phxi;WaLi;EES}('';\ p_{11};\ h_i;\ w_{11} : T_i)$ (for $i = start_{cond}+1$ to end_{cond}) *Urceni T_i*

$dQ_{cond;i} = m_1 \cdot dh_{cond}$ (for $i = start_{cond}+1$ to end_{cond})

$Q_{tot;i} = Q_{tot;i-1} + dQ_{cond;i}$ (for $i = start_{cond}+1$ to end_{cond})

$h_{fluid;i-1} - h_{fluid;i} = \frac{dQ_{cond;i}}{m_{31}}$ (for $i = start_{cond}+1$ to end_{cond})

$h_{fluid;i} = \mathbf{h}(steam_{iapws}; T = T_{hs;i}; P = 2)$ (for $i = start_{cond}+1$ to end_{cond})

$\Delta_{T;i} = T_i - T_{hs;i}$ (for $i = start_{cond}+1$ to end_{cond})

two phase flow and concentrations

Call $\mathbf{xil}_{psts;WaLi;EES}('';\ p_{11};\ T_i : xil_i)$ (for $i = start_{cond}+1$ to end_{cond})

$xil_i = \frac{m_{liq;w;i}}{m_{liq;w;i} + m_{libr}}$ (for $i = start_{cond}+1$ to end_{cond})

$m_{liq;i} = m_{liq;w;i} + m_{libr}$ (for $i = start_{cond}+1$ to end_{cond})

$m_{vap;i} = m_{wf} - m_{liq;i}$ (for $i = start_{cond}+1$ to end_{cond})

$x_{steam;i} = \frac{m_{libr} + m_w - m_{liq;i}}{m_{libr} + m_w}$ (for $i = start_{cond}+1$ to end_{cond})

Call $\mathbf{vl}_{pstsxil;WaLi;EES}('';\ p_{11};\ -1;\ xil_i : v_{l;i})$ (for $i = start_{cond}+1$ to end_{cond})

Call $\mathbf{vv}_{pstsxil;WaLi;EES}('';\ p_{11};\ -1;\ xil_i : v_{v;i})$ (for $i = start_{cond}+1$ to end_{cond})

$\rho_{v;i} = \frac{1}{v_{v;i}}$ (for $i = start_{cond}+1$ to end_{cond})

$m_{abs;i} = m_{vap;i-1} - m_{vap;i}$ (for $i = start_{cond}+1$ to end_{cond}) *required absorbed mass flow in each element*

$Vol_{l;i} = v_{l;i} \cdot m_{liq;i}$ (for $i = start_{cond}+1$ to end_{cond})

$\Gamma_i = \frac{m_{liq;i}}{O_{loops}}$ (for i = start$_{cond}$+1 to end$_{cond}$)

Call **etal**$_{pstsxil;WaLi;EES}$ ('' ; p_{11} ; – 1 ; xil_i : $\mu_{l;i}$) (for i = start$_{cond}$+1 to end$_{cond}$)

$Re_i = 4 \cdot \frac{\Gamma_i}{\mu_{l;i}}$ (for i = start$_{cond}$+1 to end$_{cond}$)

$\alpha_i = 129{,}7712 \cdot (1 - xil_{i-1})^{-0{,}8058} \cdot \left[dQ_{cond;i} \cdot \frac{1000}{A_i}\right]^{0{,}2422} \cdot Re_i^{-0{,}0856}$ (for i = start$_{cond}$+1 to end$_{cond}$)

correlation from LiBr film falling evaporation

Call **hl**$_{pstsxil;WaLi;EES}$ ('' ; p_{11} ; – 1 ; xil_i : $h_{sol;i}$) (for i = start$_{cond}$+1 to end$_{cond}$) *later comment as calculated later from unequilibrium mod l*

Call **xil**$_{psts;WaLi;EES}$ ('' ; p_{10} ; $T_{L;i}$: $\xi_{Lsat;i}$) (for i = start$_{cond}$+1 to end$_{cond}$) *concentration of LiBrH2O at saturated liquid state at point i*

Call **vl**$_{pstsxil;WaLi;EES}$ ('' ; – 1 ; $T_{L;i}$; xil_i :) (for i = start$_{cond}$+1 to end$_{cond}$) *density of liquid LiBrH2O solution at i*

$m_{abs;i} = K_L \cdot (\xi_{Lsat;i} - xil_i) \cdot A_i \cdot \rho_{L;i}$ (for i = start$_{cond}$+1 to end$_{cond}$) *from here A_i is calculated*

$(T_{L;i} - T_{hs;i}) \cdot \left[\frac{A_i}{R_{wf;abs} + R_{wall;abs} + R_{cf;abs;i}}\right] = 1000 \cdot dQ_{cond;i}$ (for i = start$_{cond}$+1 to end$_{cond}$) *from here $T_{L,i}$ is calculated (in [W])*

$q_{nucl;i} = dQ_{cond;i} \cdot \frac{1000}{A_i}$ (for i = start$_{cond}$+1 to end$_{cond}$) *heat flux at i ... no need for new parameter*

$\mu_{hs;i}$ = **Visc** (steam$_{iapws}$; T = $T_{hs;i}$; P = p_{31}) (for i = start$_{cond}$+1 to end$_{cond}$)

$Pr_{hs;i}$ = **Pr** (steam$_{iapws}$; T = $T_{hs;i}$; P = p_{31}) (for i = start$_{cond}$+1 to end$_{cond}$)

$Re_{hs;i} = \frac{m_{31}}{Circles_{cw;abs} \cdot S_{cw;inner}} \cdot \frac{d_{cw}}{\mu_{hs;i}}$ (for i = start$_{cond}$+1 to end$_{cond}$)

$De_{hs;i} = Re_{hs;i} \cdot \sqrt{\frac{d_{cw}}{2 \cdot \frac{d_{cw;axis;51}}{2}}}$ (for i = start$_{cond}$+1 to end$_{cond}$)

$Nuss_{hs;De;i} = 0{,}0551 \cdot De_{hs;i}^{0{,}864} \cdot Pr_{hs;i}^{0{,}4}$ (for i = start$_{cond}$+1 to end$_{cond}$)

$f_{coef;i} = (0{,}79 \cdot \ln(Re_{hs;i}) - 1{,}64)^{-2}$ (for i = start$_{cond}$+1 to end$_{cond}$)

$Nuss_{hs;i} = \frac{f_{coef;i}}{8} \cdot (Re_{hs;i} - 1000) \cdot \left[\frac{Pr_{hs;i}}{1 + 12{,}7 \cdot \left[\frac{f_{coef;i}}{8}\right]^{(1/2)} \cdot (Pr_{hs;i}^{(2/3)} - 1)}\right]$ (for i = start$_{cond}$+1 to end$_{cond}$)

Gnielinski correlation: Re(3000-5000000)

$Nuss_{hs;De;i} = d_{cw} \cdot \frac{\alpha_{hs1;De;i}}{k_{hs;i}}$ (for i = start$_{cond}$+1 to end$_{cond}$) *not used*

$\alpha_{hs1;i} = 0{,}023 \cdot \frac{k_{hs;i}}{d_{cw}} \cdot Re_{hs;i}^{0{,}8} \cdot Pr_{hs;i}^{0{,}4} \cdot \left[1 + 82{,}4 \cdot \left[\frac{d_{cw}}{d_{cw;axis;51}}\right]^3\right]$ (for i = start$_{cond}$+1 to end$_{cond}$) *not used*

$\alpha_{hs4;i} = 0{,}023 \cdot \frac{k_{hs;i}}{d_{cw}} \cdot Re_{hs;i}^{0{,}8} \cdot Pr_{hs;i}^{0{,}4} \cdot \left[1 + 82{,}4 \cdot \left[\frac{d_{cw}}{d_{cw;axis;54}}\right]^3\right]$ (for i = start$_{cond}$+1 to end$_{cond}$) *not used*

$k_{hs;i}$ = **k** (steam$_{iapws}$; T = $T_{hs;i}$; P = p_{31}) (for i = start$_{cond}$+1 to end$_{cond}$)

$Nuss_{hs;i} = d_{cw} \cdot \frac{\alpha_{hs;i}}{k_{hs;i}}$ (for i = start$_{cond}$+1 to end$_{cond}$) *from here alpha$_{hs,i}$ is calculated*

$R_{cf;abs;i} = \frac{1}{\alpha_{hs;i}}$ (for i = start$_{cond}$+1 to end$_{cond}$)

$A_{tot;i} = A_{tot;i-1} + A_i$ (for i = start$_{cond}$+1 to end$_{cond}$)

$\Delta_{T;vl;i} = T_i - T_{L;i}$ (for i = start$_{cond}$+1 to end$_{cond}$)

PP_{cold} = **Min** ($\Delta_{T;start;cond..end;cond}$) *to find minimal temperature difference*

$PP_{cold} = 10$ *definition of minimal temperature difference to be used in above equations*

A_{cond} = **Sum** ($A_{151..end;cond}$) *surface area of the condenser*

$Q_{flux;abs} = \frac{Q_{rej}}{A_{cond}}$

Velikost HX

$D_{cw;abs} = \frac{21{,}3}{1000}$ *DN15 diameter of cooling fluid pipes in [m]*

DN10-10/1; DN12-12/1; DN15-15/1; DN18-18/1; DN22-22/1

$thick_{abs} = \frac{2}{1000}$ *wall thickness in [m]*

$d_{cw} = D_{cw;abs} - 2 \cdot thick_{abs}$ *pro trubku DN15*

$pipe_{cw;abs} = 1$ *# of cooling fluid sections with the absorber?*

$S_{cw;abs} = D_{cw;abs}^2 \cdot \frac{3{,}14159}{4} \cdot pipe_{cw;abs}$ *prurez cw trubkou*

$m_{31} \cdot$ **v** (steam$_{iapws}$; P = p_{31} ; T = T_{31}) = $S_{cw;inner} \cdot veloc_{cw;abs}$ *calculation of cw velocity*

$D_{cw;abs} \cdot 3{,}14159 \cdot L_{abs;pipe} = A_{cond}$ *calculation of $L_{abs,pipe}$ = total lenght f pipes needed*

$D_{column;abs}$ = **Round** ($14 \cdot D_{cw;abs}$; 0,01) *Vnejsi prumer jadra in [m]*

$Circles_{cw;abs} = 4$ ----------*# of pipes*

$dq_{cond} = \frac{Q_{rej}}{L_{abs;pipe}}$ *heat transfered per meter of the cw pipe*

$space_{abs} = 1 \cdot D_{cw;abs}$

space between the pipes in radial horizontal position

g=9,81

$n3 = Circles_{cw;abs} - 1$

$start_{cw;pipe} = 51$

$end_{cw;pipe} = 51 + n3$

$\frac{d_{cw;axis;51}}{2} = \frac{D_{column;abs}}{2} + space_{abs} + 2 \cdot \frac{D_{cw;abs}}{2}$

$\frac{d_{cw;inner;51}}{2} = \frac{d_{cw;axis;51}}{2} - \frac{D_{cw;abs}}{2}$

$circumf_{51} = \pi \cdot d_{cw;axis;51}$

$L_{cw;51} = \frac{L_{abs;pipe}}{Circles_{cw;abs}}$

$Q_{tot;51} = L_{cw;51} \cdot dq_{cond}$

$m_{51} = \frac{m_{31}}{Circles_{cw;abs}}$

$\Delta_{T;51} = \frac{Q_{tot;51}}{m_{51} \cdot \mathbf{Cp}(steam_{iapws}; T = T_{31}; P = p_{31})}$

$\mu_{l;51} = \mathbf{Visc}(steam_{iapws}; T = T_{35;51}; P = p_{31})$

$Re_{51} = \frac{m_{51}}{S_{cw;inner}} \cdot \frac{d_{cw}}{\mu_{l;51}}$

$T_{35;51} = T_{31} + \Delta_{T;51}$

$pitch_{cw;51} = 1{,}5 \cdot D_{cw;abs}$ *setting the vertical pitch (roztec) in the most inner pipe.*

$\left[\frac{L_{cw;51}}{rot_{cw;51}}\right]^2 = pitch_{cw;51}^2 + circumf_{51}^2$ *calculation of the number of rotations per each pipe*

$height_{cw;pipe} = rot_{cw;51} \cdot pitch_{cw;51}$ *height of the pipes spiral*

$\frac{d_{cw;axis;i}}{2} = \frac{d_{cw;axis;i-1}}{2} + space_{abs} + 2 \cdot \frac{D_{cw;abs}}{2}$ (for $i = start_{cw;pipe}+1$ to $end_{cw;pipe}$) *horizontal axis diameter of each of the pipe at one layer*

$\frac{d_{cw;inner;i}}{2} = \frac{d_{cw;axis;i}}{2} - \frac{D_{cw;abs}}{2}$ (for $i = start_{cw;pipe}+1$ to $end_{cw;pipe}$) *horizontal inner diameter*

$circumf_i = \pi \cdot d_{cw;axis;i}$ (for $i = start_{cw;pipe}+1$ to $end_{cw;pipe}$) *circumference of each pipe at one layer*

$L_{cw;i} = \frac{L_{abs;pipe}}{Circles_{cw;abs}}$ (for $i = start_{cw;pipe}+1$ to $end_{cw;pipe}$) *total length of each of the cw pipes*

$Q_{tot;i} = L_{cw;i} \cdot dq_{cond}$ (for $i = start_{cw;pipe}+1$ to $end_{cw;pipe}$) *Total heat tranfered for each of the cw pipes*

$m_i = \frac{m_{31}}{Circles_{cw;abs}}$ (for $i = start_{cw;pipe}+1$ to $end_{cw;pipe}$) *setting the same mass flow for each of the pipes*

$\Delta_{T;i} = \frac{Q_{tot;i}}{m_i \cdot \mathbf{Cp}(steam_{iapws}; T = T_{31}; P = p_{31})}$ (for $i = start_{cw;pipe}+1$ to $end_{cw;pipe}$) *absolute temperature difference in each of the pipes*

$\mu_{l;i} = \mathbf{Visc}(steam_{iapws}; T = T_{35;i}; P = p_{31})$ (for $i = start_{cw;pipe}+1$ to $end_{cw;pipe}$) *dyn. viscosity*

$Re_i = \frac{m_i}{S_{cw;inner}} \cdot \frac{d_{cw}}{\mu_{l;i}}$ (for $i = start_{cw;pipe}+1$ to $end_{cw;pipe}$) *Reynolds number at the cw pipe outlet in each of the pipes*

$T_{35;i} = T_{31} + \Delta_{T;i}$ (for $i = start_{cw;pipe}+1$ to $end_{cw;pipe}$)

$L_{cw;i}^2 = (rot_{cw;i} \cdot \pi \cdot d_{cw;axis;i})^2 + height_{cw;pipe}^2$ (for $i = start_{cw;pipe}+1$ to $end_{cw;pipe}$) *calculation of the number of rotations*

$pitch_{cw;i} = \frac{height_{cw;pipe}}{rot_{cw;i}}$ (for $i = start_{cw;pipe}+1$ to $end_{cw;pipe}$) *calculation of pitches*

$O_{loops} = \mathbf{Sum}(circumf_{51..end;cw;pipe})$

Absober design - additional information

$h_{distr} = 0{,}05$ *height of the distributor layer in [m]*

$h_{spray} = 0{,}04$ *height of the solution spraying layer in [m]*

$h_{pool} = 0{,}05$ *height of the hladinka in absorber in [m]*

$h_{absorber} = h_{spray} + h_{distr} + 0{,}02 + height_{cw;pipe} + h_{spray} + h_{distr} + 0{,}02 + height_{cw;pipe} + 0{,}02 + h_{pool}$ *aproximate height of the absorber*

$thick_{abs;shell} = \frac{2}{1000}$ *aproximate thickness of the Absorber shell in [m]*

$\frac{D_{abs;ext}}{2} = \frac{d_{cw;axis;54}}{2} + \frac{D_{cw;abs}}{2} + space_{abs} + thick_{abs;shell}$ *aproximate external diameter of the absorber*

COOLING LOOP

$h_{31} = \mathbf{h}(steam_{iapws}; T = T_{31}; P = p_{31})$

$s_{31} = \mathbf{s}(steam_{iapws}; T = T_{31}; P = p_{31})$

$\mu_{l;31} = \mathbf{Visc}(steam_{iapws}; T = T_{31}; P = p_{31})$

$S_{cw;inner} = \pi \cdot \frac{d_{cw}^2}{4}$

$Re_{31} = \frac{m_{31}}{Circles_{cw;abs} \cdot S_{cw;inner}} \cdot \frac{d_{cw}}{\mu_{l;31}}$ *Reynolds*

$T_{35} = \mathbf{T}(steam_{iapws}; h = h_{35}; P = 2)$

$s_{35} = \mathbf{s}(steam_{iapws}; T = T_{35}; P = p_{31})$

$\mu_{l;35} = \mathbf{Visc}(steam_{iapws}; T = T_{35}; P = 2)$

$Re_{35} = \frac{m_{31}}{Circles_{cw;abs} \cdot S_{cw;inner}} \cdot \frac{d_{cw}}{\mu_{l;35}}$ *Reynolds at the outlet*

$\Delta_{P;DC} = 200$

$\Delta_{P;H2O} = 80000$

$W_{cwpump} = m_{31} \cdot \mathbf{v}(steam_{iapws}; T = T_{31}; P = 1,5) \cdot \frac{\Delta_{P;H2O}}{0,5 \cdot 1000}$

$h_{30} = h_{31}$

DC

$T_{41} = t_e$

$RH = 0,7$

$\omega = \omega(AIRH2O; T = T_{41}; R = RH; P = 1,01)$

$\Delta T_{min;DC} = 10$

$\Delta_{P;acc} = 200$ [Pa] *ACC air pressure loss*

$\eta_{fan} = 0,7$ *fan efficiency*

$h_{41} = \mathbf{h}(AIRH2O; T = T_{41}; R = RH; P = 1,01)$

$Q_{DC} = m_{31} \cdot (h_{35} - h_{30})$

$T_{35} = T_{42} + \Delta T_{min;DC}$

$T_{31} = T_{41} + \Delta T_{min;DC}$

$h_{42} = \mathbf{h}(AIRH2O; T = T_{42}; R = RH; P = 1,01)$

$Q_{DC} = m_{41} \cdot (h_{42} - h_{41})$

$W_{fan} = m_{41} \cdot \mathbf{v}(AIRH2O; T = T_{42}; w = \omega; P = 1,01) \cdot \frac{\Delta_{P;DC}}{\eta_{fan} \cdot 1000}$ *Fan power [kW]*

QT diagram DC

$T_{hs;141} = T_{41}$

$T_{141} = T_{31}$

$Q_{tot;141} = 0$

$T_{hs;142} = T_{42}$

$T_{142} = T_{35}$

$Q_{tot;142} = Q_{DC}$

$W_{net} = W_{plant} - W_{fan} - W_{cwpump}$ *net power output*

$s_0 = \mathbf{s}(steam_{iapws}; T = T_{31}; P = p_{21})$ *dead state entropy*

$h_0 = \mathbf{h}(steam_{iapws}; T = T_{31}; P = p_{21})$ *dead state enthalpy*

$e_{hs} = h_{21} - h_0 - ((T_{31} + 273,15) \cdot (s_{21} - s_0))$ *exergy of heat source kW/kg s*

$Ex_{hs} = e_{hs} \cdot m_{21}$ *exergy of heat source kW*

$\eta_c = \frac{W_{net}}{Q_{in}}$

$\eta_{1;gross} = \frac{W_{plant}}{Q_{in}}$

$\eta_{1;net} = \frac{W_{net}}{Q_{in}}$

$\eta_{ex;net} = \frac{W_{net}}{Ex_{hs}}$

Vypocet rychlosti v potrubni siti

DN80 - pred turbinou

$D_{o;5} = 88,9 \cdot \frac{1}{1000}$

$thickn_5 = 2,11 \cdot \frac{1}{1000}$

$D_{i;5} = D_{o;5} - 2 \cdot thickn_5$

$v_{v;5} = \mathbf{v}(steam_{iapws}; T = T_5; P = p_5)$

$c_5 = \frac{m_5 \cdot v_{v;5}}{\pi \cdot \frac{D_{i;5}^2}{4}}$

DN65 - za turbinou

$D_{o;6} = 73,03 \cdot \frac{1}{1000}$

$thickn_6 = 2,11 \cdot \frac{1}{1000}$

$D_{i;6} = D_{o;6} - 2 \cdot thickn_6$

$v_{v;6} = \mathbf{v}(steam_{iapws}; h = h_6; P = p_6)$

$c_6 = \frac{m_6 \cdot v_{v;6}}{\pi \cdot \frac{D_{i;6}^2}{4}}$

T-S diagram

$Ss_{ii} = s_{ii} \cdot m_{ii}$ (for ii = 1 to 11)

T-s diagram vztazena na hmotnostni prutok pary

$s_{rel;steam;ii} = s_{ii} \cdot \frac{m_{ii}}{m_5}$ (for ii = 1 to 11)

p-h diagram vztazena na hmotnostni prutok pary

$h_{rel;steam;ii} = h_{ii} \cdot \frac{m_{ii}}{m_5}$ (for ii = 1 to 11)

.....h-x diagram....

$\xi_i = 0{,}4$

Call **hl**$_{pstsxil;WaLi;EES}$ ('' ; p_{11} ; – 1 ; ξ_i : $h_{L;x0}$) *saturacni krivky*

Call **hl**$_{pstsxil;WaLi;EES}$ ('' ; p_1 ; – 1 ; ξ_i : $h_{H;x0}$)

Call **hv**$_{pstsxil;WaLi;EES}$ ('' ; p_{11} ; – 1 ; ξ_i : $h_{L;x1}$)

Call **hv**$_{pstsxil;WaLi;EES}$ ('' ; p_1 ; – 1 ; ξ_i : $h_{H;x1}$)

.....Saturacni krivky T-s diagram.....

$T_{ii} = 100$

Call **sl**$_{pstsxil;WaLi;EES}$ ('' ; p_{11} ; T_{ii} ; – 1 : $s_{L;x0}$) *odsud xil*

Call **sl**$_{pstsxil;WaLi;EES}$ ('' ; p_1 ; T_{ii} ; – 1 : $s_{H;x0}$) *odsud xil*

Call **sv**$_{pstsxil;WaLi;EES}$ ('' ; p_{11} ; T_{ii} ; – 1 : $s_{L;x1}$) *odsud xil*

Call **sv**$_{pstsxil;WaLi;EES}$ ('' ; p_1 ; T_{ii} ; – 1 : $s_{H;x1}$) *odsud xil*

$s_{H2O;0} =$ **s** ($steam_{iapws}$; T = T_{ii} ; x = 0) *saturacnu krivka x=0*

$s_{H2O;1} =$ **s** ($steam_{iapws}$; T = T_{ii} ; x = 1) *saturacnu krivka x=1*

C

Print of main solutions of the joint model from EES

Generated in EES program based on the model from Ing. Novotný.

SOLUTION

Unit Settings: SI C bar kJ mass deg

$\alpha_{boil,des,aver}$ = 841,8
$\alpha_{wf,abs}$ = 2000
AoptT$_{21}$ = 90 [C]
AoptW$_{7}$ = 0,5
A_{cond} = 5,695 [m^2]
Circles$_{cw,abs}$ = 4
dD$_{ratio}$ = 0,6519
ΔT$_{min,DC}$ = 10 [C]
ΔP$_{,DC}$ = 200
des$_{S,LiBr}$ = 0,002704
dh$_{eva}$ = 25,59 [kJ/kg]
Dratio$_{sh,bu,actual}$ = 1,55
dTse = 21 [K]
D$_{column,abs}$ = 0,3
D$_{cw,abs}$ = 0,0213
d$_{tube,i}$ = 0,0088
end$_{cond}$ = 180
end$_{eva}$ = 130
$\eta_{1,net}$ = 0,01482
$\eta_{ex,net}$ = 0,0186 [kW-s/kg]
η_{p} = 0,2
Ex$_{hs}$ = 15,94 [kg/s]
height$_{cw,pipe}$ = 0,5616 [m]
h$_{1,ad}$ = 100,1 [kJ/kg]
h$_{cv}$ = 2612 [kJ/kg]
h$_{e,ad}$ = 2516 [kJ/kg]
h$_{H,x1}$ = 2690
h$_{L,x1}$ = 2652
h$_{orc,real}$ = 696,5 [kJ/kg]
h$_{pool}$ = 0,05
k$_{Cu}$ = 393,1
k$_{wall,abs}$ = 15,26 [W/m-K]
L$_{abs,pipe}$ = 85,11 [m]
L$_{tube,need}$ = 1,035 [m]
m$_{cv}$ = 0,007597 [kg/s]
m$_{orc}$ = 0,06453
m$_{wf}$ = 0,02603 [kg/s]
n = 30
n3 = 3
n$_{coef}$ = 0,85
O$_{loops}$ = 6,447
PP$_{cold}$ = 10 [K]
p$_{orc}$ = 0,8649
Q$_{DC}$ = 19,57 [kJ/kg-s]
Q$_{flux,abs}$ = 3,437 [kW/m^2]
Q$_{FWH}$ = 0,01529 [kW]
Q$_{reg}$ = 1,228 [kW]
Re$_{hs,des,aver}$ = 4743 [m/dim]
R$_{trubky}$ = 0,000002544
R$_{wall,des}$ = 0,0001616 [m-K/W]
σ_{LiBr} = 0,06
start$_{cond}$ = 150
start$_{eva}$ = 100
s$_{10,l}$ = 0,426
S$_{cw,inner}$ = 0,0002351
s$_{H2O,1}$ = 7,354
s$_{H,x1}$ = 8,273
s$_{L,x1}$ = 8,686
S$_{pipes}$ = 0,01002

$\alpha_{hs,des,aver}$ = 1854
AoptT$_{11}$ = 44,5 [C]
AoptW$_{1}$ = 0,65
aux$_{q,avg}$ = 6,512 [kW/m^2]
A_{des} = 3,071 [m^2]
C$_{sf}$ = 0,0136
ΔTmin$_{hot}$ = 10 [K]
ΔP$_{,acc}$ = 200 [Pa]
ΔP$_{,H2O}$ = 80000
dh$_{cond}$ = 25,06 [kJ/kg]
dq$_{cond}$ = 0,23 [kW/m]
Dratio$_{sh,bu,the,max}$ = 1,217
D$_{abs,ext}$ = 0,7087
d$_{cw}$ = 0,0173
d$_{h,des}$ = 0,0088
d$_{tube,o}$ = 0,0135
end$_{cw,pipe}$ = 54
$\eta_{1,gross}$ = 0,02059
η_{c} = 0,01482
η_{fan} = 0,7
η_{turb} = 0,4
e$_{hs}$ = 22,02
h$_{0}$ = 125,9 [kJ/kg]
h$_{absorber}$ = 1,413 [m]
h$_{distr}$ = 0,05
h$_{H,x0}$ = 236,2
h$_{L,x0}$ = 196,7
h$_{orc,end,ie}$ = 676,2 [kJ/kg]
h$_{orc,turb}$ = 716,7 [kJ/kg]
h$_{spray}$ = 0,04
K$_{L}$ = 0,00001
k$_{wall,des}$ = 14,54 [W/m-K]
l$_{trubky}$ = 0,001
m$_{cl}$ = 0,01843 [kg/s]
m$_{libr}$ = 0,009111 [kg/s]
m$_{w}$ = 0,01692 [kg/s]
m$_{w,separ}$ = 0,009111 [kg/s]
n2 = 30
nr$_{tube}$ = 70
ω = 0,01025
pipe$_{cw,abs}$ = 1
PP$_{hot}$ = 10 [K]
p$_{orc,eva}$ = 6,524 [bar]
Q$_{eva}$ = 19,98 [kW]
Q$_{flux,des}$ = 6,512 [kW/m^2]
Q$_{in}$ = 20 [kW]
Q$_{rej}$ = 19,57 [kW]
RH = 0,7
R$_{wall,abs}$ = 0,0001311 [m-K/W]
R$_{wf,abs}$ = 0,0005 [m-K/W]
space$_{abs}$ = 0,0213
start$_{cw,pipe}$ = 51
s$_{0}$ = 0,4367 [kJ/kg-K]
S$_{cw,abs}$ = 0,0003563
s$_{H2O,0}$ = 1,307
s$_{H,x0}$ = 0,5686
s$_{L,x0}$ = 0,5039
s$_{orc}$ = 2,354
S$_{shell}$ = 0,01272

$thick_{abs}$ = 0,002
$thick_{des}$ = 0,00235
$t_{1,ad}$ = 44,5
T_{ii} = 100
$veloc_{cw,abs}$ = 1,118
W_{fan} = 0,07326 [kW]
W_{plant} = 0,4118 [kW]
W_{turb} = 0,4126 [kW]
x_{sep} = 0,3

$thick_{abs,shell}$ = 0,002
TTD = 5 [C]
t_e = 20 [C]
$T_{orc,eva}$ = 180
W_{cwpump} = 0,04204 [kW]
W_{net} = 0,2965 [kW]
W_{pump} = 0,0008575 [kW]
ξ_i = 0,4
$x_{steam,e}$ = 100 [-]

797 potential unit problems were detected.
EES suggested units (shown in purple) for AoptT_11 AoptT_21 aux_q_avg alpha[151] alpha[152] alpha[153] .